T H E U N I V E R S I T Y O F M I C H I G A N

COLLEGE OF ENGINEERING
Department of Aeronautical and Astronautical Engineering

Final Report

FALLING-SPHERE INSTRUMENTATION DEVELOPMENT

Prepared for the Project by:

J. W. Peterson
D. A. Robinson
H. F. Schulte

Approved by:
L. M. Jones

UMRI Project 2649

under contract with:

UNITED STATES AIR FORCE
AIR RESEARCH AND DEVELOPMENT COMMAND
AIR FORCE CAMBRIDGE RESEARCH CENTER
GEOPHYSICS RESEARCH DIRECTORATE
CONTRACT NO. AF 19(604)-2415
BEDFORD, MASSACHUSETTS

administered by:

THE UNIVERSITY OF MICHIGAN RESEARCH INSTITUTE ANN ARBOR

February 1960

TABLE OF CONTENTS

LIST OF FIGURES

LIST OF FIGURES (Concluded)

ABSTRACT

Work on the continuing development of the falling-sphere technique for measuring upper-air density and temperature is described. The factors limiting the performance of the transit-time accelerometer were investigated, and a design concept was reached which, it is anticipated, will improve the performance. The data-reduction process for the sphere experiment was completely computerized and is reported. An investigation of the phenomenon of antenna breakdown in flight is described.

THE UNIVERSITY OF MICHIGAN PROJECT PERSONNEL
(BOTH FULL-TIME AND PART-TIME)

Finkbeiner, Richard G., Electronic Technician

Gleason, Kermit L., Instrument Maker

Harrison, Lillian, Secretary

Jones, Leslie M., B.S., Project Supervisor

Malkani, Sundru J., M.Sc., Assistant in Research

Mosakewicz, Mary C., Secretary

Pattinson, Theodore R., Electronic Technician

Peterson, John W., M.S., Associate Research Engineer

Robinson, Douglas A., Technician

Schulte, Hal. F., Jr., M.S.E.(EE), Associate Research Engineer

Thornton, Charles H., Consultant

Wenk, Norman J., B.S.E.(ME), Research Engineer

1. INTRODUCTION

This is the final report of a project carried on in the Department of Aeronautical and Astronautical Engineering of The University of Michigan, the purpose of which was to continue with certain developments of the falling-sphere method for measuring upper-air density and temperature. The work is a continuation of a program started in 1954 and continuing through 1958 in which the small-falling-sphere technique was developed and used. Support for that period was received under Air Force Contracts No. AF 19(604)-999 and No. AF 19(604)-1871. The former contract encompassed the International Geophysical Year as well as the so-called "pre-IGY" period, July, 1956, to July, 1957. Within this 2-1/2-year interval, seven successful (of a total of 10) flights of the small-sphere experiment were carried out. The results of these flights, together with a single small-sphere flight in 1955 and some still earlier work with large inflatable spheres, include a comparison of winter upper-air densities at 32°N vs. 58°N, the detection of a latitude density gradient, and the detection of "explosive warming" at rocket altitudes in the winter Arctic atmosphere. Background information is contained in Refs. 1 through 8.

The tasks of the contract of this report included the delivery to AFCRC of two Michigan-type accelerometers and one complete 7-in. falling sphere of the type used during the IGY. These items were delivered. In addition, the following research and development tasks were undertaken:

"Conduct experiments and studies directed toward the determination of the lower limit of acceleration which can be measured with the existing Michigan-type transit-time accelerometer and directed toward the refinements in design of that accelerometer for extending the range to lower values."

"Initiate the development of a refined falling-sphere accelerometer system consisting of the following:

a. A refined time of fall accelerometer of the type indicated in the statement above.

b. A light rigid drag envelope communicating directly with the accelerometer bobbin in a manner consistent with a practical minimum mass-to-area-ratio for the envelope-bobbin structure and suspended or supported relative to the internal mass in a manner such that during rocket flight only, the system will withstand the associated accelerations.

c. A radio transmitter system complete with power supply, slot antenna and necessary external controls and monitor mechanisms designed to make its performance equal to or better than the transmitter developed for the spheres flown in November 1956."

"Initiate the development of a device for holding the falling-sphere accelerometer system during rocket flight and for ejecting the falling-sphere accelerometer system from the rocket upon signal from a timer sometime after the end of powered flight."

By Modification 3 of the contract, the following task was added:

"Research and develop computer methods for reducing data from the small sphere experiment with the ultimate aim of developing an automatic data reduction system."

Some of the development goals of the contract of this report have been achieved and some have not. To complete the work and bring the improved techniques to field test, a new contract, AF 19(604)-6185, to be carried out in the calendar year 1960, has been entered upon.

2. ACCELEROMETER INVESTIGATIONS

In previous work with the transit-time accelerometer at low accelerations, an Attwood's machine technique described in Ref. 3 was used. With this apparatus, checks of the accelerometer at somewhat less than 0.01 g were successfully carried out. As a first step in exploring the practical lower limit of accelerations which could be measured with the existing accelerometer, a technique for accurately applying lower accelerations of 10^{-3} or perhaps 10^{-4} g was sought. Measurement of the moment of inertia of the pulley was improved by construction of a magnetic tong release which eliminated the slack in the thread and the lost motion in the trigger of the previous setup. A crystal microphone was used to provide a stop pulse to the counter at the time of contact of the small calibrating weight. These devices are shown in Fig. 1.

Some improvements were also made in the heavy-bullet technique for calibrating the accelerometer. A light-beam and photo-cell apparatus was installed for starting the counter at the beginning of the fall of the accelerometer and "bullet" to eliminate the varied starting effects of the previously used micro-switch. A further improvement was the employment of a double "bullet" consisting of similar massive pieces mounted symmetrically on either end of the accelerometer. This arrangement placed the bobbin at the center of a very slight rotary motion which was observed to occur upon dropping the mass. The cause of the rotation was not investigated further but its effect was eliminated.

With the new setup, an acceleration of 0.0067 g was measured. The apparatus is shown in Fig. 2.

The Attwood's machine technique appears capable of being extended to 10^{-3} g and perhaps further merely by increasing the mass of the drop bullet. A practical difficulty peculiar to the technique is that of raising the mass through the larger and larger drop distances required for the increasing transit times of the decreasing accelerations. The larger drop-distance problem and the problem of air drag are, of course, common to any drop tester. To avoid the heavy mass of the Attwood's machine, a new technique described in the next paragraph was attempted. The results so far have been unsatisfactory. It may be that the best method will prove to be the Attwood's machine with some provision for conveniently handling the massive bullet. A variation of the Attwood's machine was considered in which, instead of accelerating a pulley, a small mass attached by cord to the falling big mass is accelerated upward. In this case the cord must reverse direction over either one or two pulleys or smooth rods. To eliminate unwanted inertia of the pulleys, they are kept small or replaced with smooth rods. In either case the friction in these "reversers" has caused unacceptably large errors, and this variation of the drop technique has not been made to work well.

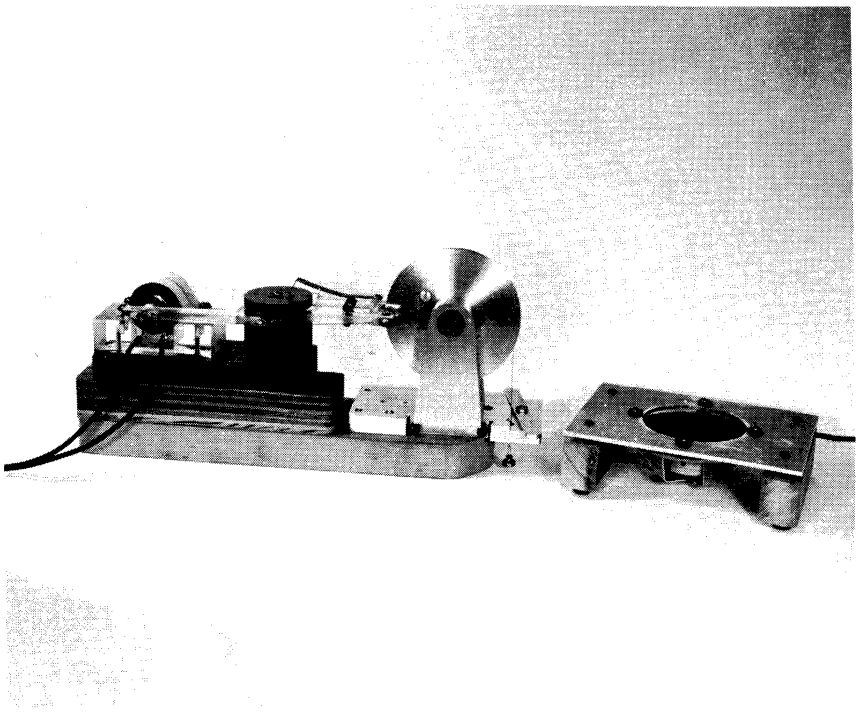

Fig. 1. Magnetic tong release and microphone used in measuring moment of inertia of calibrating pulley.

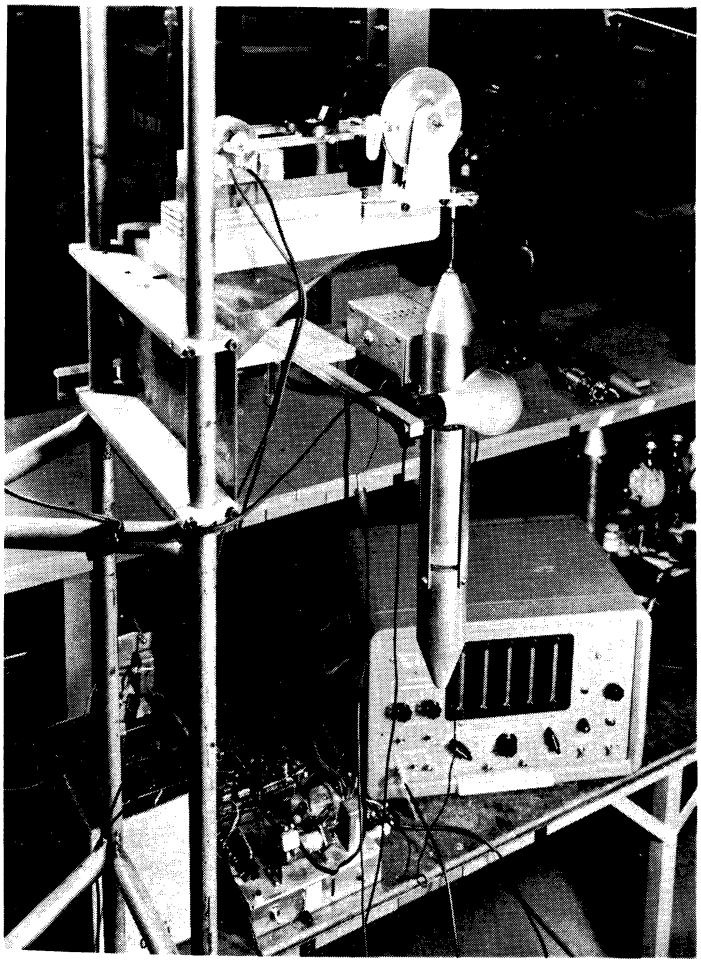

Fig. 2. Double-ended bullet and photocell drop indicator used in calibrating accelerometer.

As mentioned above, an apparatus was conceived and built which induced test accelerations magnetically. Small permanent magnets were fastened to the accelerometer unit and to a weighted windshield which was released simultaneously with the accelerometer. The geometric arrangement of the magnets was designed so that the magnetic forces are substantially constant in the small range of motion which results from the test force and the air drag force on the windshield. The accelerometer coils were energized by batteries external to the falling bodies.

The initial work with this device was not successful. The difficulties are obscure, but may be due to inability to release the two bodies and break the current to the accelerometer coils at precisely the same instant. Perhaps satisfactory techniques could have been developed. In any case, other tests of accelerometer characteristics seemed more attractive at the time and were therefore given priority. However, the principle of reducing air drag by enclosing the accelerometer with a windshield should be of value whenever the low range of acceleration is tested. The magnetic drop tester is illustrated in Figs. 3 and 4.

In Ref. 2, three sources of error in the accelerometer are discussed: (a) error in transit distance, (b) error in measuring transit time, and (c) error due to initial velocity of the bobbin upon release. The first two can be made acceptably small and are not proportional to the acceleration being measured. The magnitude of the error in acceleration due to initial velocity in per cent is

$$\delta a_{v_o} = 200\, v_o/at \qquad (1)$$

where

v_o = initial velocity

a = acceleration

t = time

Various sources of initial velocity can be supposed. If the center of the bobbin is displaced from the center of rotation of the sphere by an amount r, then $v_o = \omega r$, where ω is the spin angular velocity. This source of initial velocity is avoided in flight by achieving a low rocket spin and precise bobbin location ("balance"). Under no-spin conditions, initial velocity can result from mechanical imperfections in the uncaging process, perturbations due to collapse of the magnetic field of the caging coils, and perhaps others. In view of the difficulties encountered with the drop testers, an alternate approach, namely, attempting to assess the initial velocity errors, was undertaken. From the equation above it may be seen that for a 1% error in acceleration due to initial velocity v_o, the magnitude of v_o is

$$v_o = (1/200)\sqrt{2\, sa} \qquad (2)$$

where

s = transit distance = .187 in.

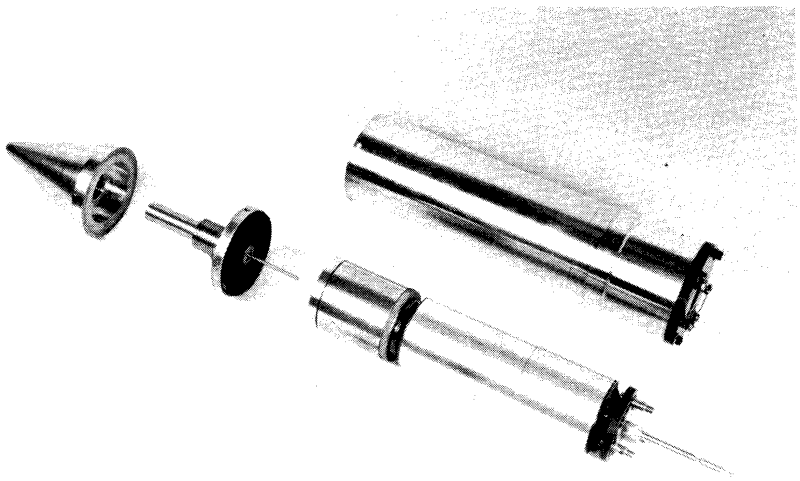

Fig. 3. Magnetic drop tester for accelerometers, disassembled.

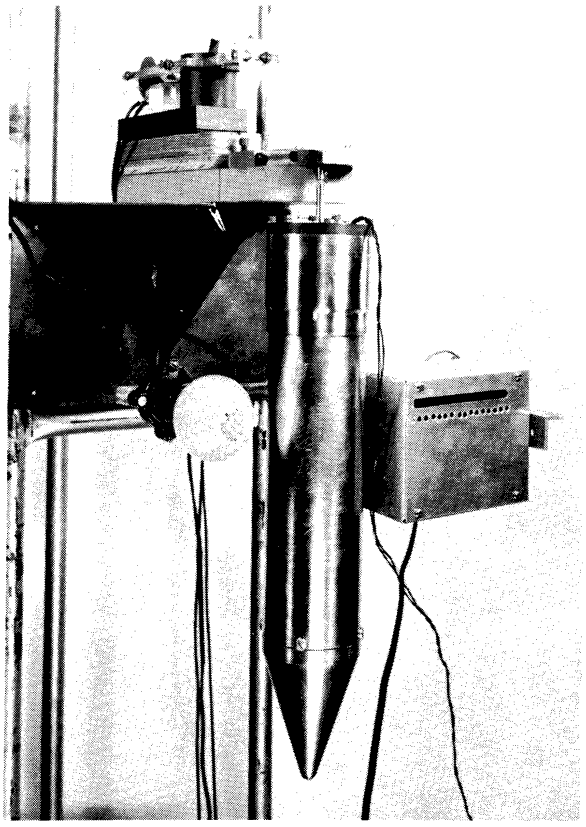

Fig. 4. Magnetic drop tester with photoelectric drop indicator.

Thus $v_o = 1.9 \times 10^{-3}$ in./sec at 10^{-3} g for 1% error.

$= 0.6 \times 10^{-3}$ in./sec at 10^{-4} g for 1% error.

The collapse of the magnetic field of the caging coils was disposed of as a source of significant initial velocity in the following manner. The bobbin was supported on a thread three feet in length in its normal cage position within the cavities. Considerable time and effort were required to reach a condition of no motion even with the aid of an air-motion shield. With the bobbin in place, the caging coils were energized and de-energized and the bobbin observed for motion. To increase the sensitivity of the system, a shadow image of the bobbin was cast on a screen with an optical multiplication of 10 to 1. It can be shown that, with this experimental setup, initial velocities of .006 in./sec, .0019 in./sec, and .0006 in./sec (which would yield 1% errors at 10^{-2}, 10^{-3} and 10^{-4} g, respectively) would result in lateral displacements of the bobbin image of about .02 in., 0.006 in., and 0.002 in., respectively. Since no motion of the image whatever was observed, it was concluded that perturbations of the bobbin due to magnetic field are negligible.

Next, an experiment was performed to assess the magnitude of initial velocity resulting from release of the caging mechanism. An accelerometer from which the contact wire and cavities had been removed was set up over a free drop distance of 46.5 in. The bobbin was dropped on a piece of carbon paper resting on a piece of paper to mark the point of impact (see Fig. 5). The target to be hit in the absence of initial velocity was determined with the aid of a plumb bob. The initial velocity was then calculated from the displacement R between the impact point of the bobbin and the target point:

$$v_o = R\sqrt{g/2h} \qquad (3)$$

$$h = 46.5 \text{ in.}$$

$$g = 386 \text{ in./sec}^2$$

The test was applied to three bobbins: (A) an aluminum bobbin of standard design with the caging surfaces in good condition; (B) an aluminum bobbin with a square caging hole, the caging surfaces in good condition (this bobbin was designed for a test on the contact wire described later); and (C) a magnesium bobbin of standard design. The average displacements R and calculated initial velocities v_o with the standard deviations of 10 drops each are given in Table I. If we take the results for A and B to be typical of bobbins whose caging surfaces are in good condition and assume that the same impulse is available to move C as A and B, the initial velocity of C may be expected to be inversely proportional to its mass, say perhaps .06 in./sec. The fact that the measured v_o is more than twice as large may reasonably be attributed to a major defect in the caging action. The fact that the random error in the case of C is about the same as the other two supports this view. Even in the cases of A and B, the initial velocities are marginal at 10^{-2} g and too large for 10^{-3} g.

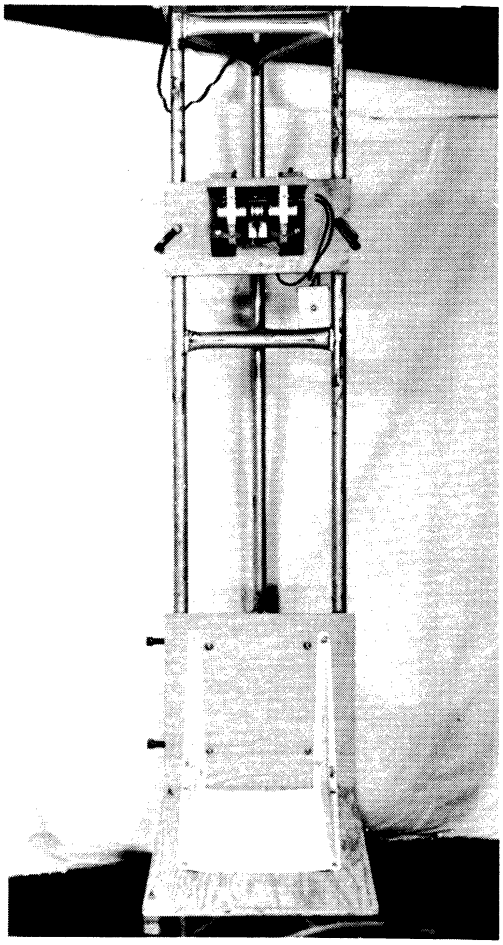

Fig. 5. Bobbin drop test for initial velocity.

TABLE I

Bobbin	Weight grams	Weight lb	R in.	v_o in./sec
A	32.2	.071	.017 ± .015	.04 ± .03
B	33.2	.073	.014 ± .011	.03 ± .02
C	14.9	.033	.068 ± .018	.14 ± .04

Having eliminated the collapse of the magnetic field as a source of significant initial velocity, we may attribute the above values of initial velocity to the caging mechanism with one reservation. It is necessary to show that the aerodynamic forces on the falling bobbin in the test contribute only a negligible portion of the measured deflections.

The first step is to determine the aerodynamic flow regime within which the bobbin falls. Since the bobbin is a relatively massive object, we can make the vacuum calculation for the velocity after a fall of 4 ft. The velocity is 16 ft/sec. The Reynolds number is defined by

$$Re = \frac{\rho V d}{\mu} , \tag{4}$$

where ρ and μ are the air density and viscosity and d is the bobbin diameter. The Reynolds number is therefore zero at the beginning of the fall and increases to 2000 at the end. The drag coefficient of a spherical bobbin in this range of Reynolds numbers is 0.4, approximately.

To estimate an upper limit of the lateral displacement of the falling bobbin due to aerodynamic effects, let us assume a lateral force 10% of the drag. The lateral motion is therefore defined by

$$m \frac{d^2x}{dt^2} = \frac{C_D}{10} A \frac{1}{2} \rho V^2 , \tag{5}$$

where $V = gt$

A = bobbin cross-sectional area.

Integrating, the result is

$$x = \frac{C_D A}{240\ m} \rho\ g^2 t^4 . \tag{6}$$

But $y = \frac{1}{2} gt^2$; thus

$$x = \frac{C_D A}{60m} \rho\ y^2 . \tag{7}$$

In the case of bobbin "A" above which weighed .071 lb and with a drop distance of 3.88 ft,

$$x = .007 \text{ in.}$$

In the case of bobbin "C", which weighed .033 lb, and with the same drop distance:

$$x = .016 \text{ in.}$$

These values compare with measured deflections of .017 in. and .068 in., respectively. Thus we conclude that, although a small part of the measured deflections may be due

to aerodynamic forces, some of it is probably due to initial velocities of the magnitudes shown in Table I. The technique shows promise of working well for detecting initial velocity and is capable of improvement in making the spurious aerodynamic effects negligible.

Having examined the effect of drag in the case of the bobbin drop test for initial velocity, we will find it instructive to investigate whether or not, at the very low accelerations it is hoped to measure, drag on the bobbin in traversing its normal transit distance may introduce an error.

If appreciable error from this cause were indicated, it would be necessary to evacuate the accelerometer. We know from laboratory and flight tests that, if drag on the bobbin causes any error, it is at most a few percent, so that, for purposes of establishing the Reynolds number regime, we may use the drag-free velocities. In Table II velocities and Reynolds numbers at impact of the bobbin are shown. It is assumed that the accelerometer cavities are filled with air at sea-level pressure at room temperature and that the outside drag acceleration a_D is constant at the values shown.

TABLE II

Drag on Sphere (a_D)		Transit Dist.		Impact		Drag-Free
g	ft/sec^2	in.	ft	vel, ft/sec	Re	Time, sec
10^{-3}	3.22×10^{-2}	.187	.0156	3.17×10^{-2}	17.1	.98
10^{-3}	3.22×10^{-2}	.050	.0042	1.64×10^{-2}	8.9	.51
10^{-4}	3.22×10^{-3}	.187	.0156	1.003×10^{-2}	5.4	3.11
10^{-4}	3.22×10^{-3}	.050	.0042	$.518 \times 10^{-2}$	2.8	1.64

At impact the Reynolds numbers are of the order of 10 and are less before impact. Thus throughout the transit the bobbin is in the Stokes regime. The drag of a sphere not under the influence of cavity walls is

$$D = 3\pi \mu dV, \tag{8}$$

where

D = drag force
μ = viscosity
d = diameter
V = velocity

The presence of the cavity walls tends to increase the drag but probably not enough to invalidate this order of magnitude analysis. The equation of motion is therefore

$$\frac{d^2y}{dt^2} = a_D - \frac{3\pi\mu D}{m}\frac{dy}{dt} \qquad m = \text{mass} \tag{9}$$

Integrating:

$$t = \frac{m}{-3\pi\mu d} \ell n \left(a_D - \frac{3\pi\mu d}{m}\frac{dy}{dt}\right) + C_1 \tag{10}$$

when

$$t = 0,\ \frac{dy}{dt} = 0,\ C_1 = \frac{m}{3\pi\mu d}\ \ell n\ a_D.$$

Substituting for C_1 and solving for $\frac{dy}{dt}$:

$$\frac{dy}{dt} = \frac{ma_D}{3\pi\mu d}\left(1 - e^{\frac{-3\pi\mu dt}{m}}\right) \tag{11}$$

Substituting this value of $\frac{dy}{dt}$ in the equation of motion, we have:

$$\frac{d^2y}{dt^2} = a_D e^{\frac{-3\pi\mu dt}{m}} \tag{12}$$

Taking

$\mu = 3.7 \times 10^{-7}$ lb f sec/ft^2
$d = 1/12$ ft
$m = 1.025 \times 10^{-3}$ lb f sec^2/ft

we have

$$\frac{d^2y}{dt^2} = a_D e^{-2.83 \times 10^{-4} t} . \tag{13}$$

Since the exponent of e is small, we may expand and write

$$\frac{d^2y}{dt^2} = a_D(1 - 2.83 \times 10^{-4}t) \tag{14}$$

Thus for any transit time up to 35 seconds, the error due to drag on the bobbin will be less than 1% and we may ignore it completely in the "old" as well as the contemplated accelerometers.

The final investigations of the characteristics of the "old" accelerometer concerned the contact wire. The contact wire is a pair of drawn gold wires 0.002 in. in diameter mounted in such a way as to resemble two cantilever beams (springs) each 1 in. long with mutually opposing forces. For a single spring:

$$P = \frac{3yEI}{\ell^3} \tag{15}$$

where

P = force in lb
E = Young's modulus = 11.4×10^6 lb/in.
I = moment of inertia = 0.8×10^{-12} in.^{4}
ℓ = length = 1 in.
y = deflection in.
P = 2.69×10^{-5}y lb for a single spring. For two springs the over-all spring constant is
k = 5.38×10^{-5} lb/in.

For that orientation of the sphere where the longitudinal axis of the accelerometer is perpendicular to the drag vector, the spring, acting as a cantilever, will oppose the drag force and the equation of motion is:

$$\frac{d^2y}{dt^2} = a_D - \frac{ky}{m} \tag{16}$$

where

y = displacement of bobbin
t = time
a_D = drag acceleration of sphere
k = spring constant of contact wire
m = mass of bobbin

Integrating, and noting that both constants of integration are zero, we have:

$$y = \frac{ma_D}{k} - \frac{ma_D}{k} \cos \sqrt{\frac{k}{m}}\, t \tag{17}$$

and

$$t = \sqrt{\frac{m}{k}} \cos^{-1} \left(1 - \frac{yk}{ma_D}\right) \tag{18}$$

In the last expression, if y is taken as the complete transit distance, t will be the transit time in the presence of drag force and spring force. Without the spring, the transit time is:

$$t_1 = \sqrt{\frac{2y}{a_D}} \tag{19}$$

Since the percentage error in acceleration caused by an error in transit time is

$$\delta a_t = 200 \frac{t - t_1}{t_1} , \tag{20}$$

we have an expression for the percentage error in acceleration caused by the contact wire:

$$\delta a_\omega = 200\sqrt{\frac{m}{k}}\,\frac{\cos^{-1}\left(1 - \frac{ky}{ma_D}\right) - \sqrt{\frac{2y}{a_D}}}{\sqrt{\frac{2y}{a_D}}} \qquad (21)$$

Expanding the $\cos^{-1}$ term and using the first two terms, we may write:

$$\delta a_\omega = \frac{100\ ky}{6ma_D} \qquad (22)$$

In Table III values of this error are tabulated for various values of acceleration and two transit distances. It is apparent that for a transit distance of 0.1875 in. the contact wire causes an unacceptable error at 10^{-3} g, and with a transit distance of .050 in. the error is too large at 10^{-4} g. The bobbin in this instance is taken to be a magnesium one of weight 14.9 grams or 3.3×10^{-2} lb, i.e., bobbin "C" above. Other orientations of the accelerometer axis with respect to the drag vector will no doubt result in similar errors, but it is sufficient to demonstrate the difficulty in a single case.

TABLE III

Acceleration (g) (1 g = 386 in./sec^2)	Percentage error in Acceleration Due to Wire $100\ \Delta a/a$	
	For transit distance = 0.188 in.	For transit distance = .050 in.
10^{-2}	0.5	0.14
5×10^{-3}	1.0	0.28
10^{-3}	5.0	1.40
10^{-4}		14.0

Electrical contact between the contact wire and the bobbin and between the bobbin and cavity was investigated. To check the bobbin to cavity contact at 1 g, a lead was soldered to the bobbin. The accelerometer was operated 100 times at various orientations in a circuit which would trigger the indicating counter at a resistance of 3000 ohms. There were no misses. To investigate contact reliability at smaller impact velocities, the bobbin was suspended on a fine wire as a pendulum and swung against a replica of the cavity wall. At that impact velocity which would be experienced at 10^{-2} g, there were 50% "no-contacts" in 100 tries, but this was reduced to 5% after polishing the surfaces.

The contact wire was checked at 1 g only. In flight the force of the wire against the bobbin does not fall below that of the wire acting as a spring. A lead, in addition to the contact wire, was soldered to the bobbin. The accelerometer was then operated with two counters, one stopped through the contact-wire

circuit, the other through the soldered lead circuit. In 100 tries the contact wire circuit missed 5 times, the other did not miss at all. With interchanged counters the results were repeated.

In anticipation of using a soldered lead instead of the contact wire to improve circuit reliability, a bobbin was fitted on one end with a square hole and a square pyramidal caging finger was placed in the corresponding end of the accelerometer. This arrangement prevented rotation of the bobbin (except for a small angle) to prevent breaking of the lead. In the drop test for initial velocity, the special bobbin and finger performed as well as the standard design, as noted previously. The new caging finger and bobbin are shown in Fig. 6.

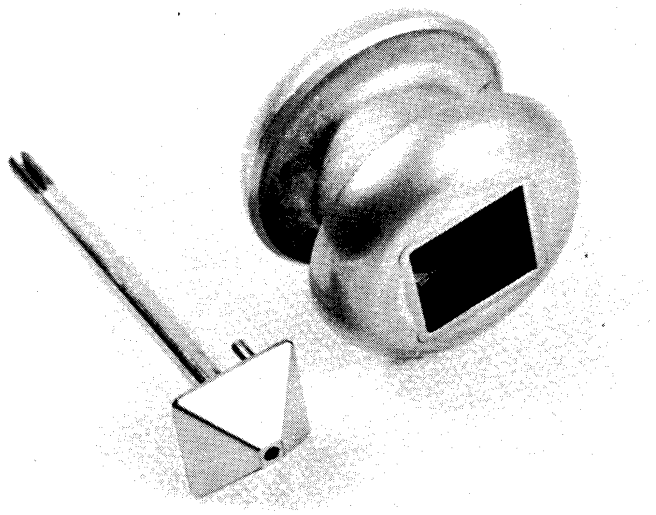

Fig. 6. Pyramidal caging finger to prevent bobbin rotation.

In summary, the results of the investigations of the accelerometer were that neither the magnetic field nor drag on the bobbin are sources of error but that initial velocity imparted by the caging mechanism and an error in transit time introduced by the contact wire begin to become appreciable sources of error in the measurement of accelerations below 10^{-2} g. In view of this, it was decided to design and construct a new accelerometer with three major changes in characteristics:

(a) A free bobbin with no contact wire;
(b) Precision construction to perhaps ±.0001 in.; and
(c) Mounting arrangement to permit precision balancing.

In addition, an attempt would be made to decrease the power consumption.

3. ELIMINATION OF CONTACT WIRE

Various schemes were conceived to eliminate the contact wire. Included were:

(a) A double conductor, perhaps a double spiral printed circuit on the cavity. Contact by the bobbin would connect the conductors.

(b) A mechanically vibrating cavity. Contact by the bobbin would damp the vibration causing amplitude and phase changes.

(c) A displacement or velocity detector, i.e., a transducer attached to the cavity. Contact by the bobbin would generate an electrical signal in the transducer.

(d) A multiple cavity with the segments separated electrically. Contact by the bobbin would connect the segments electrically. This is similar in principle to but considerably more practical than (a).

Scheme (a) was rejected after tests with a small model in planar form showed that contact was obtained in only a small percentage of tries. Considerable effort was expended on (b), (c), and (d).

3.1. VIBRATING CAVITY

An accelerometer based on the conception of a vibrating cavity is shown in Fig. 7. The cavity consists of a hollow, light-weight plastic sphere such as a ping-pong ball. The cavity is supported in a mounting which permits it to vibrate

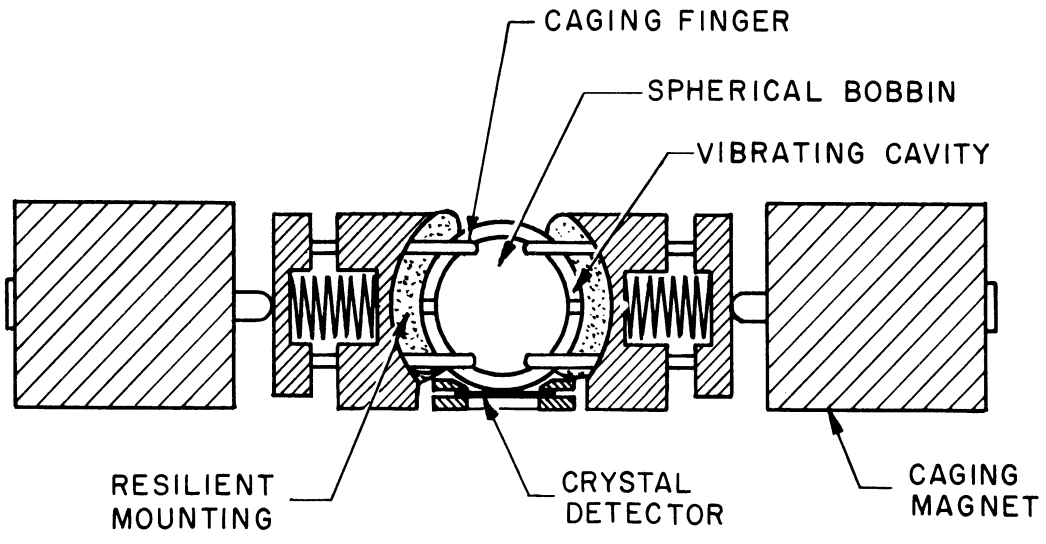

Fig. 7. Vibrating cavity accelerometer schematic.

and is attached to the combined driver-sensor which could be a piezoelectric crystal. The caging fingers pass through holes in the cavity. The bobbin is a metallic sphere with no contacts or attachments when in free fall. Ideally, the cavity and crystal would vibrate as a whole with no nodal patterns at a frequency just off resonance. Contact by the bobbin mass would cause damping as well as a phase shift accompanying the change in resonant frequency. Since it is desired to detect transit times of 0.010 sec with an error of ± 1% or better, a natural frequency of the order of 10^4 cps is indicated to avoid elaborate phase-sensitive circuits.

In the first attempt a ping-pong ball was mounted on a steel reed driven electromagnetically. The resonant frequency of the combination was only about 450 cps and the device was abandoned. Next, a ping-pong ball was attached to a crystal by means of a thin Micarta wafer in the form of a yoke, as shown in Fig. 8. This combination resonated at 5900 cps but was too flimsy for practical application. In an attempt to increase the strength of the device, a second crystal-and-yoke combination was attached to the ball in one case 90° displaced from the first yoke and in another 180° displaced as in Fig. 9. Although matched crystals were used and an attempt was made to make the yokes identical, the two crystals could not be made to resonate at a common frequency. The result was a complex wave pattern on the surface of the ball with many nodal points. Therefore the attempt to use two crystals was abandoned. Returning to the single crystal and yoke, the ball was next surrounded by sponge rubber which, although it would tend to damp the resonant peak, would still permit vibration while increasing the ruggedness of the combination. This arrangement resonated at 5900 cps but had a complicated mode of vibration as indicated by many nodal points. It began to appear that it would be difficult to vibrate the ping-pong ball as a whole without setting up vibratory patterns in the surface. Two more attempts were made, however. In one, a single mounting was once more resorted to in which the ball was cemented directly to the crystal which was in turn mounted in a thin metal disc with center hole. The arrangement was more rugged than the previous single point mounting but again exhibited the troublesome nulls. Finally, the ping-pong ball was mounted in a thin annular stiffening ring which was then supported in firm rubber locator pads and which rested against the crystal. The resonant frequency was 6600 cps. The vibration of the ball surface was not eliminated with this system and no further attempts to vibrate the ping-pong ball as a whole at frequencies approaching 10^4 cps were made. The various arrangements described are illustrated in Fig. 10.

The next step was to try metal spheres in place of the ping-pong ball. Several were fabricated. The most practical in terms of weight and size was of Dural, 1-1/2 in. in diameter with a wall thickness of 0.021 in. The sphere consisted of two hemispheres bonded with Armstrong cement. Various mounts were again tried. The most successful is shown in Fig. 11. The rubber was sponge rubber slightly compressed. The sphere rests against a 1/2-in.^{2} laminated crystal. The apparatus was driven at frequencies varying over a wide range. Resonances in various modes were detected as low as 2800 cps and as high as 83,000 cps. At 8700 cps the sphere resonated with virtually no nodal points.

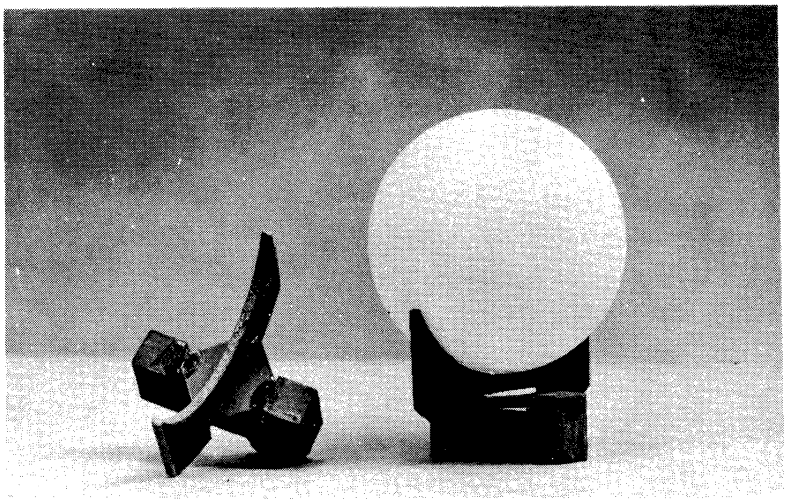

Fig. 8. Yoke mount for cavity and crystal.

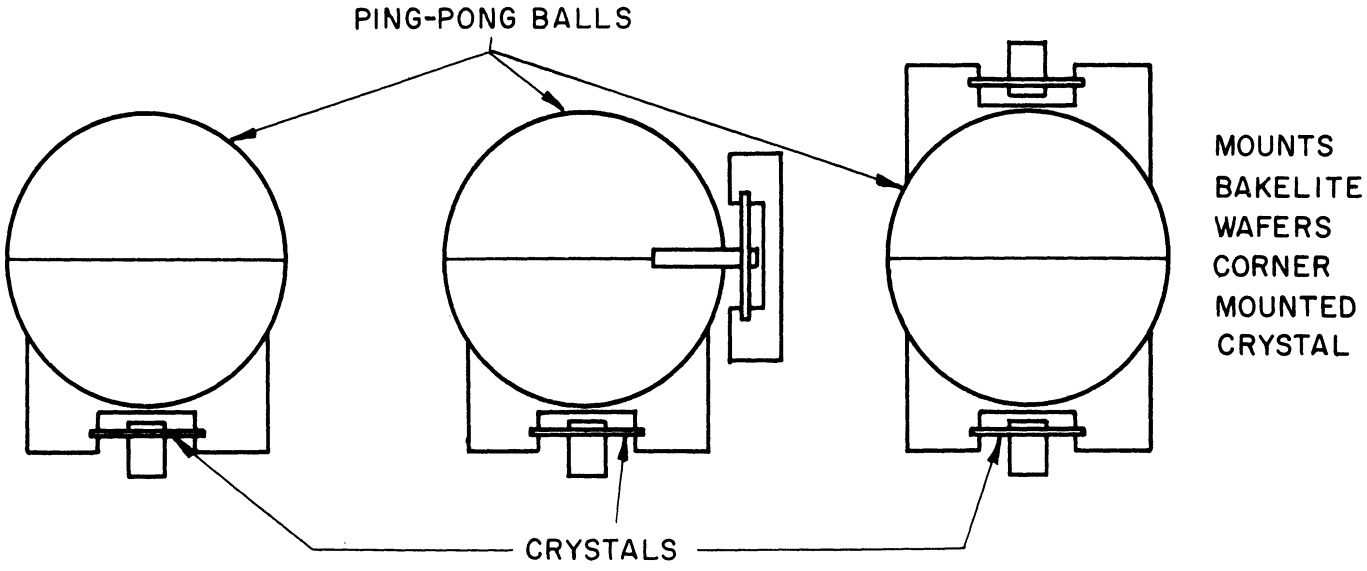

Fig. 9. Various yoke mounts for cavities and crystals.

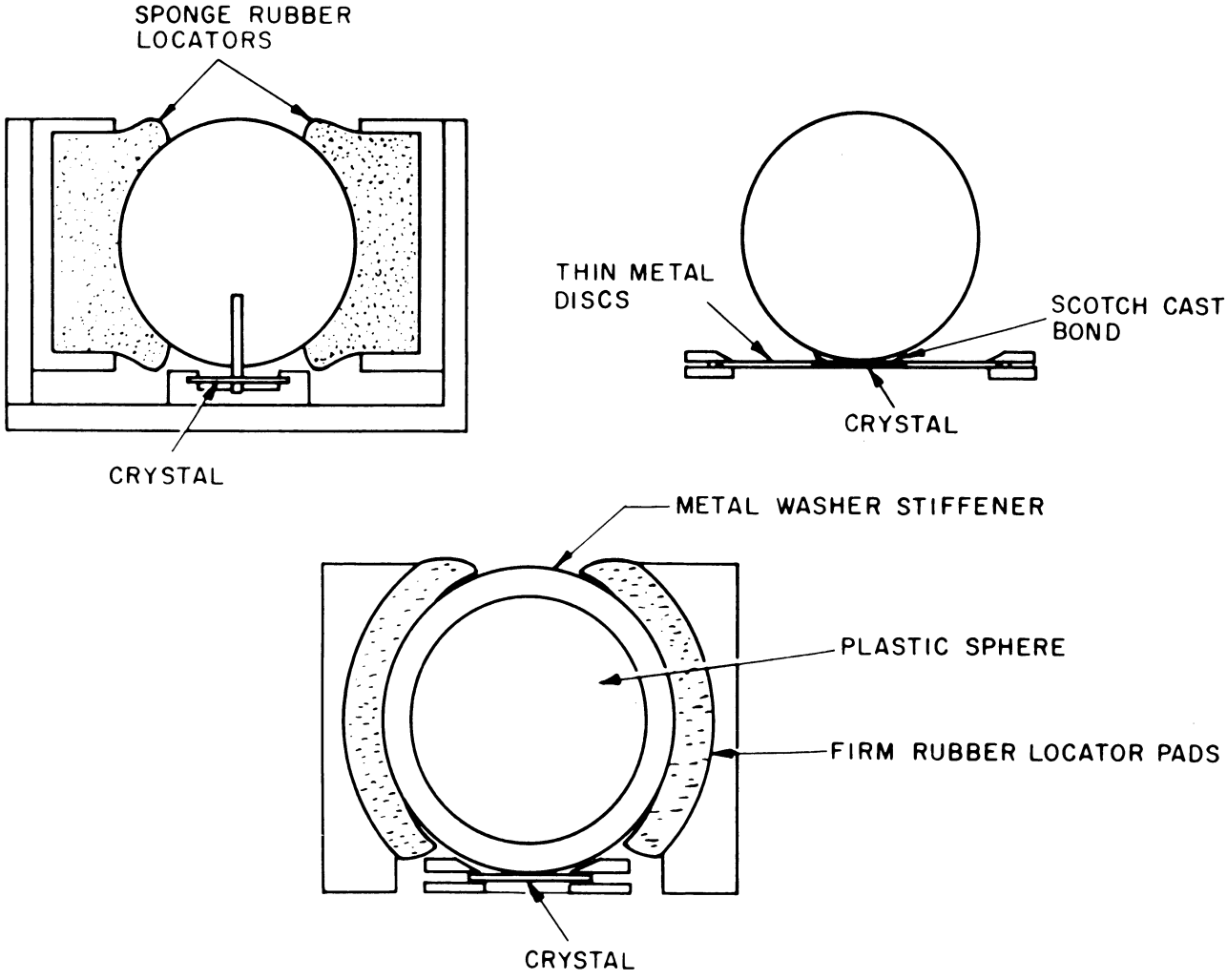

Fig. 10. Three ping-pong-ball to crystal mounts.

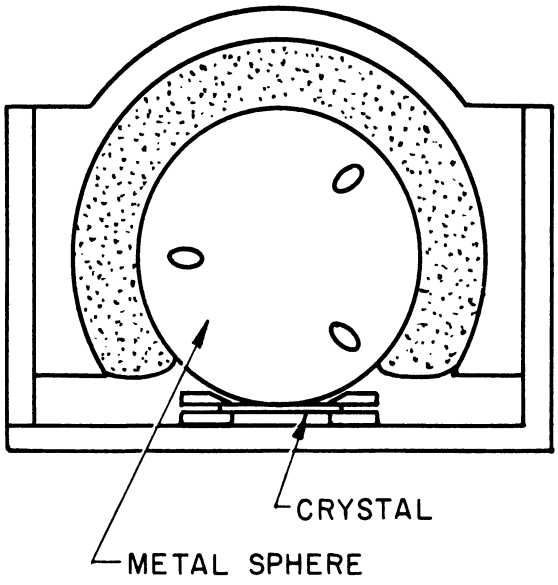

Fig. 11. Metal spherical cavity mount.

Contact at virtually any point of the sphere would produce a phase shift. At very high frequencies where resonances occurred, for instance 59,000 cps, the vibration patterns in the surface of the sphere became very pronounced, the crests being very sensitive and the nodes having no sensitivity.

The conclusions drawn from the foregoing investigations are:

(a) That a workable accelerometer meeting the design requirements can probably be designed along the lines of the final model, that is with a metal spherical cavity, vibrating at nearly 10^4 cps with contact of a spherical bobbin being detected by a phase change in the crystal signal.

(b) That certain problems which were not investigated would have to be met. These include: unwanted noise in the crystal, inaccuracies in the cavity location due to the resilient mounting, dead areas in the cavity occupied by orifices for entry of the caging fingers, the necessity for an oscillator and power supply and perhaps others.

3.2. IMPACT TRANSDUCER

Instead of detecting the phase and amplitude changes in the driving signal caused by impact loading of the cavity attached to the driver, it should be possible to detect the impact of the bobbin by the energy of impact transmitted to a transducer attached to the cavity. A variety of mounts illustrated in Figs. 12 and 13 were tried. Although in each case signals were obtained, all the devices were rejected for one or more of the following reasons: fragility, lack of sensitivity for certain directions of impact, sensitivity to spurious noise, time delay between impact and signal, variable sensitivity in different orientations, and different accelerations. In summary it may be said that while an accelerometer with a transducer impact detector might conceivably be constructed, the approach had all the weaknesses of the vibrating cavity as well as some additional ones. No further investigations of this approach were made.

In the work with the various impact detection schemes described above, bobbin impact was simulated in preliminary tests by finger pressure or with a ball probe touching the outside of the cavity. For the more successful arrangements (for example, the vibrating metal spherical cavity) the setup of Fig. 14 was used to simulate bobbin impact. A 19-gram ball was suspended on a wire in the form of a pendulum. Impacts corresponding to various accelerations were obtained by releasing the pendulum from the proper displaced position. In the case of metal cavities the circuit shown permitted measuring the time delay between impact of the pendulum and appearance of the signal at the terminals of the crystal. For a given configuration, the measured time delays were quite constant and varied from 0.2 to 0.6 millisecond among various models. Time delays of these magnitudes represent significant errors in accelerations as big as 1 g but, being constant, could be corrected for.

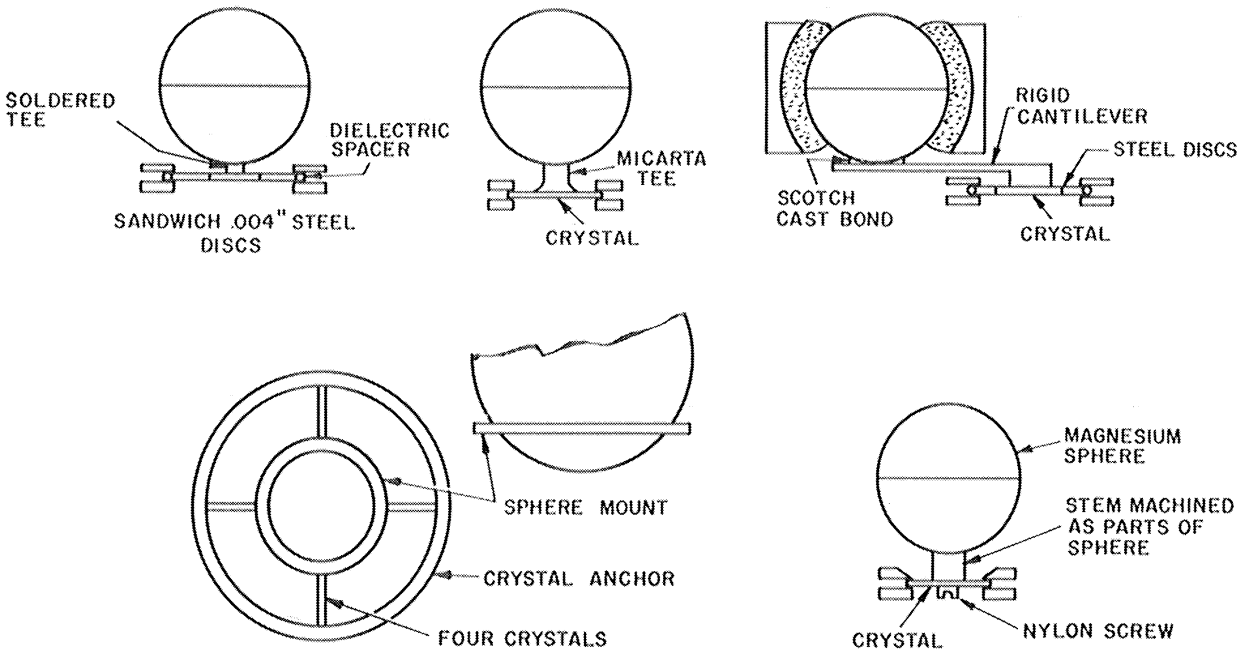

Fig. 12. Mounts used with metal spheres.

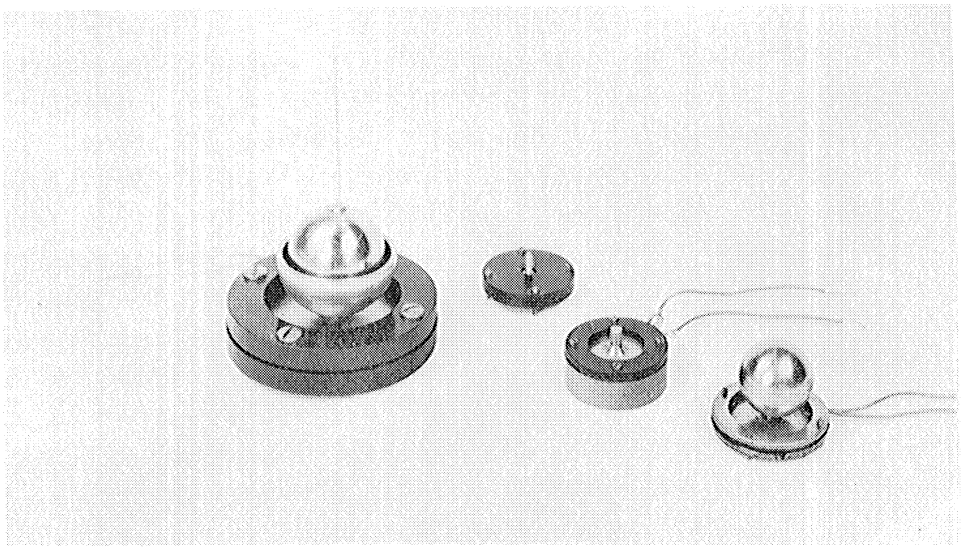

Fig. 13. Mounts used with metal spheres.

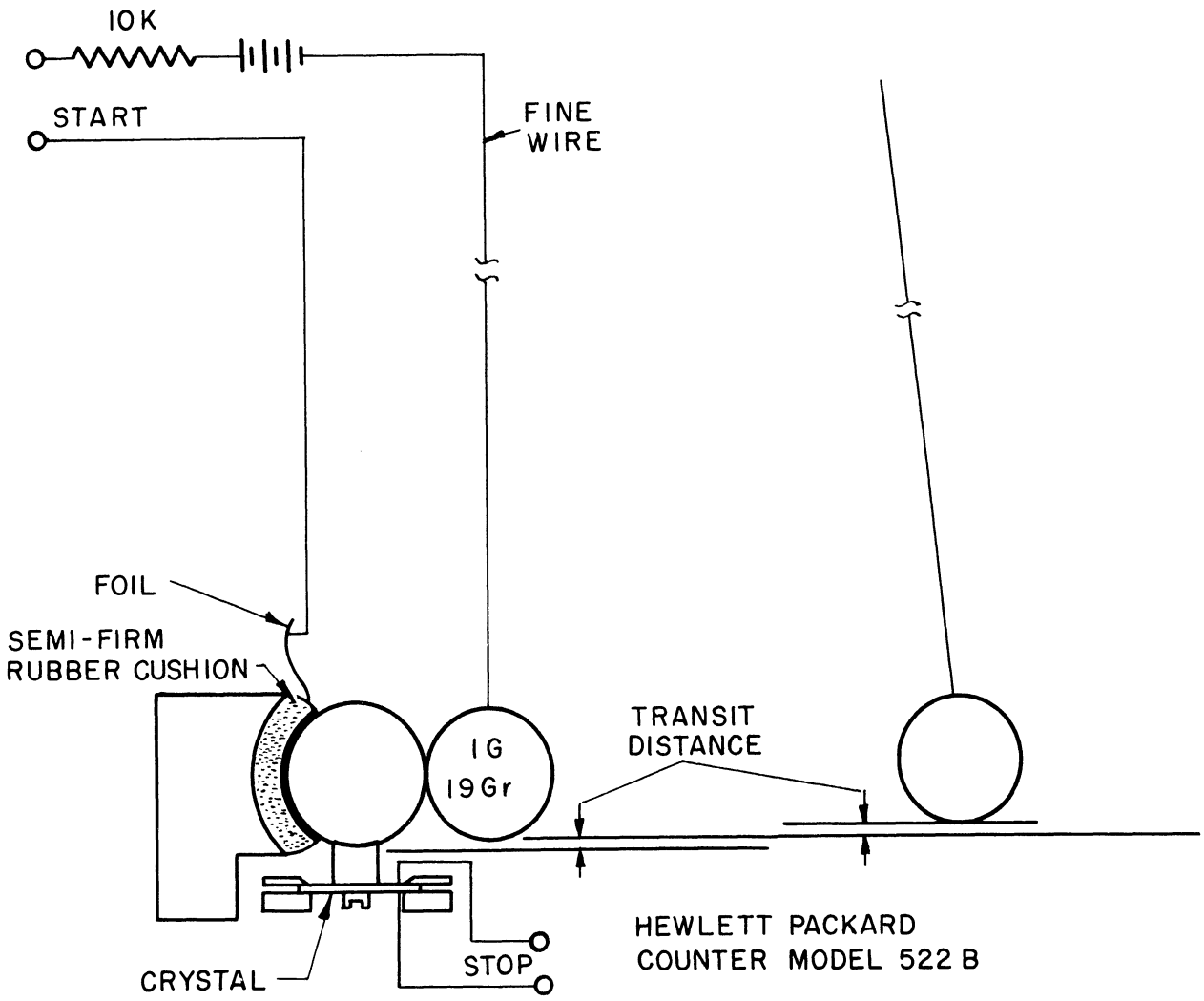

Fig. 14. Impact pendulum.

Observation of the form and magnitude of the crystal signal outputs was by means of a Tektronics type 545 oscilloscope. At 1 g a typical magnitude of voltage peak at the instant of impact was 1.2 volts, and at 0.01 g, 0.2 volt. At impacts corresponding to 0.001 g the signal peaks were often indistinguishable from noise, one source of which appeared to motions of the cavities in the resilient mountings. Under flight conditions, similar sources of noise could be expected and this situation probably constitutes a limitation on the low-acceleration end of the range of operation of an accelerometer using this method of detecting impact.

In summary, the same general remarks may be made about the use of a transducer to detect impact as were made about the vibrating cavity—namely, that an accelerometer could probably be constructed using the idea but that certain difficult problems would have to be solved.

3.3. PIEZOELECTRIC MATERIALS

Piezoelectric materials come in a large variety of physical makeups. For the applications employing the resonated or impacted cavity sphere, only those which combined a fairly high degree of physical strength and electrical sensitivity were considered. An early consideration was to make the cavity sphere entirely of a formed ceramic crystal. Consultation with engineers at Clevite Corporation, Cleveland, discouraged this approach. It seems that ceramic crystals of this nature are applicable only where the applied forces impinge large areas of the crystal—such as underwater transducers, etc. Point contacts as made between the cavity sphere and the reference sphere would be too insensitive. Several types of crystals were tested. Without entering a discussion of crystal design or the processes of elimination, the one selected had the following outline: it was a 1/2-in.^{2} laminated sandwich .025 in. thick. The segments of this sandwich were comprised of two oppositely oriented crystals. Applying a voltage across the two plates produced an elongation in one plate and contraction in the other. The resulting flexure, if reproduced mechanically, made the crystal an excellent voltage generator. Sensitivity to both bending and twisting action, good physical strength, and, when used as a driver, numerous resonant points of an acceptably high frequency made it the best all-around device. Happily, with some modifications, it proved to be the most efficient of the tested crystals for both applications. Mountings were made of two Micarta hoops which were screwed together to hold the crystal around its perimeter. The leads of gold-plated brass shim stock, .001 in. thick, could be soldered to the surfaces of the crystal, but were found to be more efficient just pressed against the opposite faces by the Micarta hoops. The only further modification to the crystals was on the one mounting the impacted cavity sphere. Here a small hole was bored through the center of the crystal through which a nylon screw passed and screwed into the stem of the cavity sphere.

3.4. CAGING

One of the disadvantages of the old accelerometer was the high power requirement of the caging mechanism. An air-core moving coil was chosen because its low mass and inductance would permit large acceleration during uncaging. The magnetic circuit was relatively inefficient, however, and the coils were operated at 54 watts to obtain the necessary caging force. A moving iron magnetic system was constructed during the course of the work with the crystals and used with the crystal accelerometer models as well as with the multiple cavity accelerometer described in the next section.

The new caging solenoid is shown in Figs. 15 and 16 together with the small caging finger scheme used with various trial accelerometers. One factor contributing to the feasibility of the solenoid is the anticipated reduction of the transit distance from 0.187 to 0.050 or even 0.020 in. The coils were wound with 890 turns of No. 28 wire and are operated at about 20 watts. The individual solenoids are 1-1/4 in. in diameter and 1-1/4 in. long; the corresponding dimensions in the previous design were 2-1/16 and 1-3/4 in. Because

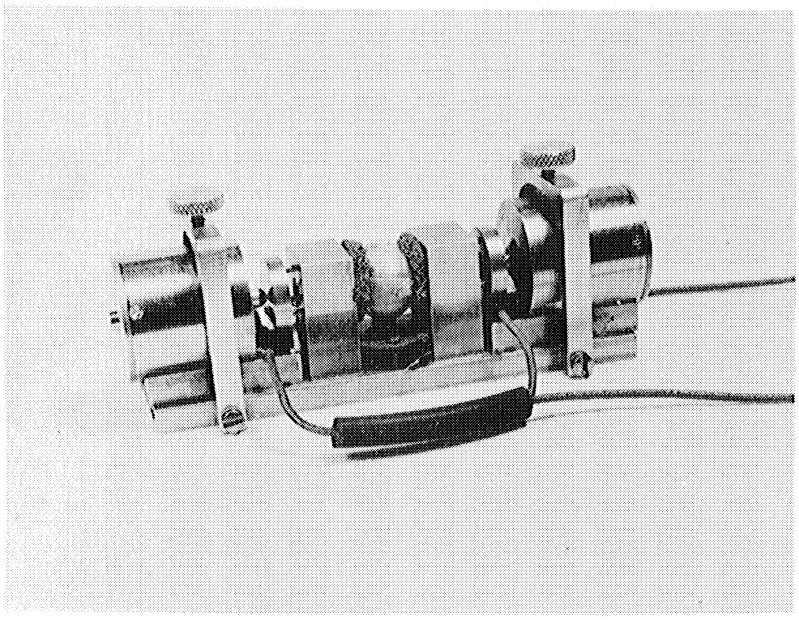

Fig. 15. Photo showing moving iron solenoids.

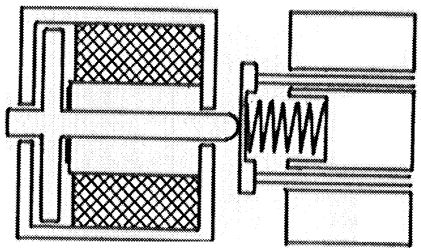

Fig. 16. Schematic showing moving iron solenoid.

the force increases with decreasing gap (as contrasted with the constant force of the old design), a relatively stiff spring can and must be used to provide sufficient initial acceleration at the instant of uncaging. The time lag of the motion of the solenoid was reduced to the order of 1 millisecond by the incorporation of a 0.009-in. nonmagnetic shim between the slug and the core. In a flight accelerometer the residual time lag would be eliminated as a source of error by taking the start pulse from the break of contact between fingers and bobbin.

3.5. MULTIPLE CIRCUIT CAVITY

At this point a promising new idea for cavity and bobbin was conceived. It is illustrated in Fig. 17. The bobbin consists of a cube on the face-centers of which are mounted six spheres. Four of the spheres are surrounded by hemispherical cavities separated by an appropriate transit distance. The distance which the bobbin travels from the caged position to the cavities is, as before, the same in any direction. In this case, however, the bobbin approaches at least two and sometimes three (depending on the direction) cavity segments. This permits the bobbin to be employed as the circuit-completing element between two cavity segments which are electrically insulated, thus eliminating the contact wire. One important difference between this scheme and the one mentioned previously (in which the cavity would have had printed on it a double spiral circuit) is that, in the case of an accelerometer made with no dimensional error, the bobbin of the new type will contact two surfaces simultaneously, whereas in the spiral circuit scheme this will happen only a fraction of the time.

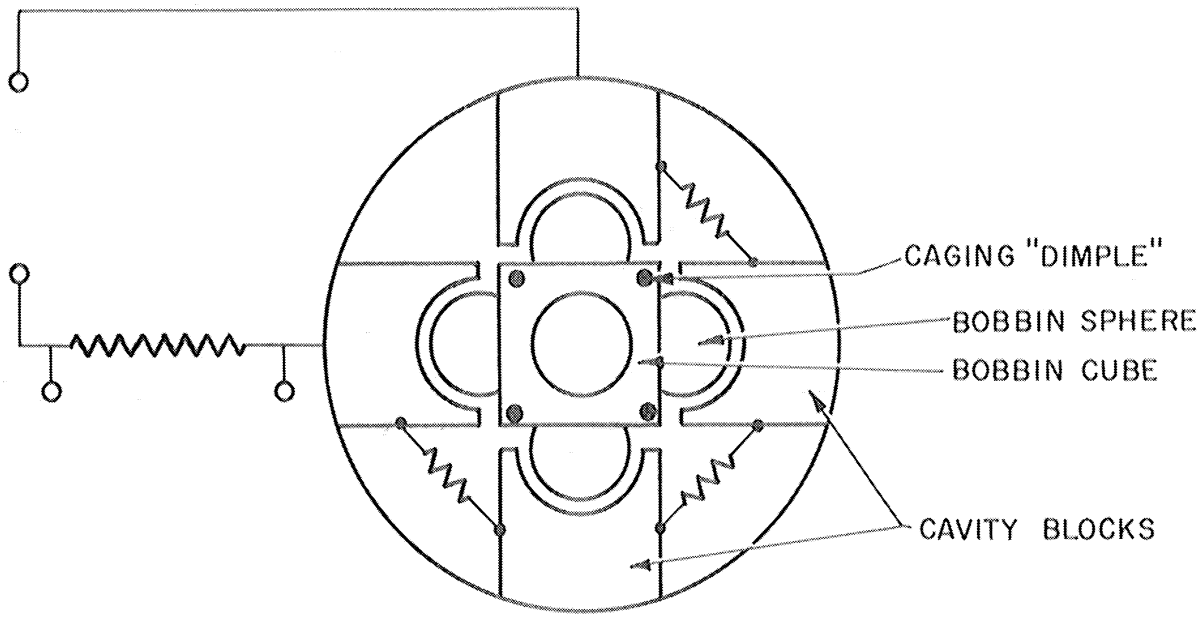

Fig. 17. Multiple cavity accelerometer schematic.

An experimental model of the new configuration was constructed and preliminary tests were made. It is shown in Fig. 18. The hemispherical cavities were machined in four brass cubes, the final shape being obtained by pressing

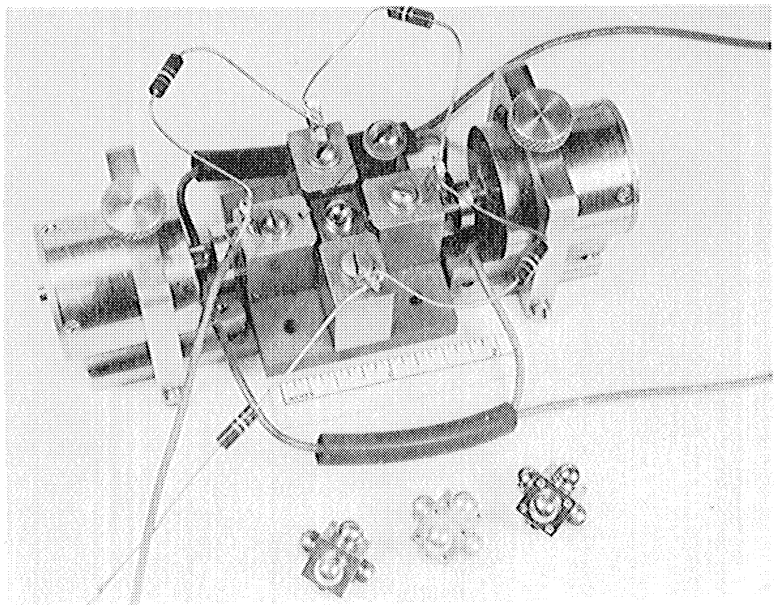

Fig. 18. Model of multiple cavity accelerometer.

a steel ball into the machined cavity. They were mounted on a base with clamping screws which permitted positional adjustment. The bobbin was formed of a square, soft iron cube 0.4 in. on a side, through each face of which a 0.228-in.-diameter hole was bored on center. Into each hole a 0.25-in.-diameter chrome steel ball was placed and soldered. Before installing the sixth ball the center chamber of the cube was filled with solder. Various jigs and fixtures were constructed to aid in the assembly. The transit distance was 0.020 in. Because the bobbin was not a figure of revolution, it was necessary to orient it, each time it was caged, about the longitudinal axis of the device. This was accomplished by means of four small caging fingers, two on each end, engaging corresponding "dimples" in the opposite faces of the bobbin cube. The cavities were connected in series with series resistances. On bobbin contact, a change in voltage across one of the series resistances resulted from the connection of two or three cavity segments by the bobbin.

In the first tests (with steel bobbin and brass cavities), contact was made in 30% of the tries. Gold-plating the bobbin and cavities improved this figure to 75%. It had been anticipated that shop tolerances would prevent simultaneous contact in all cases. The first tests indicated that, while there were some misses, the percentage of contacts was encouragingly high. With the old accelerometer, contact was obtained in somewhat better than 95% of the tries. To improve the percentage of contacts, new bobbins were constructed with the spheres resiliently mounted to the cubes. In one case an adhesive, resilient when dry, was used. In another, opposite spheres were connected with fine wires. In both instances contact was obtained in better than 90% of the tries.

Work with the preliminary model of the multiple cavity accelerometer was very encouraging. The design of a prototype flight model was consequently undertaken.

4. SPHERE DATA-PROCESSING BY COMPUTER

A major portion of the effort of the project was expended on the task specified in Modification 3 of the contract: "Research and develop computer methods for reducing data from the small sphere experiment with the ultimate aim of developing an automatic data reduction system." The work was accomplished with the aid of the LGP-30 digital computer of the High Altitude Engineering Laboratory. By Modification 5 of the contract, funds were made available by the Air Force Cambridge Research Center to purchase a high-speed Tape Punch and Reader Unit manufactured by Ferranti Electric, Inc., for the Royal Precision LGP-30 System (computer). The new equipment when working with the LGP-30 is capable of reading tapes at 150 characters per second and punching tapes at 20 per second. These speeds compare with about 10 per second for both reading and punching for the Flexowriter which is furnished as standard equipment with the LFP-30 computer. The increased input-output speeds greatly facilitated the data work described in the following sections.

The analysis of falling-sphere data using the LGP-30 digital computer was previously reported.[6] Some of the parts of the analysis were carried out by hand calculation at that time. The present program performs all the data analysis automatically. Some refinements of the trajectory equations were also included in the new program. Three new functions are accomplished by the present program:

(1) Accelerometer raw data are processed to obtain corrected time and acceleration data.

(2) Trajectory peak time is derived from the acceleration data.

(3) Trajectory peak altitude is adjusted by comparing sphere-derived densities with balloon-sonde densities. Trajectory iterations and density-pressure-temperature calculations are performed in essentially the same way as before.

Data from three sphere flights were processed by the new program with satisfactory results. These were Nike-Cajuns AM 6.02, AM 6.03, and AM 6.05 fired at Fort Churchill in the winter of 1958. A condensed flow diagram for the over-all data-processing is shown in Fig. 19 and the flow diagram for the fill-data and print-data routine is shown in Fig. 20.

4.1. ANALYSIS OF ACCELEROMETER RAW DATA

This routine contains four subroutines:

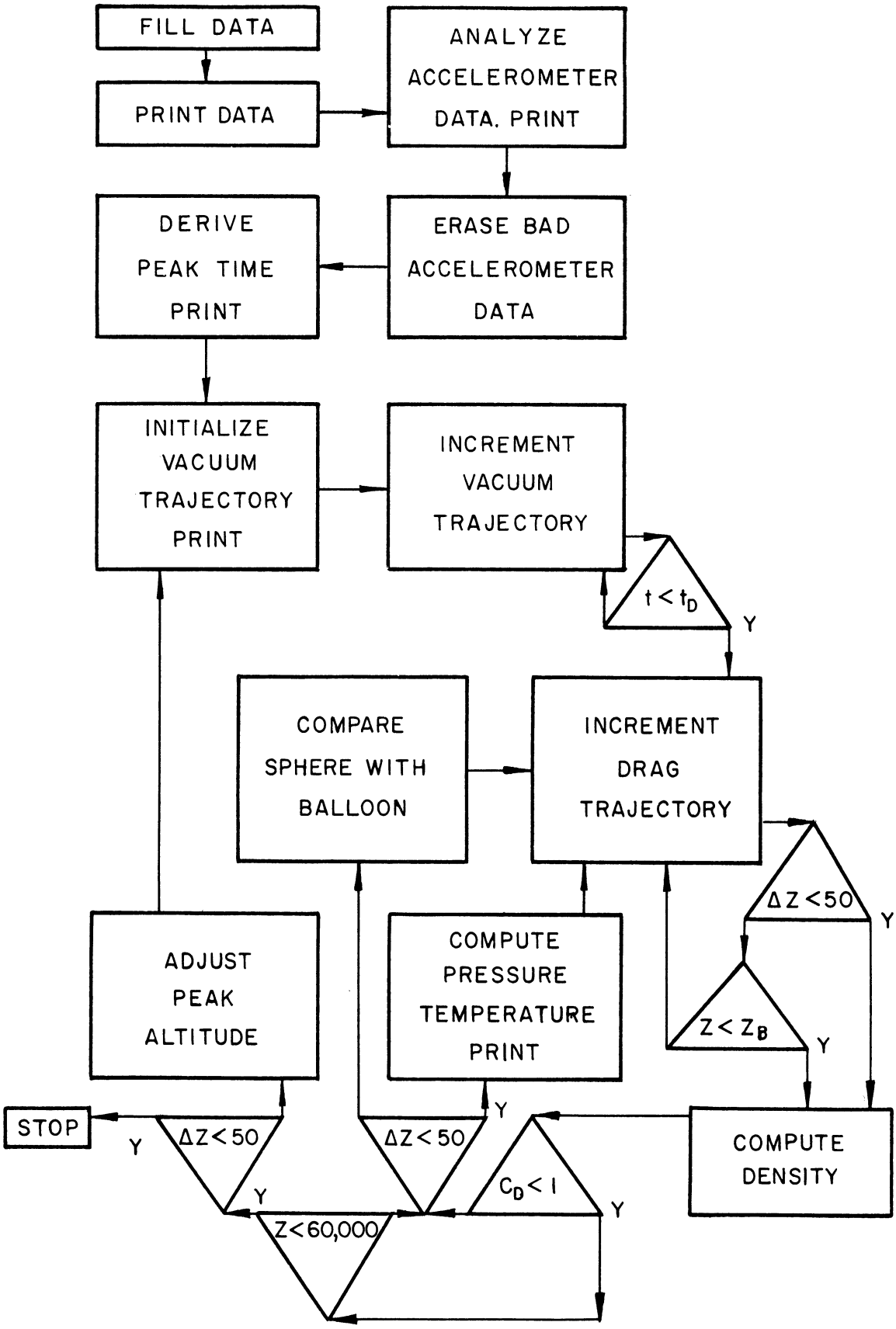

Fig. 19. Flow diagram for over-all data processing.

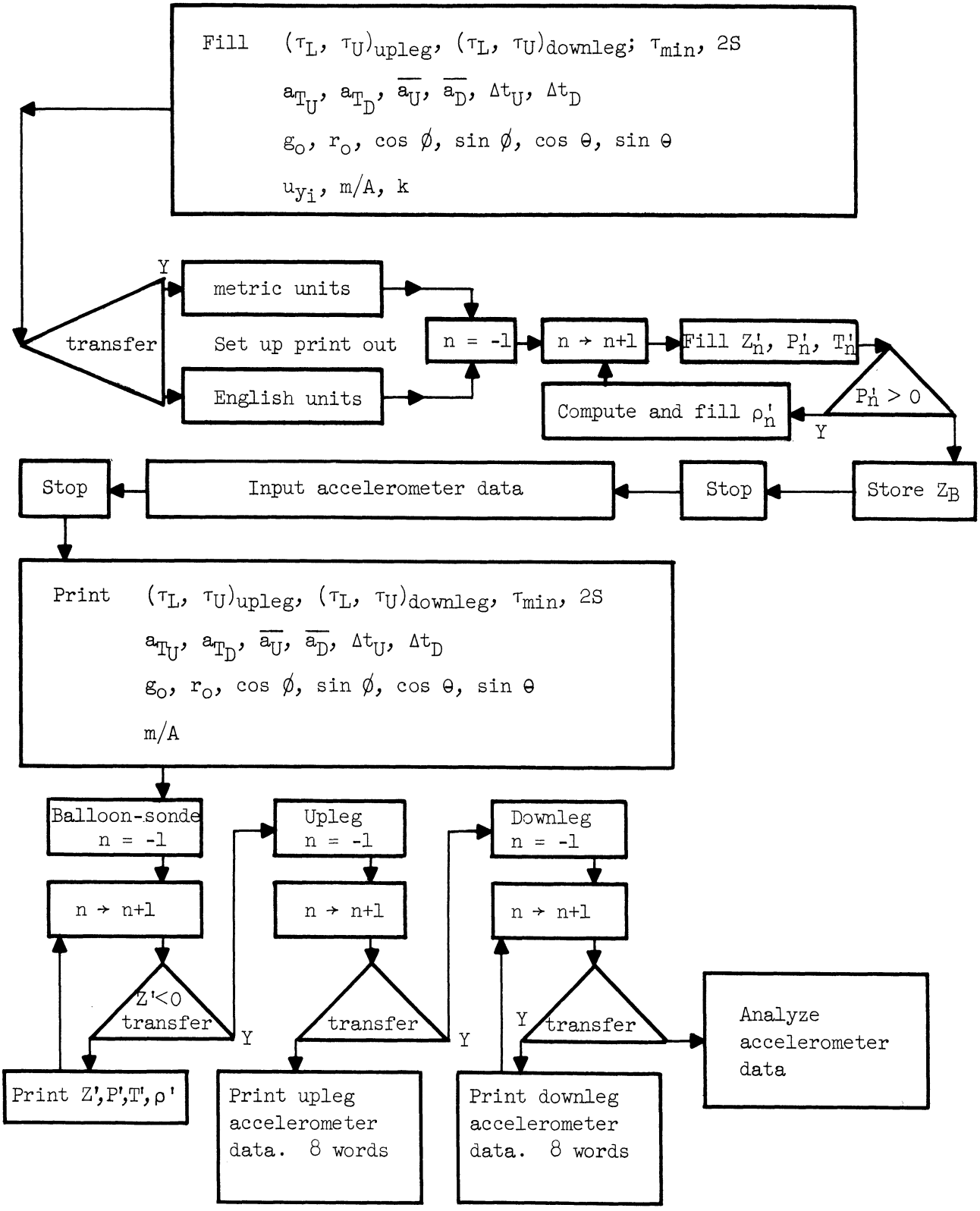

Fig. 20. Flow diagram for fill-data and print-data routines.

(1) Find release pulses;
(2) Compute transit time;
(3) Reject noisy data;
(4) Compute corrected time and acceleration.

See Fig. 21 for the flow diagram. The accelerometer raw data consist of the times at which the accelerometer release pulses and contact pulses are recorded. These numbers, stored in sequence, are therefore monotonically increasing. Two tracks are reserved for upleg data and six tracks for downleg data; 64 numbers can be stored in each track. The release pulses are spaced equally in time because the accelerometer recycles periodically. The upper and lower limits which define the recycle period are denoted by τ_L and τ_U. If a pair of pulse times are separated by more than τ_L but less than τ_U, they are identified as release times. This is accomplished by storing the negative of the release time in place of the release time. At high accelerations the release time and contact time are closely spaced and both may satisfy these conditions. In this case, the first pulse of the pair is selected as the release pulse and no further pulses are considered until the elapsed time is τ_L. The presence of noise may also cause pulses to be closely spaced. Exit from this subroutine occurs when a pulse time is found which is smaller than the preceding release pulse time. The transit-time subroutine replaces each positive time by the difference between it and the preceding release time.

The normal sequence is alternating release and contact pulses. In the presence of noise there may be two or more pulses between each pair of release pulses. In this case the subroutine which rejects noisy data chooses the transit time most nearly equal to the transit time of the preceding cycle and fills it in place of the last one in sequence and fills zeroes into the remainder of the sequence.

The corrected time is equal to the sum of the release time and half the transit time. The drag acceleration is

$$a_D = \frac{2s}{\tau^2} .$$

If the transit time is smaller than eight milliseconds, a zero is filled in place of the acceleration. If the transfer control button is depressed, corrected time and drag acceleration will be printed by the typewriter.

4.2. DERIVE PEAK TIME ROUTINE

See Fig. 22 for the flow diagram. Peak time is computed by assuming that the drag function is symmetrical with respect to peak time. The upper portions of the trajectory where the drag accelerations are small give the best results. At lower altitudes the drag destroys the symmerty. On the other hand at very small drag accelerations the data become too scattered for the purpose of de-

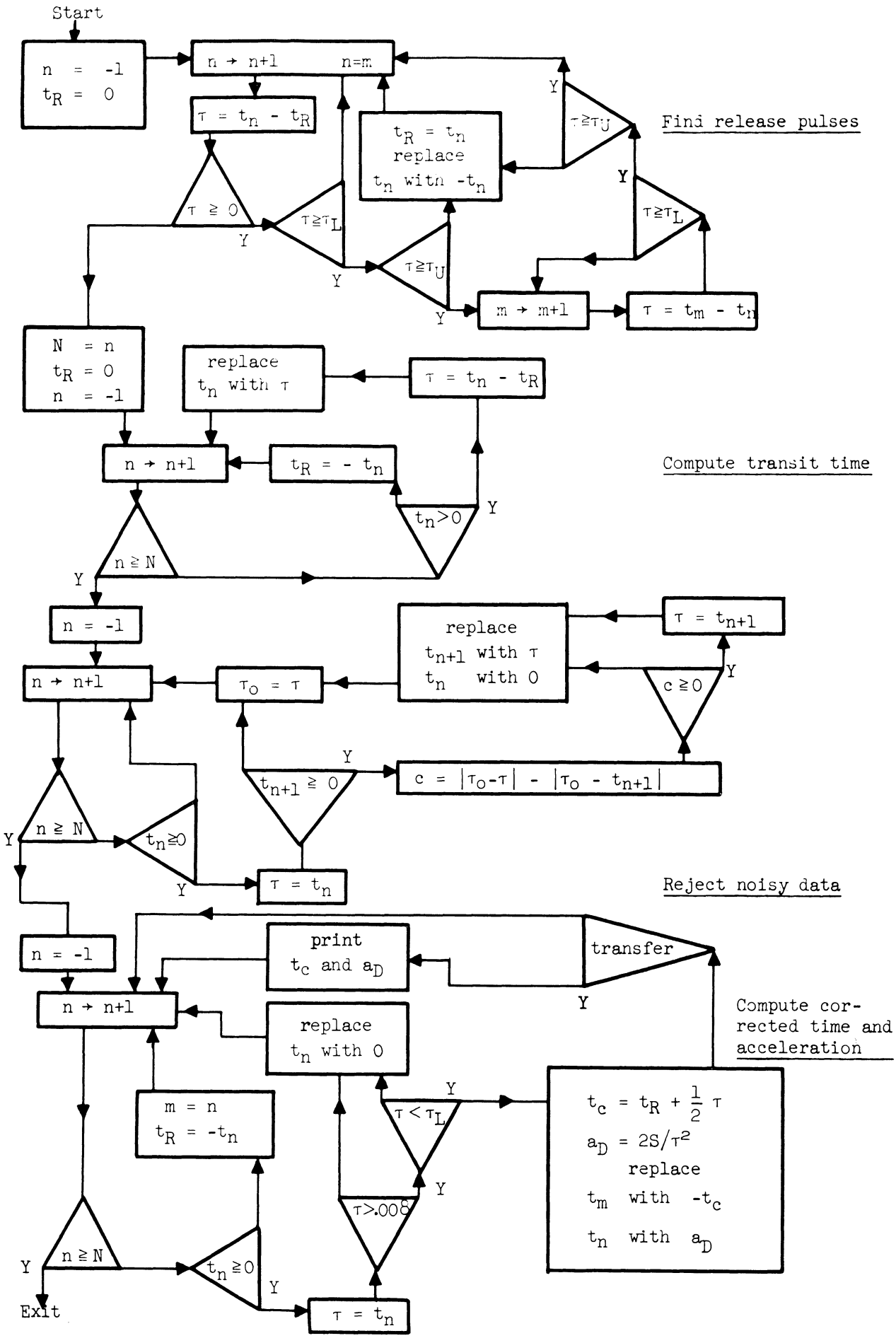

Fig. 21. Flow diagram for analyze-accelerometer-data routine.

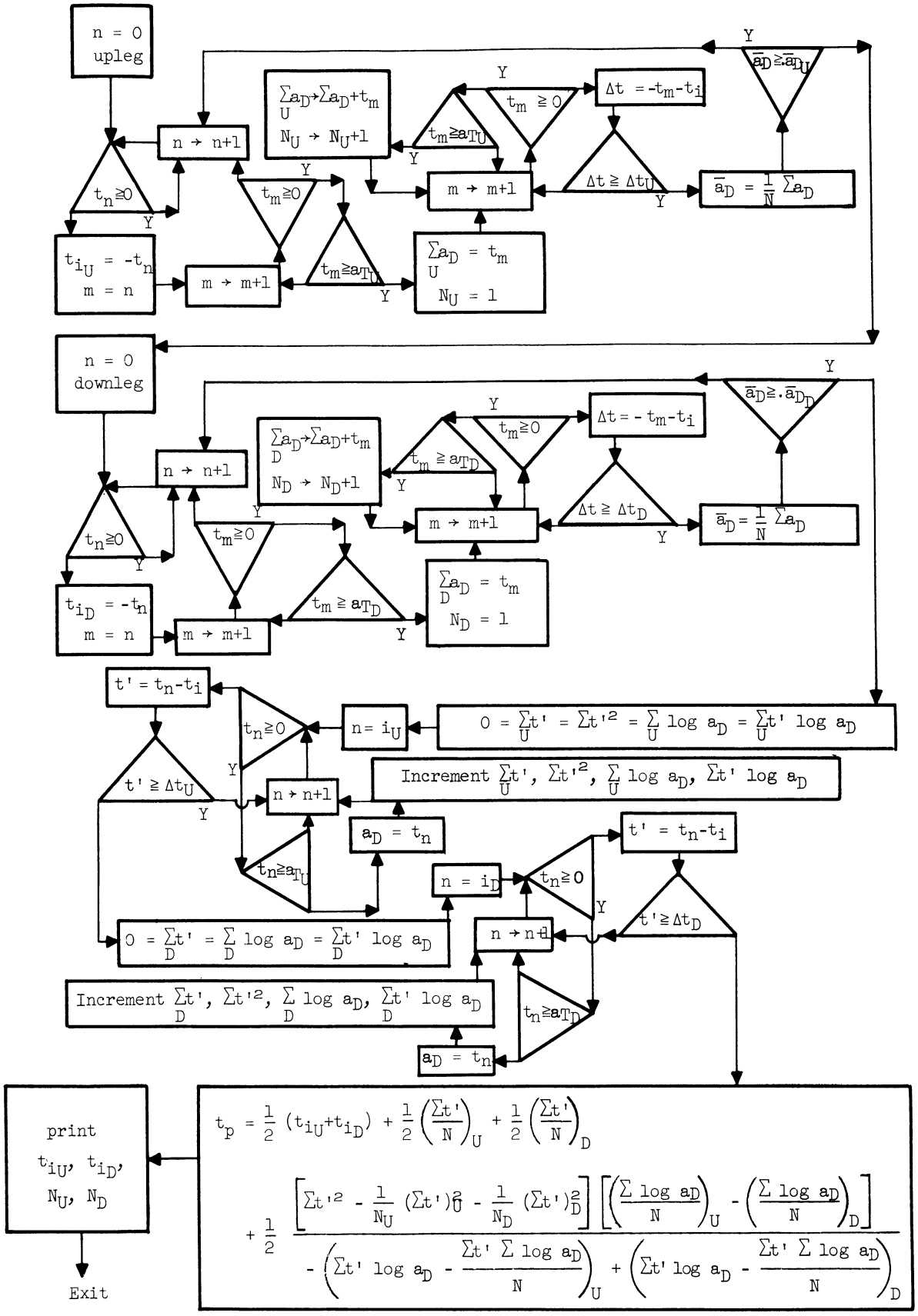

Fig. 22. Flow diagram for peak-time routine.

riving peak time. A compromise value is therefore chosen. Several data points are used in a least-squares analysis. Three parameters must be specified: threshold acceleration, mean acceleration, and elapsed time. Data points for which the drag acceleration exceeds the threshold are taken in sequence until the elapsed time measured from the first point is exceeded. Then the mean drag acceleration is computed and compared with the specified value. If it is too high on the upleg or too low on the downleg, the first point is rejected and the process is repeated. A plot of drag acceleration logarithm vs. time is a good approximation to a straight line if the elapsed time is not too great. A least-squares formula for the peak time was derived on this basis.

$$t_p = \frac{1}{2}(t_U + t_D) + \frac{1}{2}\left(\frac{1}{n_U}\sum_U t' + \frac{1}{n_D}\sum_D t'\right)$$

$$+ \frac{1}{2}\cdot\frac{\left[\sum_U t'^2 + \sum_D t'^2 - \frac{1}{n_U}\left(\sum_U t'\right)^2 - \frac{1}{n_D}\left(\sum_D t'\right)^2\right]\left(\frac{1}{n_U}\sum_U \log a - \frac{1}{n_D}\sum_D \log a\right)}{-\sum_U t' \log a + \sum_D t' \log a + \frac{1}{n_U}\sum_U t' \sum_U \log a - \frac{1}{n_D}\sum_D t' \sum_D \log a}$$

Upleg values are denoted by U, downleg values by D. The time of the first upleg point is t_U, downleg, t_D. $t'_U = t - t_U$, $t'_D = t - t_D$. t_U, t_D, n_U, n_D are printed.

4.3. TRAJECTORY ROUTINE

See Fig. 23 for the flow diagram. The equations used for computing the trajectory are:

$$\frac{\Delta u_z}{\Delta t} = -\bar{g} - \bar{a}_D\left(\frac{u_z}{V}\right) + u_y\left(\frac{u_y}{\bar{r}} + 2\Omega\cos\phi\sin\theta\right) + \bar{r}\,\Omega^2\cos^2\phi$$

$$\frac{\Delta u_y}{\Delta t} = -\bar{a}_D\left(\frac{\bar{u}_y}{V}\right) - u_z\left(\frac{u_y}{\bar{r}} + \Omega\cos\phi\sin\theta\right) - \bar{r}\,\Omega^2\sin\phi\cos\phi\cos\theta$$

$$\frac{\Delta r}{\Delta t} = \bar{u}_z$$

$$\bar{r} = r + \frac{1}{2}u_z\,\Delta t$$

$$\bar{g} = g_o r_o^2/\bar{r}^2$$

$$\bar{a}_D = \frac{1}{2}(a_D + a_D^+)$$

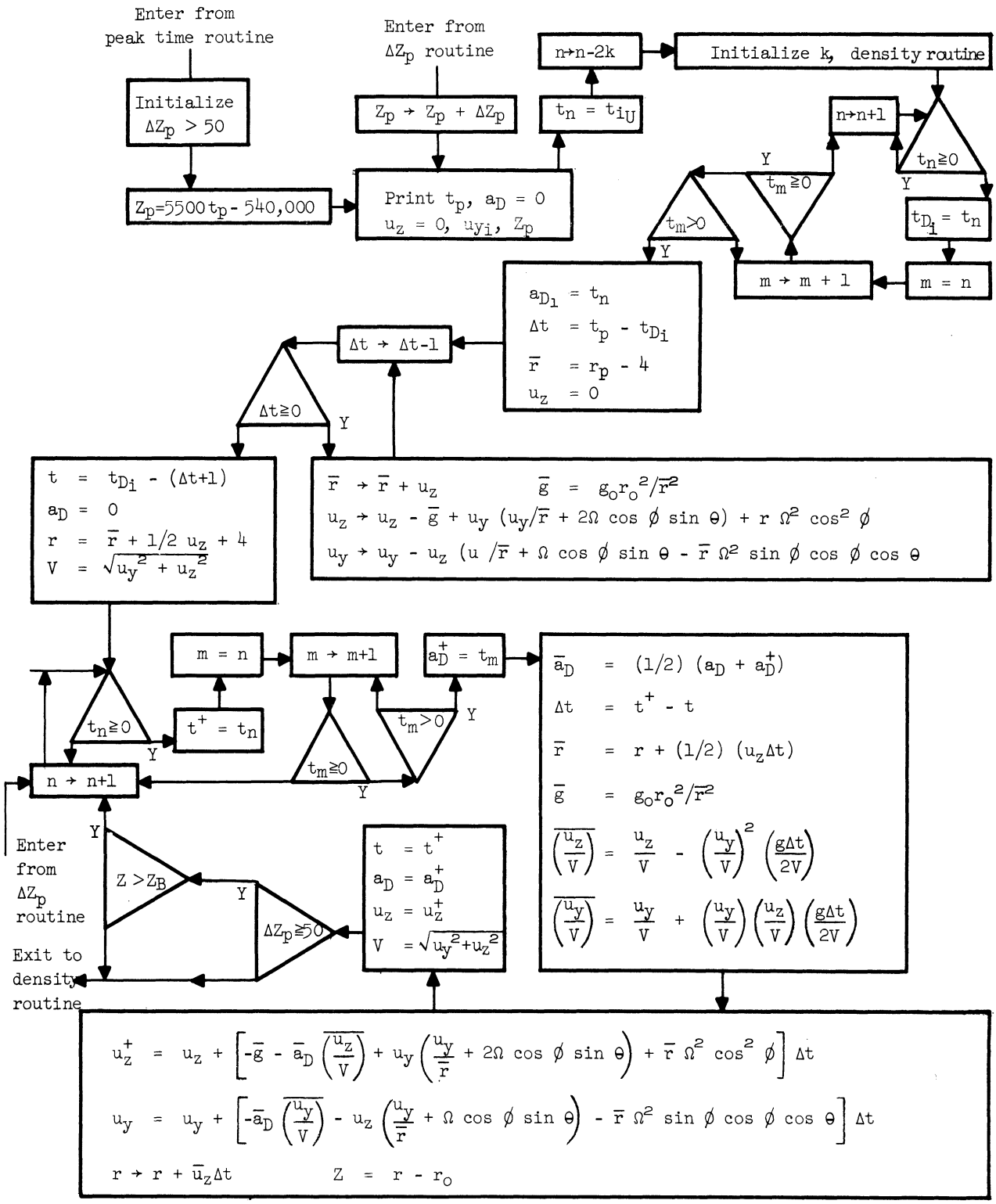

Fig. 23. Flow diagram for trajectory routine.

$$\left(\frac{\overline{u_z}}{V}\right) = \frac{u_z}{V} - \left(\frac{u_y}{V}\right)^2 \left(\frac{g\Delta t}{2V}\right)$$

$$\left(\frac{\overline{u_y}}{V}\right) = \frac{u_y}{V} + \left(\frac{u_y}{V}\right)\left(\frac{u_z}{V}\right)\left(\frac{g\Delta t}{2V}\right)$$

The horizontal and vertical velocity components, u_y and u_z, are referred to the earth's surface, a rotating coordinate system. The equations therefore contain Coriolis terms involving the earth's rotational velocity Ω. The radius to the earth's center is r; g is the acceleration of gravity. The increments of the numerical integration, Δt, are approximately one second. Mean values, denoted by $\overline{(\ )}$, are required for some of the parameters. The latitude angle and azimuth angle of rocket launch are ϕ and θ. The absolute gravity at zero altitude is g_o.

The present formulation of the equations is more satisfactory than the one employed previously[6] where an inertial reference was used. Certain inaccuracies in resolving velocities led to small errors in the horizontal velocity component in the old system. The errors were not large enough to influence the density calculations, however. The initial peak altitude is computed from the peak time and is a function of the rocket and launch parameters.[10] The following formula is applicable to Nike-Cajun rockets launched at 85°.

$$Z_p = 5500\ t_p - 540{,}000$$

The peak altitude must be adjusted by comparing with balloon-sonde data at the lower end of the trajectory. The initial vertical velocity at peak altitude is of course zero. The initial horizontal velocity depends principally upon the rocket launch angle. Nike-Cajun rockets launched at 85° have about 500 ft/sec velocity at the peak altitude. It has been found that this is not a very critical parameter since an assumed vertical trajectory results in essentially unchanged density data.

4.4. AIR-DENSITY ROUTINE

See Fig. 24 for the flow diagram. The air-density calculations are essentially the same as reported previously.[6] The air density is related to the drag acceleration by the equation

$$\rho = \frac{2m}{C_D A}\ \frac{a_D}{V^2}$$

The sphere cross-sectional area, A, and the mass of the sphere, m, are constants. The drag coefficient C_D is a function of Mach number M and Reynolds number Re; it is plotted in Fig. 25. It was found that all the useful information in Fig. 25 is contained in the two single-parameter functions of Fig. 26, which are the ones actually used in the data-processing. The Mach number is defined by

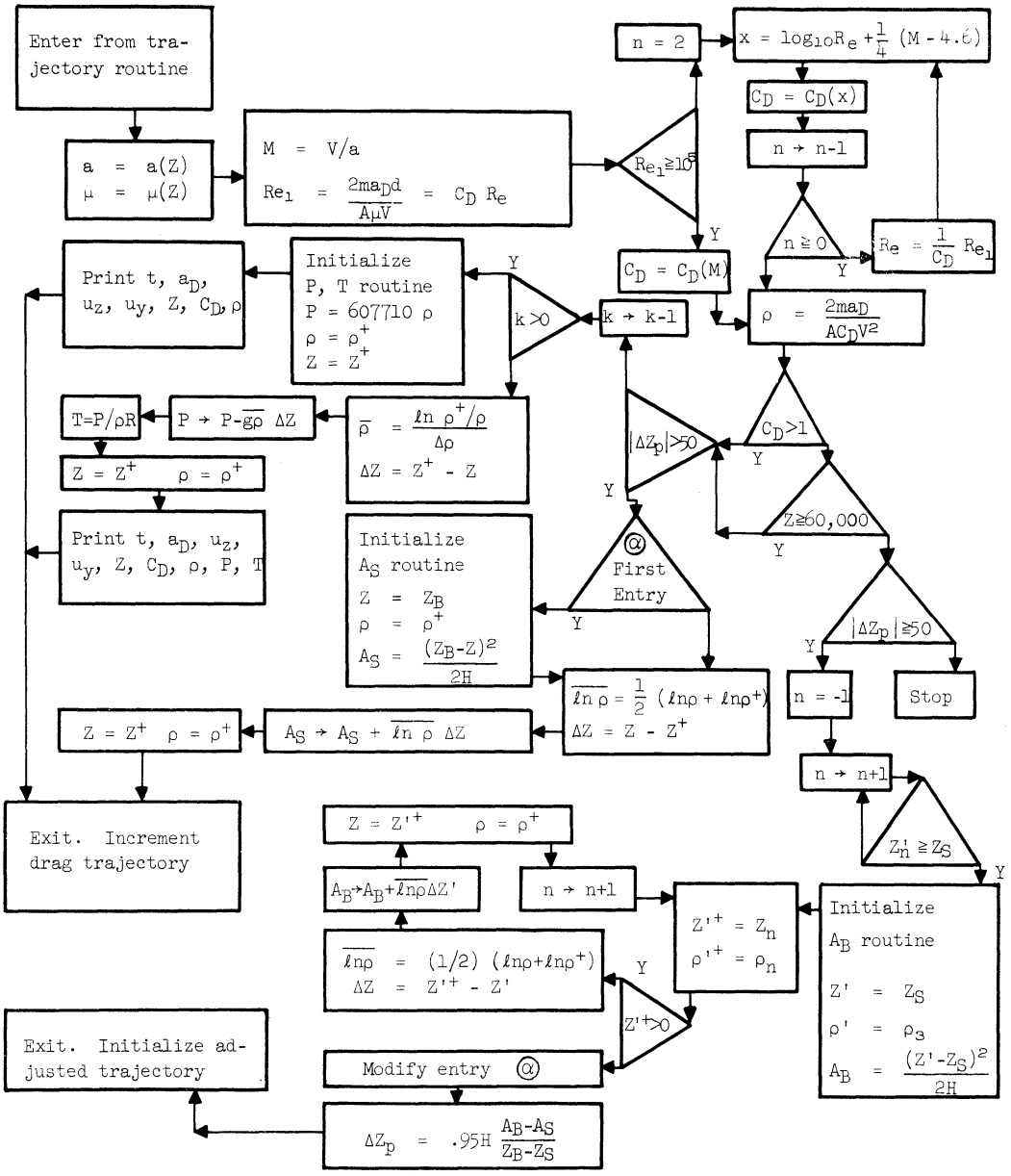

Fig. 24. Flow diagram for density routine and adjust-peak-altitude routine.

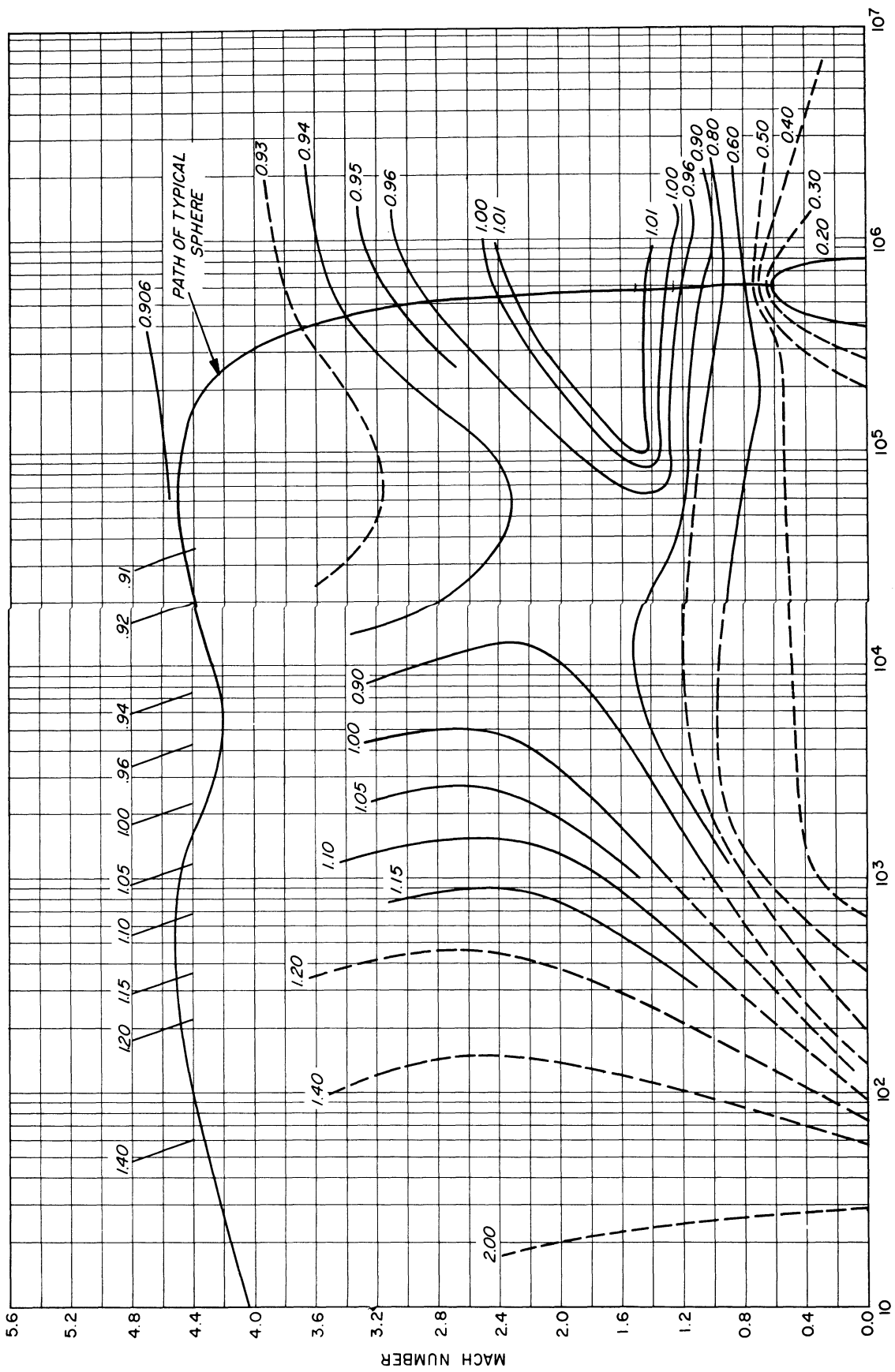

Fig. 25. C_D as a function of Mach number and Reynolds number.

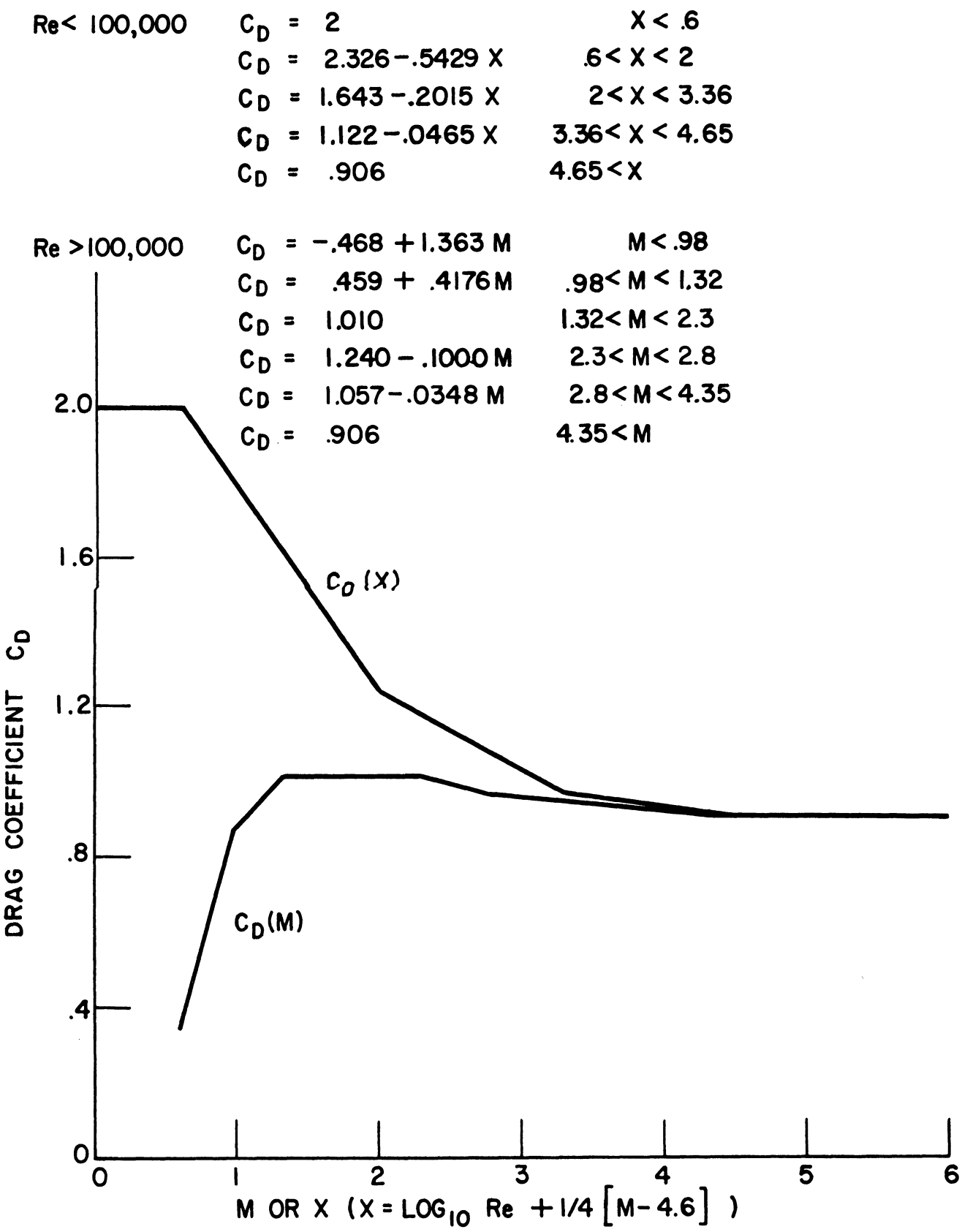

Fig. 26. Empirical drag coefficient functions.

$$M = V/a$$

The speed of sound a is a function of altitude.[9] The Reynolds number is defined by

$$Re = \rho V d/\mu$$

or, eliminating the density,

$$Re = \frac{2md}{A} \frac{a_D}{C_D \mu V} ,$$

where d is the sphere diameter. The viscosity μ is also a function of the altitude.[9]

The atmospheric pressure is derived from the differential formula

$$\Delta p = - \bar{\rho} \bar{g} \Delta z$$

The logarithmic mean of the densities ρ and ρ^+ is found from the formula

$$\bar{\rho} = \frac{\ell n \, \rho^+/\rho}{\rho^+ - \rho}$$

Since the pressure equation is differential, one must begin the integration from an initial pressure at a high altitude. The initial pressure is found by assuming the temperature to be -105.34°F from Ref. 9. At low altitudes the drag coefficient becomes smaller and its value less reliable. This point was previously discussed.[6] The low altitude limit of the density data is defined by a drag coefficient of one if the altitude is less than 60,000 feet.

4.5. ADJUST PEAK ALTITUDE ROUTINE

See Fig. 24 for flow diagram. The atmospheric density logarithm plotted as a function of altitude is approximately a straight line. The balloon-sonde-density plot must overlap the sphere-density plot if this routine is to function. Adjustments to the peak altitude are made so that the area between the two density lines is reduced to zero. The peak-altitude correction is found by the formula

$$Z = .95 \, H \frac{\Delta\rho}{\rho} .$$

The average difference in density between the sphere and balloon-sonde plots is $\Delta\rho$, H is the scale height, and .95 is an altitude correction factor. The last adjustment is considered satisfactory if it is less than 50 ft.

4.6. DATA-PROCESSING

The first step of the data-processing is to load the program into the computer. The program fills 39 tracks of the computer. About seven minutes are required if the photoelectric tape reader is used. The data associated with each sphere flight must then be filled. This consists of various constants, balloon-sonde data, and the raw accelerometer data. Two tracks are reserved for the balloon-sonde data, two for the upleg accelerometer data, and six for the downleg accelerometer data. About two minutes are required.

When all the data have been filled, the computer begins to print all such data to verify that everything is correct. About twenty minutes are required. It is possible to omit the printing of balloon-sonde data and accelerometer data by depressing the transfer control button. The computer then processes the upleg accelerometer data and prints corrected time and drag acceleration if the transfer control button has been depressed. The computer stops at the end of the upleg data and the operator inspects these data to see if there are some which should be suppressed. If there are some bad data, the operator punches a tape with time he wants erased and fills it into the computer. See Fig. 27 for the flow diagram. The computer makes the necessary changes and then processes the downleg data in the same way. The peak time is then computed and the data points on which peak time depends are printed. The initial values for the first trial trajectory are printed. The first trial trajectory is then calculated and compared with the balloon-sonde results. The peak altitude is adjusted and the second trajectory computed. These adjustments are continued until the correction is less than 50 ft. Approximately three preliminary trajectories are required. Only initial values are printed for each trial. Each trajectory requires about three minutes. When the last trajectory is calculated, all trajectory data and density data are printed at each step where there is an accelerometer data point. This requires about twenty minutes. Approximately an hour is required for the entire data-processing, mostly for printing data. The typewriter output for this computer is relatively slow since only ten characters per second can be printed. The faster punch unit can be used when the operator does not need to observe the results as they come out of the computer. The reading of the magnetic tapes which contain the raw accelerometer data can be accomplished in approximately two hours if done routinely. These data must then be punched onto paper tape for filling into the computer. Approximately one hour is required. With this system it should be possible to obtain processed data on the day of the sphere flight. The results of the use of the new computer program on Nike-Cajun flights AM 6.02, 6.03, and 6.05 are given in Appendix B.

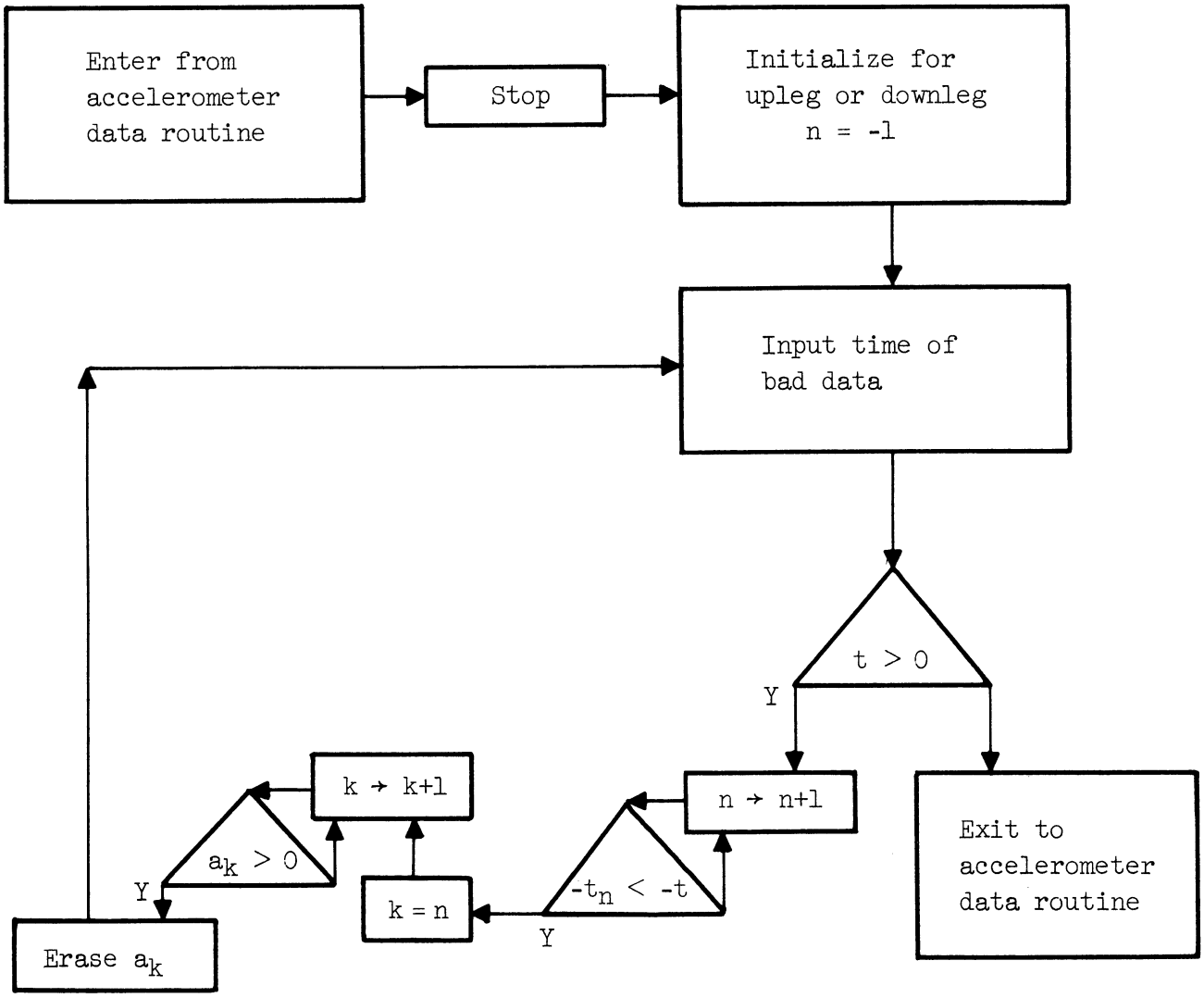

Fig. 27. Flow diagram for erase-bad-data routine.

5. SPHERE ANTENNA BREAKDOWN

The received signal strength from spheres in flight has been observed to exhibit a significant attenuation in the region of from 20 to 60 miles. A group at Boeing Airplane Company, Seattle, became interested in the problem in the course of work with antennas on hypersonic high-altitude vehicles and performed some simulation tests in the Boeing laboratory on a Michigan sphere. Mr. Howard Steele of Boeing and Mr. Hal Schulte of The University of Michigan cooperated in the investigation and prepared a paper[11] (with coauthors) on the subject. The paper was presented at a symposium entitled "Aerodynamics of the Upper Atmosphere," sponsored by the RAND Corporation, and held at Santa Monica in June, 1959. The paper is reproduced as Appendix A, following the list of references.

6. RECOMMENDATIONS

In view of the demonstration of the source of errors in the transit-time accelerometer and the real possibility of reducing the errors with a multiple-cavity design, continuation of work on the accelerometer to extend its useful range is recommended.

Since computer techniques have been successfully applied to the complete data-reduction process of the sphere technique, the next logical step in the development is to accomplish automatic data read-out of the telemeter magnetic tapes. Completion of such a development is recommended.

The sphere experiment continues to show potential for development. It is a nearly synoptic technique at present and could become more so (with an extended altitude range as well) if the recommended developments were carried out.

7. ACKNOWLEDGMENTS

We are indebted to the Geophysics Research Directorate, Air Force Cambridge Research Center, for cooperation and financial support throughout the entire program.

8. REFERENCES

1. Bartman, F. L., Chaney, L. W., Jones, L. M., and Liu, V. C., "Upper-Air Density and Temperature by the Falling Sphere Method," J. Appl. Phys., 27, 706-712 (1956).

2. Jones, L. M., "Transit-Time Accelerometer," Rev. Sci. Instr., 27, 374-377 (1956).

3. Jones, L. M., and Bartman, F. L., A Simplified Falling-Sphere Method for Upper-Air Density, Univ. of Mich. Eng. Res. Inst. Rept. 2215-10-T, Ann Arbor, 1956.

4. Peterson, J. W., Analytical Study of the Falling-Sphere Experiment for Upper-Air Density Measurement," Univ. of Mich. Eng. Res. Inst. Rept. 2533-2-T, Ann Arbor, 1956.

5. Jones, L. M., Fischbach, F. F., and Peterson, J. W., "Seasonal and Latitude Variations in Upper Air Density," Natl. Acad. Sci., IGY Rocket Rept. Series, 1, 47-57 (1958).

6. Peterson, J. W., Schulte, H. F., and Schaefer, E. J., A Simplified Falling-Sphere Method for Upper-Air Density, Part II. Density and Temperature Results from Eight Flights, Univ. of Mich. Res. Inst. Rept. 2215-19-F, Ann Arbor, 1959.

7. Jones, L. M., Peterson, J. W., Schulte, H. F., and Schaefer, E. J., "Upper-Air Densities and Temperatures from Eight IGY Rocket Flights by the Falling-Sphere Method," Natl. Acad. Sci., IGY Rocket Rept. Series, 5 (1959).

8. Jones, L. M., Peterson, J. W., Schulte, H. F., and Schaefer, E. J., "Upper-Air Density and Temperature: Some Variations and an Abrupt Warming in the Mesosphere," J. Geoph. Res., 64, 2331-2340 (1959).

9. Minzner, R. A., Champion, K.S.W., and Pond, H. L., The ARDC Model Atmosphere 1959, Air Force Cambridge Research Center Report TR-59-267, 1959.

10. Hansen, W. H., and Fischbach, F. F., The Nike Cajun Sounding Rocket, Univ. of Mich. Eng. Res. Inst. Report 2453-1-F, Ann Arbor, 1957.

11. Burns, G. A., Linder, W. J., Schorsch, J. F., Steele, H. L., and Schulte, H. F., Formation of a Radiofrequency Plasma at an Antenna During Falling-Sphere Measurements, RAND Corp. Rept. R-339, pp. 18-1 to 18-25, 1959.

APPENDIX A

FORMATION OF A RADIOFREQUENCY PLASMA AT AN ANTENNA DURING FALLING-SPHERE MEASUREMENTS

FORMATION OF A RADIOFREQUENCY PLASMA AT AN ANTENNA DURING FALLING-SPHERE MEASUREMENTS

G. A. Burns, W. J. Linder, J. F. Schorsch, and H. L. Steele
Boeing Airplane Company, Seattle, Washington,
and
H. F. Schulte,
The University of Michigan, Ann Arbor, Michigan

Abstract

A 7-in.-diameter sphere has been used extensively by University of Michigan personnel to measure air density up to 65 miles. The sphere is ejected from the nose of a Nike-Cajun rocket as it climbs past 35 miles and it continues up to over 100 miles. It telemeters to the ground its deceleration caused by the upper atmosphere as the sphere exits and then re-enters that atmosphere. The telemeter pulses are abnormally attenuated on the upward and downward passage in a region of from 20 to 60 miles. Boeing experiments show that a radiofrequency plasma occurs at the 400-Mc slot antenna at pressures simulating these altitudes. However, the attenuation of pulses does not cause a loss of data in the present case. The effect would be important in specific vehicles.

Electrons near the antenna acquire sufficient energy from the radiofrequency power being radiated to ionize the low-density gas. Breakdown occurs and a plasma forms when the production of new electrons by ionization is equal to loss by various mechanisms. The breakdown field necessary is lowest at the altitude (35 miles) where the frequency at which the excited electrons collide with ambient gas atoms is equal to the radiofrequency. A survey of experimental data indicates that within engineering accuracy diffusion and/or attachment predomi-

nates as the loss mechanism, and therefore scaling laws can be used. The breakdown field for the antenna in the sphere is nonuniform. The breakdown voltages are roughly half the breakdown voltages measured in uniform field cavities scaled to the appropriate gap length, pressure, and frequency. This experience demonstrates that the breakdown characteristics of short gap or slot antenna at other frequencies can be predicted.

Introduction

Hypersonic vehicles traveling in or through the upper atmosphere expose their antennas to low pressures. The high-frequency energy from the antenna can sufficiently increase the electron energy to produce ionization in the neighborhood of the antenna. A loss in the power radiated by the antenna results. Since future communication, radar, and guidance systems demand high reliability, it is essential to study the case where the production of new electrons by ionization is greater than the loss by diffusion or other mechanisms. Of course the problem is solved for the antenna designer if the vehicle operates at a high enough altitude so that there are an insufficient number of ionizable atoms present. Few data were available on a specific antenna which had been tested in the laboratory and then carefully checked on an actual flight. Where both laboratory and flight data were available, the breakdown was influenced by the rocket exhaust of the vehicle so that correlation was uncertain. It was the objective of the experiments reported herein to test a given antenna under both flight and simulated conditions. The physics of this process will be discussed here so that the basic principles can be applied to other cases. The antenna selected for study

was that designed and developed by The University of Michigan for telemetering upper-atmosphere density measurements from a 7-in.-diameter sphere. The antenna is a 400-Mc slot 1 in. by 11 in. long, flush-mounted in the surface of the sphere.

Flight Technique in The University of Michigan Experiments

A technique for obtaining upper-air density and temperature by measuring the drag of a falling sphere was developed by The University of Michigan Aeronautical Engineering Department. The deceleration of the sphere as it re-enters the atmosphere was telemetered[1-3] to the ground so that the ambient density could be calculated directly from the drag equation. By careful design it was possible to pack within this sphere the accelerometer, the batteries, the telemetering transmitter and the antenna. Figure 1 shows the sphere components and assembly.

A typical sphere trajectory is given in Fig. 2. Other flights went as high as 594,000 ft. In this figure the NACA radar data and estimated upleg trajectory for the rocket nose cone are shown for comparison with the calculated sphere trajectory. Note that the sphere is ejected from the rocket at 180,000 ft.

The transmitter used in the high-altitude experiments was a master-oscillator power amplifier, operating at 400 Mc. The output was a square 10μ-sec pulse occurring at a repetition rate of two pulses per second. These pulses are referred to as the start pulse and the stop pulse. The start pulse was generated when a small metal bobbin was released in the hollow cavity of the accelerometer.[1,2] It occurs at a rate of one pulse per second. The stop pulse was generated when the bobbin contacts the wall of the cavity. It varies from 5 msec for maximum acceleration to 750 msec for minimum acceleration. These pulses, when telemetered to

the ground, constituted the primary data of the high-altitude experiments.

The antenna is a boxed-in slot extending half the circumference of the sphere. This type of antenna uses the surface of the sphere itself as a radiating element. Patterns were obtained using the sphere as the transmitting antenna and the ground-station helical antennas as the receiving elements. The helix windings of these antennas was such that the patterns obtained from the sphere were essentially omnidirectional. For structural reasons, the slot was partially filled with polystyrene, and, because of the heat generated during re-entry, the surface of the slot was covered with Teflon.

Because the length of the slot was less than a half wavelength, the antenna presented an inductive impedance to the coupling point. It was therefore necessary to load the slot with a capacitive reactance to resonate with this inductance at 400 Mc. The capacitor loading point was chosen at one-third of the way down from the edge of the slot.

At the request of the Boeing Company, the magnetic tape recordings of the pulsed telemetered signals were analyzed by the staff of The University of Michigan. The amplitudes of both the start and stop pulses were found to be attenuated identical amounts. The top part of Fig. 3 shows the amplitude of both start and stop pulses plotted against altitude. These data were for a particular flight in which the sphere antenna reached an altitude of 594,000 ft. Above a relative amplitude of 25, the magnetic tape became saturated so that the inverse square effect does not appear. Thus there is no reduction in the power level as the distance between the sphere and the receiving station varies.

This method of ground-station detection clearly shows the region of break-

down. The flight data show a marked attenuation of the signal level through an altitude range of 110,000 to 300,000 ft.

The bottom part of Fig. 3 shows the velocity and Mach number for this flight. Note that the maximum in the velocity and Mach number curves does not coincide with the breakdown region shown at the upper part of the figure. This tends to indicate that these parameters have a secondary influence upon breakdown. Thus the attenuation in the signal level from the sphere antenna is probably caused by electrical breakdown.

Experimental Procedure at Boeing

The breakdown measurements were made in terms of power. However, a knowledge of the breakdown voltage is necessary if the measurements are to be compared to theory. Thus it was necessary to measure the antenna impedance. The details of these measurements are available in Boeing Report D2-3281. Several measurements were taken at various power levels and the average value of the slot impedance was found to be 200 ohms. The breakdown voltage was then determined from the breakdown power by using this value of impedance.

The sphere was then placed in the bell jar vacuum chamber. A standard fore pump was capable of reducing the pressure to 5×10^{-2} mm Hg. A diffusion pump was added to the system and permitted pressures as low as 10^{-3} mm Hg to be obtained. This pressure was measured with an Alphatron ionization gauge which had been calibrated against a mercury McLeod gauge. The bell jar used in the experiments was 12 in. in diameter and about 18 in. in height.

The antenna voltage was varied by placing lengths of transmission line (attenuators) between an external transmitter and the antenna of the sphere. A block diagram of the experimental setup appears in Fig. 4. The power was measured by means of a 10-db attenuator, bolometer mount, and power meter. This circuit sufficed for pulse repetition rates of 50 pulses per second or greater. However, for a pulse rate of 1 pps, the pulse rate used during the flights, the power had to be determined by comparing the pulse height at 1 pps to that of 200 pps.

The external receiver is also shown in the lower right-hand corner of Fig. 4. Positive 20-volt peak square waves from the pulse generator were used to trigger the oscilloscope circuit. Breakdown was determined on this oscilloscope. The methods of determining breakdown mentioned in published literature vary with the experimenter. In our case, breakdown power is that at which the pulse shape changes from that picked up at lower power. Change in the pulse shape is shown in Fig. 5. Curve (a) is the shape of the pulses normally radiated by the sphere antenna when breakdown is not present. Curve (b) is the pulse shape at a lower pressure when breakdown is present. It was found that this method of determining breakdown power is consistent with other methods. At a still lower pressure the breakdown caused the pulse shape to look like Curve (c). Note that there is a plateau present in each case, meaning that a given power is radiated even when breakdown is present.

Breakdown was measured for various power levels by decreasing the pressure until breakdown was observed on the oscilloscope. At a given power level the breakdown would persist as the pressure was lowered until a critical pressure

was reached. The breakdown power for this low-pressure point was determined by pumping down the system to a pressure below that at which breakdown occurs. At this point the transmitter was turned on and the pressure was slowly increased until breakdown occurred. This procedure assured that fresh air was used for each determination of breakdown power. This is essential since the discharge can produce oxides of nitrogen which influence the breakdown for succeeding pulses. This procedure was repeated for various power levels to the antenna.

Experimental Results

Figure 6 shows the variation of breakdown voltage with altitude at 50 and 200 pulses per second. The altitudes corresponding to experimentally observed pressures were taken from the data of The ARDC Model Atmosphere. A second scale is shown giving the altitude calculated considering the effect of high-altitude temperature on pressure. Note that the minimum voltage needed for breakdown to occur decreased as the repetition rate was increased. This is to be expected since the electrons produced during a given pulse increased the initial electron density for the succeeding pulse.

Breakdown at 1 pulse per second was not observed at all unless a microcurie alpha source enclosed in a glass needle was placed in the high-field region of the antenna, that is, within 1/4 in. of the Teflon. The effect of the alpha source on breakdown at 50 pulses per second is shown in Fig. 7. The effect was such as to increase the pressure range over which breakdown occurs and to decrease the breakdown power. The results with 1 pulse per second using the source are

given in Fig. 8. This figure is given in terms of power using the above-mentioned impedance of 200 ohms.

Comparison with Flight Data

The University of Michigan flight data mentioned above is given at the top of Fig. 8. The transmitter in the sphere was operated at 30 watts output at 2 pps during the flight. The horizontal line drawn at 30 watts in Fig. 8 intersects the laboratory data at 107,000 and 217,000 ft. Breakdown should then occur at altitudes between these extremes. The recordings of signal strength for four different flights are summarized in the table on the following page. Figure 3 is typical of these flights.

Comparison of the flight data given above and the laboratory data in Fig. 8 indicates a discrepancy above 215,000 ft. The laboratory results do not show breakdown above this altitude for a 30-watt power if the ambient ionization is equal to or less than that produced by the radioactive source. Figure 7 indicates that at 50 pps ambient ionization has the effect of lowering breakdown power at the higher altitudes. The discrepancy could also be caused by the fact that at altitudes above 215,000 ft the mean free path for electrons is 1 mm and greater. Under these conditions, a significant number of electrons may diffuse to the wall of the bell jar. This process causes the necessary voltage for breakdown to increase. Under these conditions, agreement between flight and bell jar tests would not be expected.

Since a radioactive source was necessary to produce laboratory breakdown at 1 pps even at the most favorable altitude, it is interesting to speculate about

Flight*	Min. Altitude at Which Attenuation Was Observed, ft	Altitude of Maximum Attenuation, ft	Max. Altitude at Which Attenuation Was Observed, ft	Sphere Peak Altitude, ft	Maximum Observed Attenuation**	Power, watt
AM 6.02	180,000	230,000	270,000	515,000	4.5	20.0
AM 6.03	160,000	240,000	300,000	557,000	12	24.5
SM 2.10	110,000	202,000	310,000	481,000	11	24.0
AM 6.05	145,000	200,000	290,000	594,000	6	27.0
Average	149,000	218,000	292,000			

*These firings were conducted at Fort Churchill, Canada (59 degrees N), as a part of the IGY program for upper-atmosphere density, pressure, and temperature measurements. All flights were within one hour of noon local time during January and March of 1958.

**The attenuation observed on these flights agrees reasonably well with that calculated from Figs. 5 and 8.

the source or sources of additional energy that apparently must be present in the upper atmosphere. Ultra-violet photons, cosmic rays, soft X-rays, sphere-accumulated charge caused by friction, or other sources of additional electrons, perhaps in combination with the sphere velocity, are possibilities. It is hoped that night and also higher-altitude firings will provide additional data which will lead to a more conclusive interpretation.

Comparison with Breakdown Data at Other Frequencies: Similarity Principles and Scaling

It has been shown[4] that the breakdown of hydrogen and helium gas is controlled by diffusion in and near the pressures where breakdown is most probable. There is evidence[5] that attachment also effects the breakdown in air under high-pressure conditions. However, we now want to demonstrate that as long as diffusion or attachment are the dominant loss processes (either or both), breakdown voltages can be predicted to the accuracy needed for engineering purposes, using scaling laws.

The scaling laws of plasma physics applied to breakdown can be stated as follows. The breakdown voltage will be the same for gaps with geometrically similar electrodes if the gap spacing (d), pressures (p), and wavelength (λ), are related so that:

$$p_1\lambda_1 = p_2\lambda_2$$

and

$$p_1 d_1 = p_2 d_2$$

As a demonstration of the degree to which these scaling laws hold in air, and thus the degree to which scalable processes (diffusion and/or attachment

predominates), the breakdown data of various investigations[6,7] was assembled in the three-dimensional diagram shown in Fig. 10. The horizontal axes are $p\lambda$ and pd. The vertical axis is voltage. (The concept of diffusion length is being avoided to simplify the presentation.) Note that if gap spacing and frequency are kept constant in a given experiment and pressure is varied, one moves along the horizontal plane at a 45° angle to either the $p\lambda$ or the pd axis. Each of the vertical slabs represents a breakdown curve taken in this manner. The curves to the rear are for gaps up to 0.05 of a wavelength in size while those in the right forward part are for gaps as small as 0.001λ. The curves representing nonuniform field data[7] are lower than the general trend at lower pressures, but all the data indicate a valley near $d = .003\lambda$. A smooth surface could be made to fit the top of these curves and to this accuracy scaling laws can be used to compare even uniform and nonuniform field cases. A more practical form of the three-dimensional diagram is given by plotting contours representing voltage (the vertical dimension) on the horizontal plane. This has been done in Fig. 11 for uniform field data. Figures 10 and 11 should not be used for pulsed data unless the pressure times pulse length is great enough[8] so that the breakdown voltage is the same as the C.W. value.

The data should not be extrapolated beyond the various limits bounding the contours. However, the lowest breakdown voltage will appear within these limits. A comparison of the breakdown curve for the sphere and uniform field data for a gap of 1 cm is given in Fig. 12. The pressure times pulse length at minimum voltage breakdown is low (4 mm-μsec) but the pressure times gap spacing is low enough (0.4 mm-cm) that according to Fig. 6 of Ref. 8 the breakdown voltage for the sphere should be about 10% higher than if it had been a much longer pulse.

Summary

The object of the study reported herein was to investigate the degree of correlation existing between antenna electrical breakdown data obtained in still air in a vacuum chamber with that obtained from rocket firings which take an identical antenna transmitting 10-μsec radiofrequency pulses to an altitude of over 590,000 ft.

At the lower altitudes where the flight data showed decreased signal strengths, reasonable correlation between flight and laboratory data was possible provided that a radioactive alpha source was placed near the antenna in the vacuum chamber. Since such a source is not adjacent to the antenna during flight, several sources of energy known to be present in the upper atmosphere and which might enhance antenna radiofrequency breakdown are mentioned. At the upper altitudes, poor correlation between flight and laboratory data was observed. Electron diffusion to the bell jar walls is postulated to explain the discrepancy.

The correlation between experimental and uniform field data obtained by use of the scaling laws of plasma physics was found satisfactory. Thus scaling laws can be used for engineering predictions of the altitude at which breakdown is most probable and for prediction of the breakdown voltage at and near that altitude. These results are not directly comparable with the recent analysis by MacDonald[9] because he considered antennas with a gap-to-wavelength ratio much greater than used here.

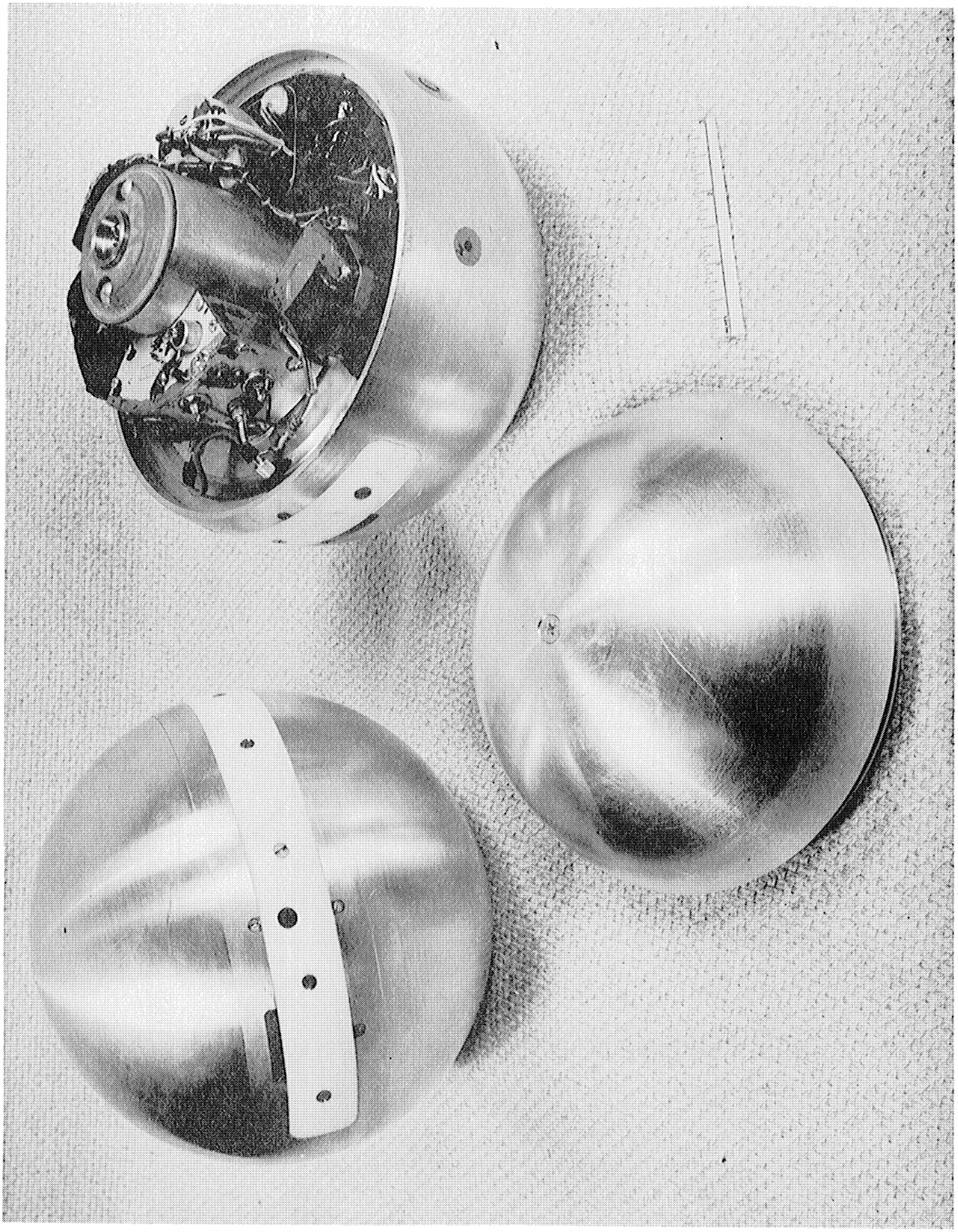

FIG. 1

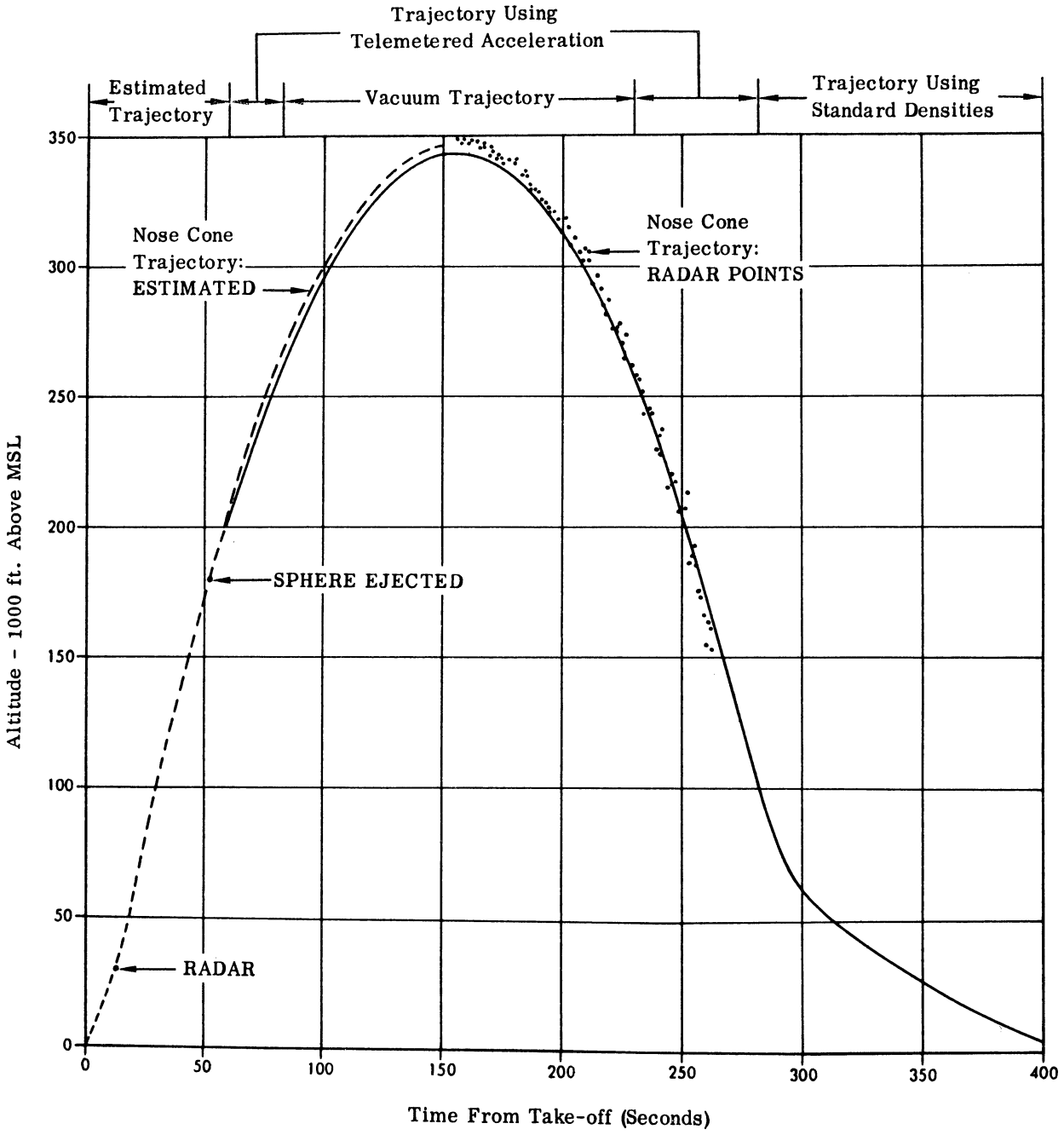

Fig. 2— Typical sphere altitude versus time

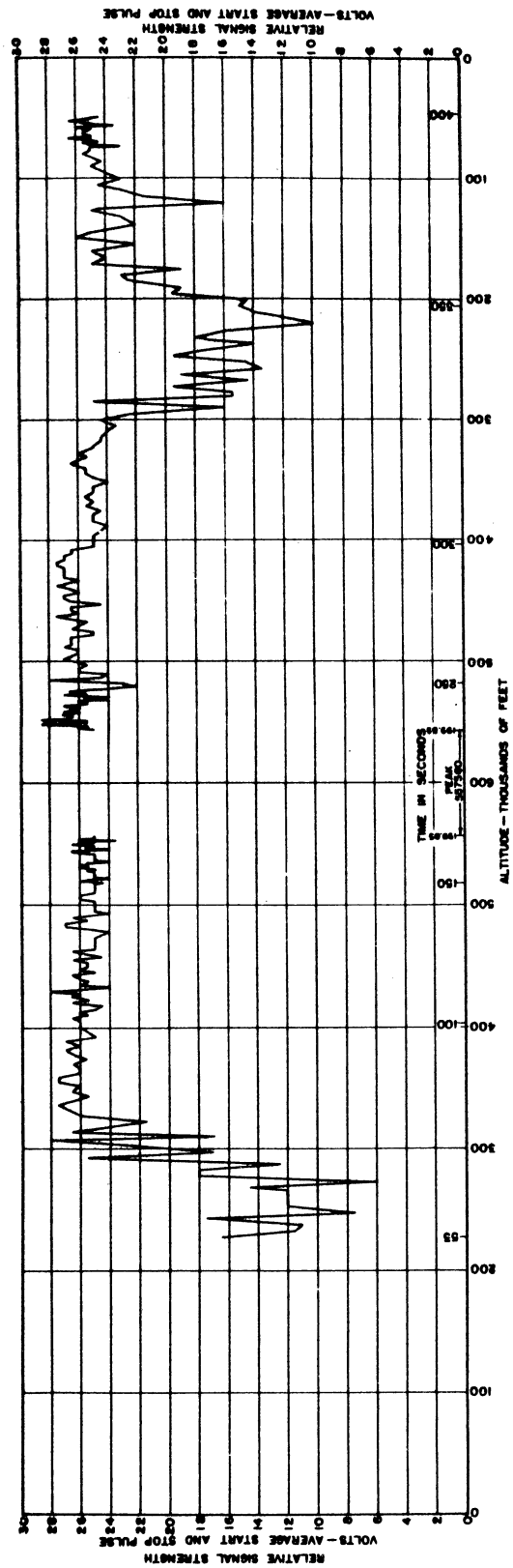

Signal strength vs. time and altitude (AM 6.03).

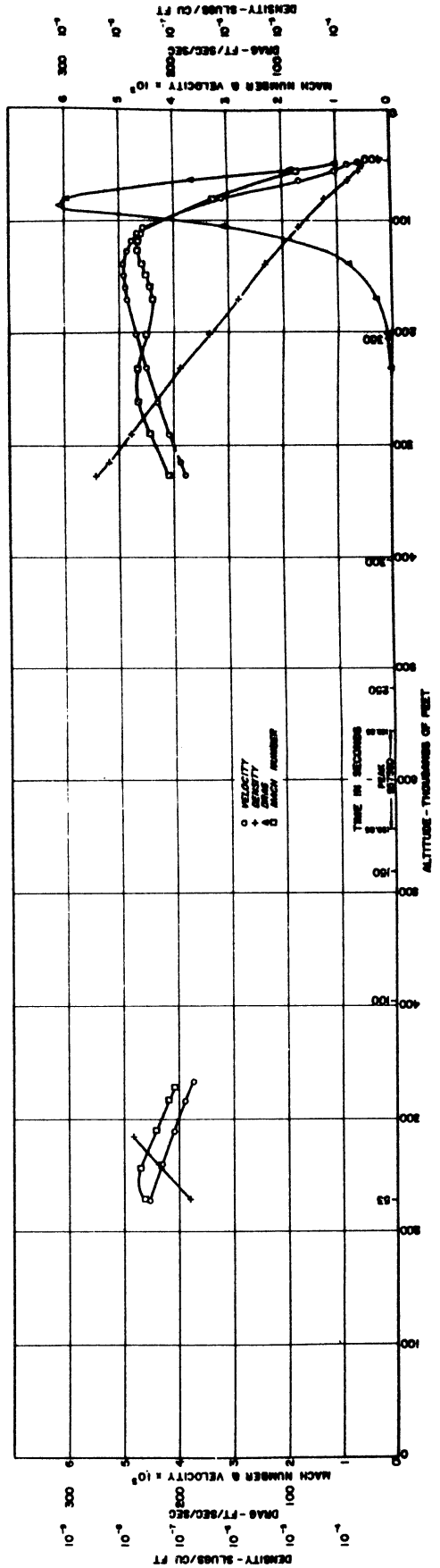

Velocity, Mach number, drag acceleration, and density vs. time and altitude (AM 6.03).

Fig 3

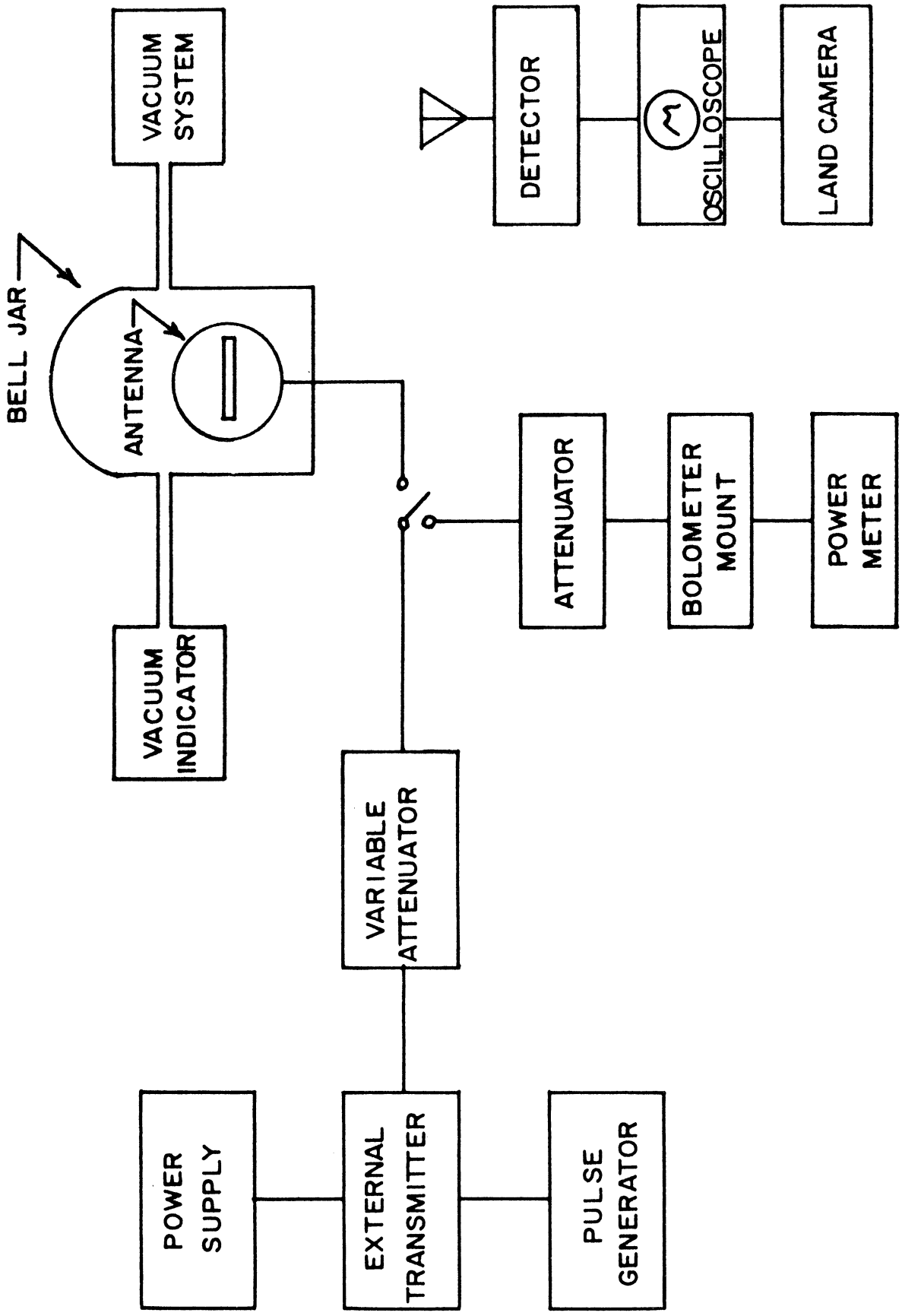

CALC			REVISED	DATE	BLOCK DIAGRAM OF EXPERIMENTAL SET-UP FOR MEASURING THE POWER AND PRESSURE AT BREAKDOWN
CHECK					
APPD					
APPD					
					BOEING AIRPLANE COMPANY SEATTLE 24, WASHINGTON

FIG. 4

PAGE

R-339
18-17

(a) ATMOSPHERIC, P_o

(b) INITIAL BREAKDOWN, P_i

(c) FINAL BREAKDOWN, P_f

$P_f < P_i < P_o$

CALC			REVISED	DATE	TYPICAL PULSE ENVELOPES
CHECK					
APR					
APR					BOEING AIRPLANE COMPANY SEATTLE 24, WASHINGTON

FIG. 5

PAGE

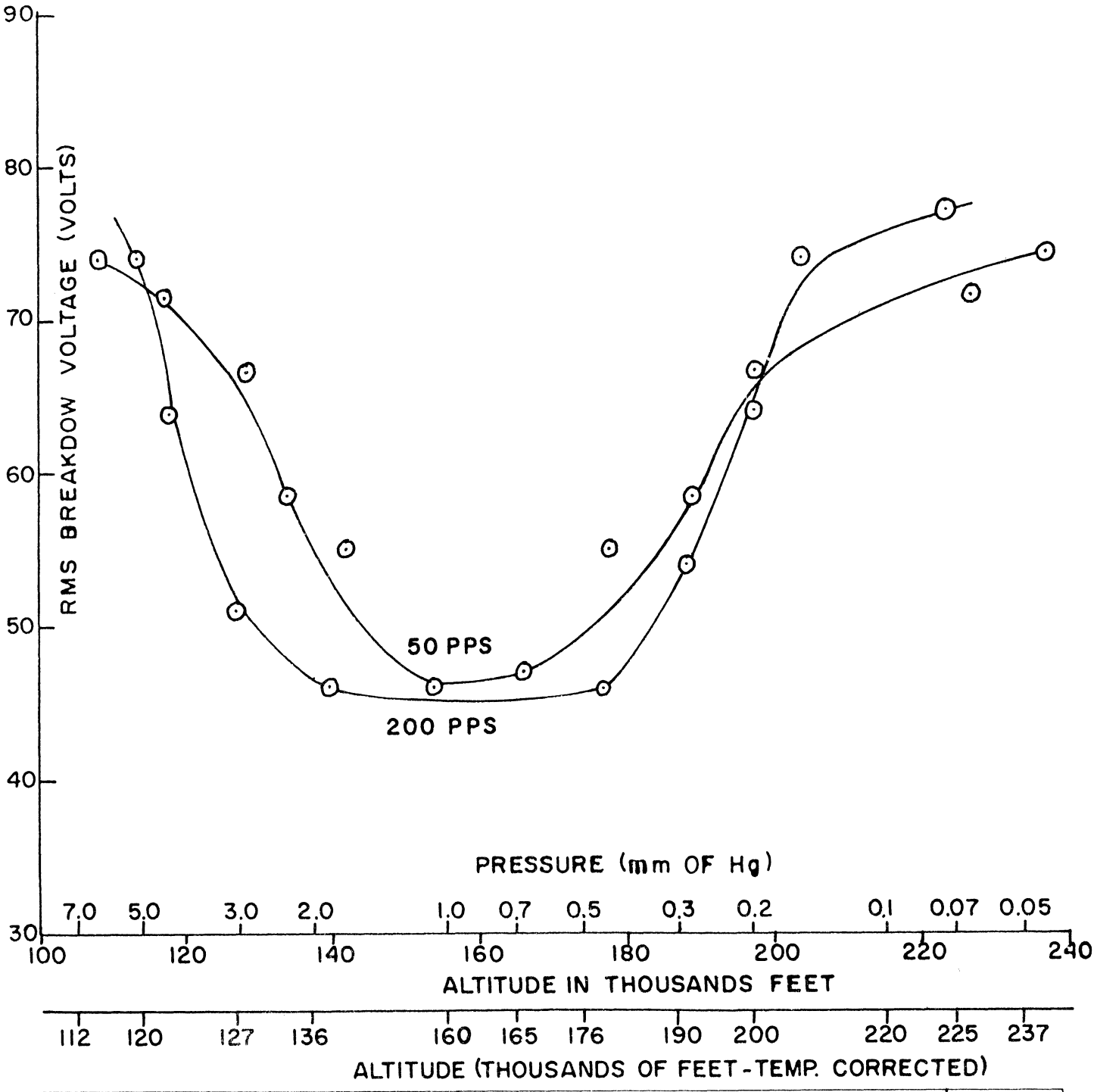

CALC			REVISED	DATE	BREAKDOWN VOLTAGE VS ALTITUDE - 50 & 200 PPS WITHOUT A RADIO-ACTIVE SOURCE	FIG. 6
CHECK						
APR						
APR					BOEING AIRPLANE COMPANY SEATTLE 24, WASHINGTON	PAGE

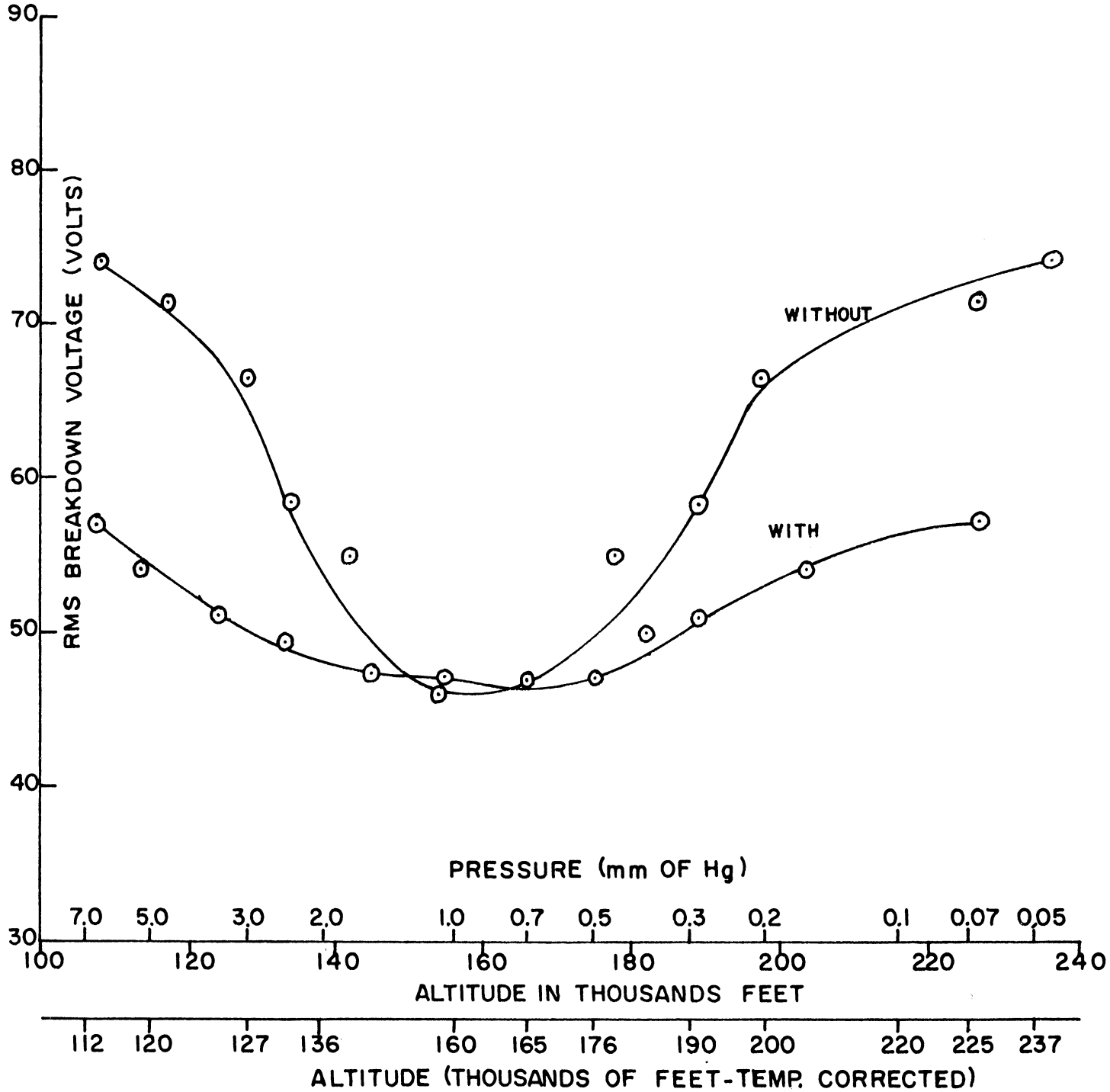

CALC			REVISED	DATE	BREAKDOWN VOLTAGE VS ALTITUDE - 50 PPS WITH AND WITHOUT A RADIOACTIVE SOURCE	FIG. 7
CHECK						
APR						
APR					BOEING AIRPLANE COMPANY SEATTLE 24, WASHINGTON	PAGE

R-339
18-20

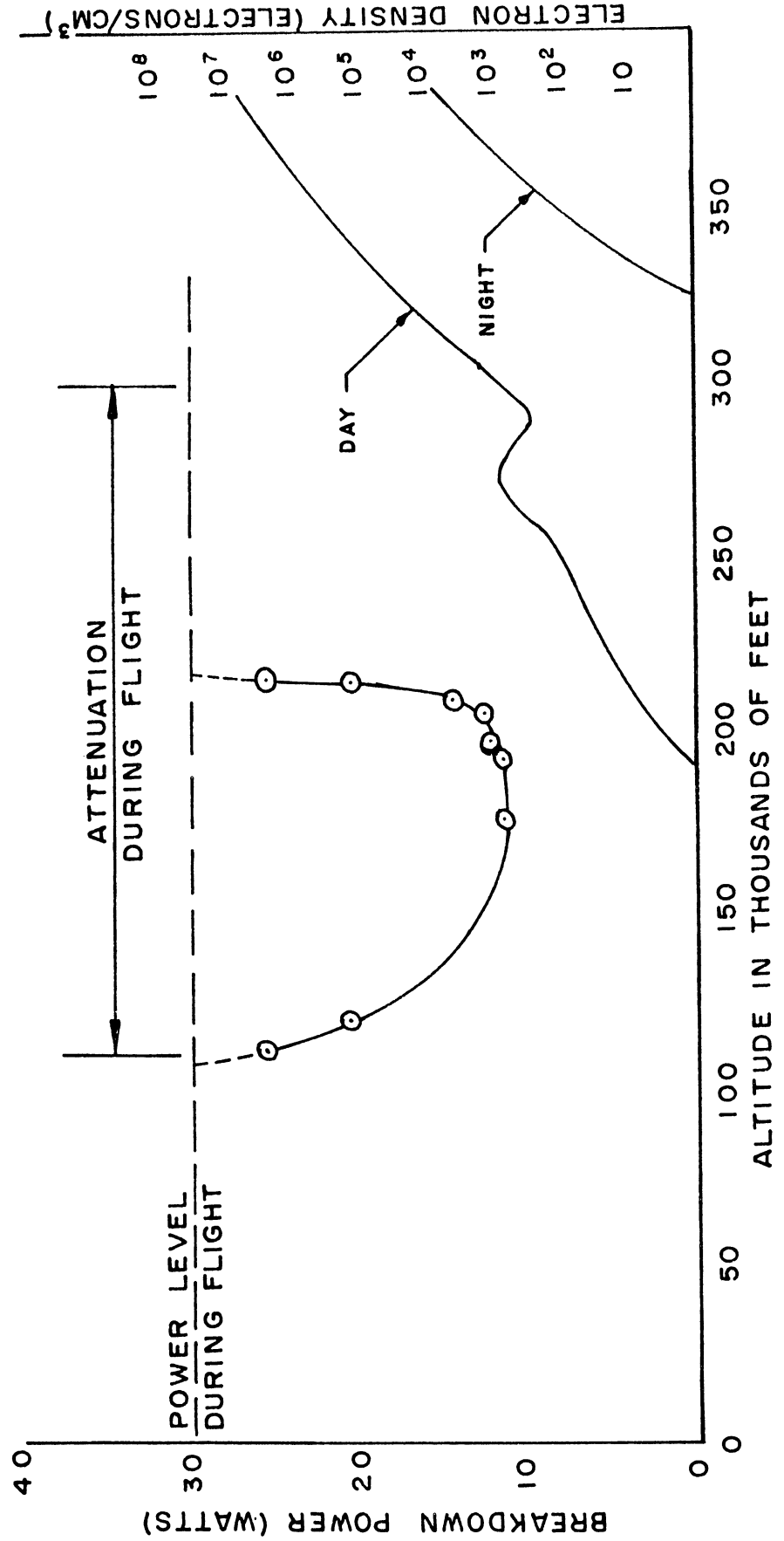

CALC			REVISED	DATE	BREAKDOWN POWER AND AMBIENT ELECTRON DENSITY VS ALTITUDE	FIG. 8
CHECK						
APR						
APR					BOEING AIRPLANE COMPANY SEATTLE 24, WASHINGTON	PAGE

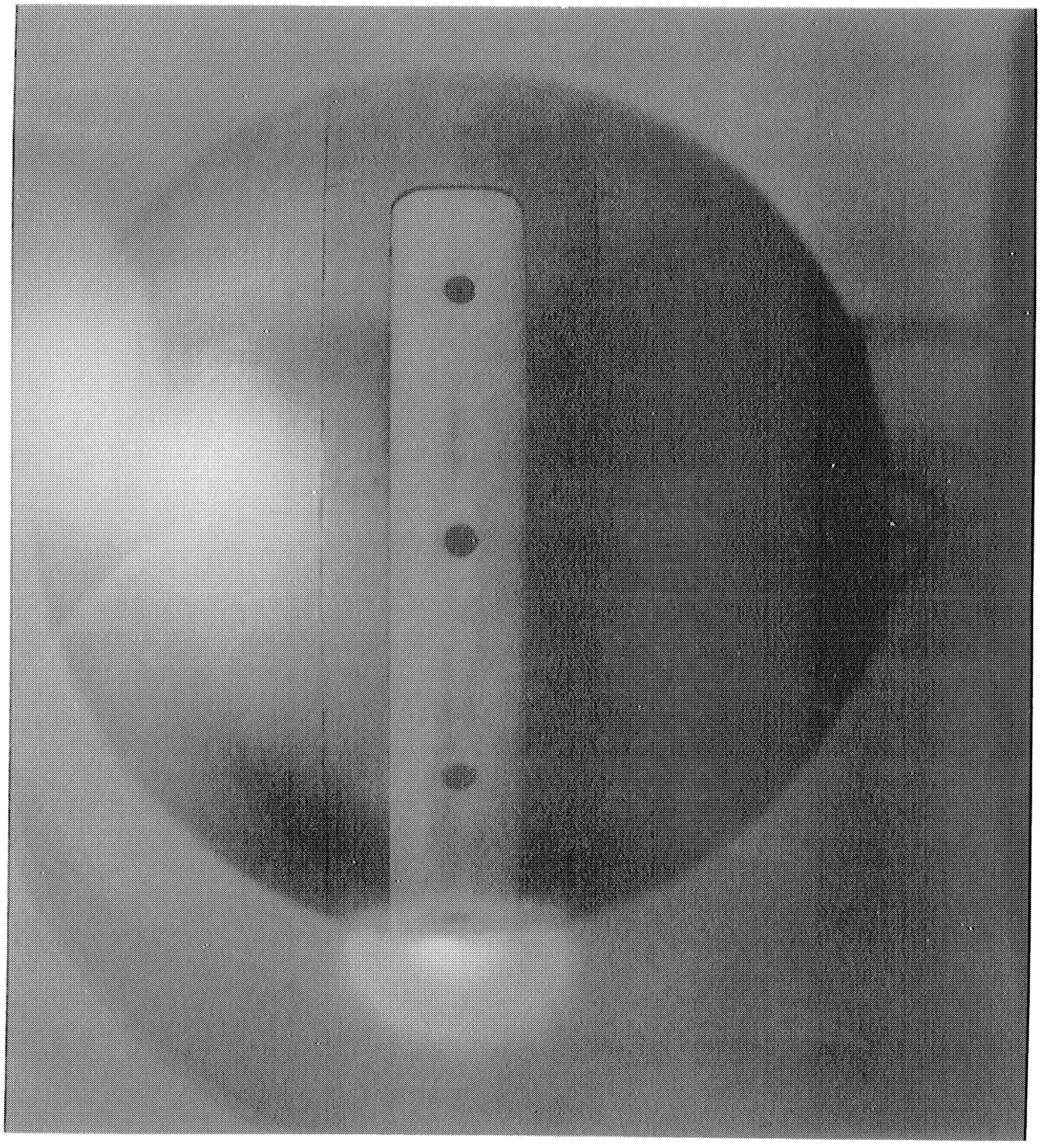

FIG. 9

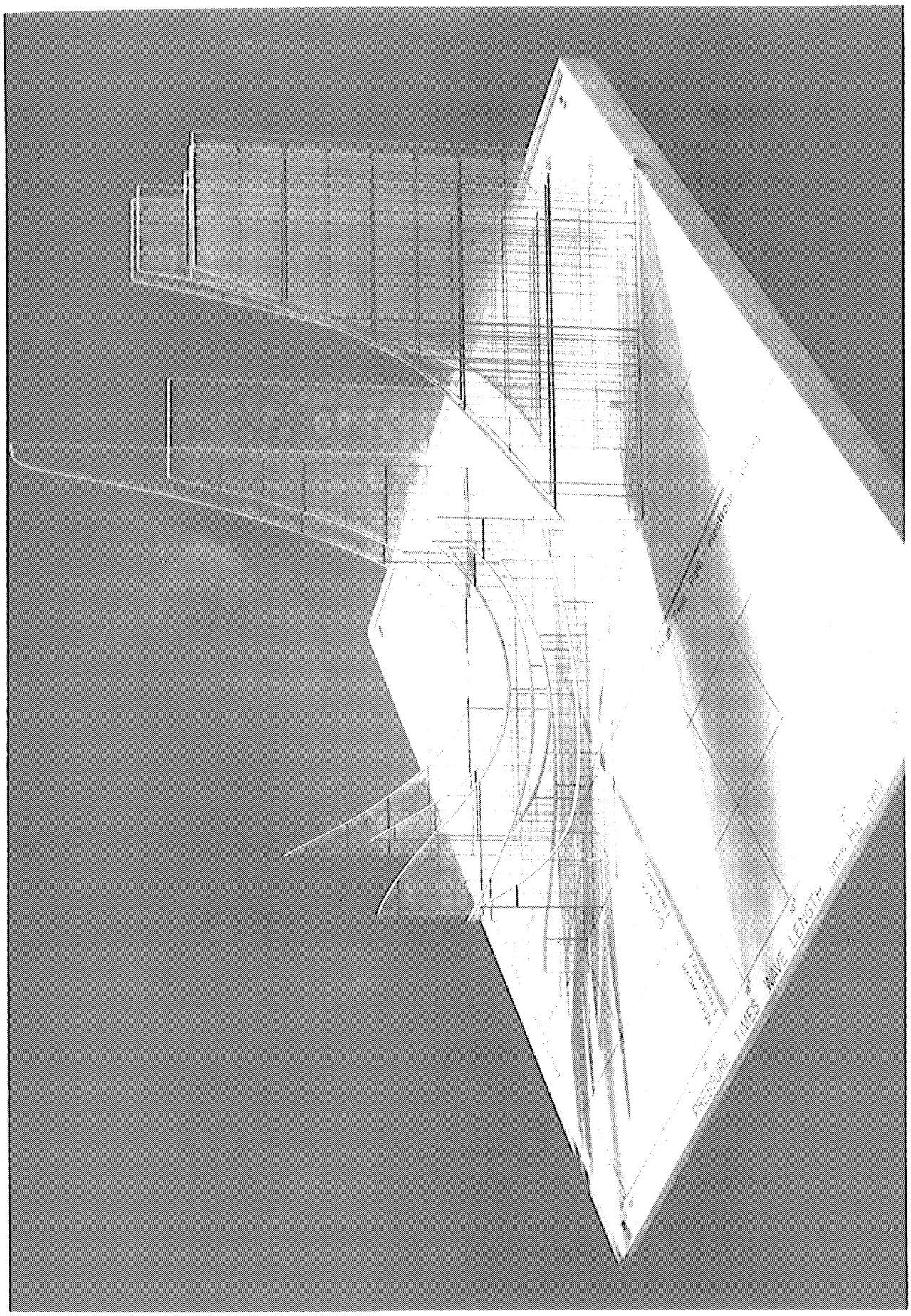

FIG. 10

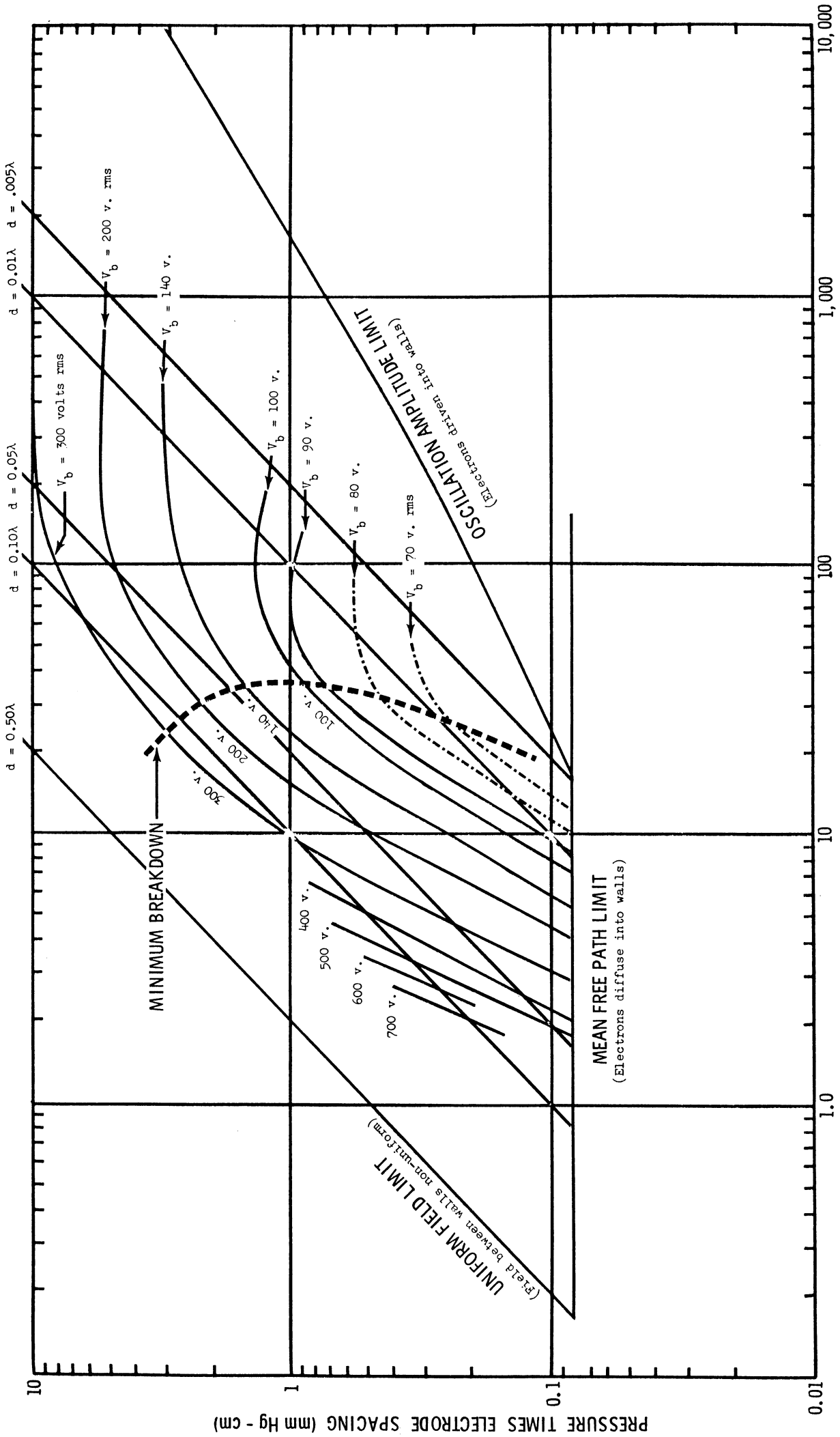
PRESSURE TIMES ELECTRODE SPACING (mm Hg - cm)
PRESSURE TIMES WAVE LENGTH (mm Hg - cm)
10
1
0.1
0.01
10,000
1,000
100
10
1.0
d = 0.50λ
d = 0.10λ
d = 0.05λ
d = 0.01λ
d = .005λ
MINIMUM BREAKDOWN
300 v.
200 v.
140 v.
100 v.
400 v.
500 v.
600 v.
700 v.
V_b = 300 volts rms
V_b = 200 v. rms
V_b = 140 v.
V_b = 100 v.
V_b = 90 v.
V_b = 80 v.
V_b = 70 v. rms
OSCILLATION AMPLITUDE LIMIT
(Electrons driven into walls)
MEAN FREE PATH LIMIT
(Electrons diffuse into walls)
UNIFORM FIELD LIMIT
(Field between walls non-uniform)

FIG. 11

R-339
18-24

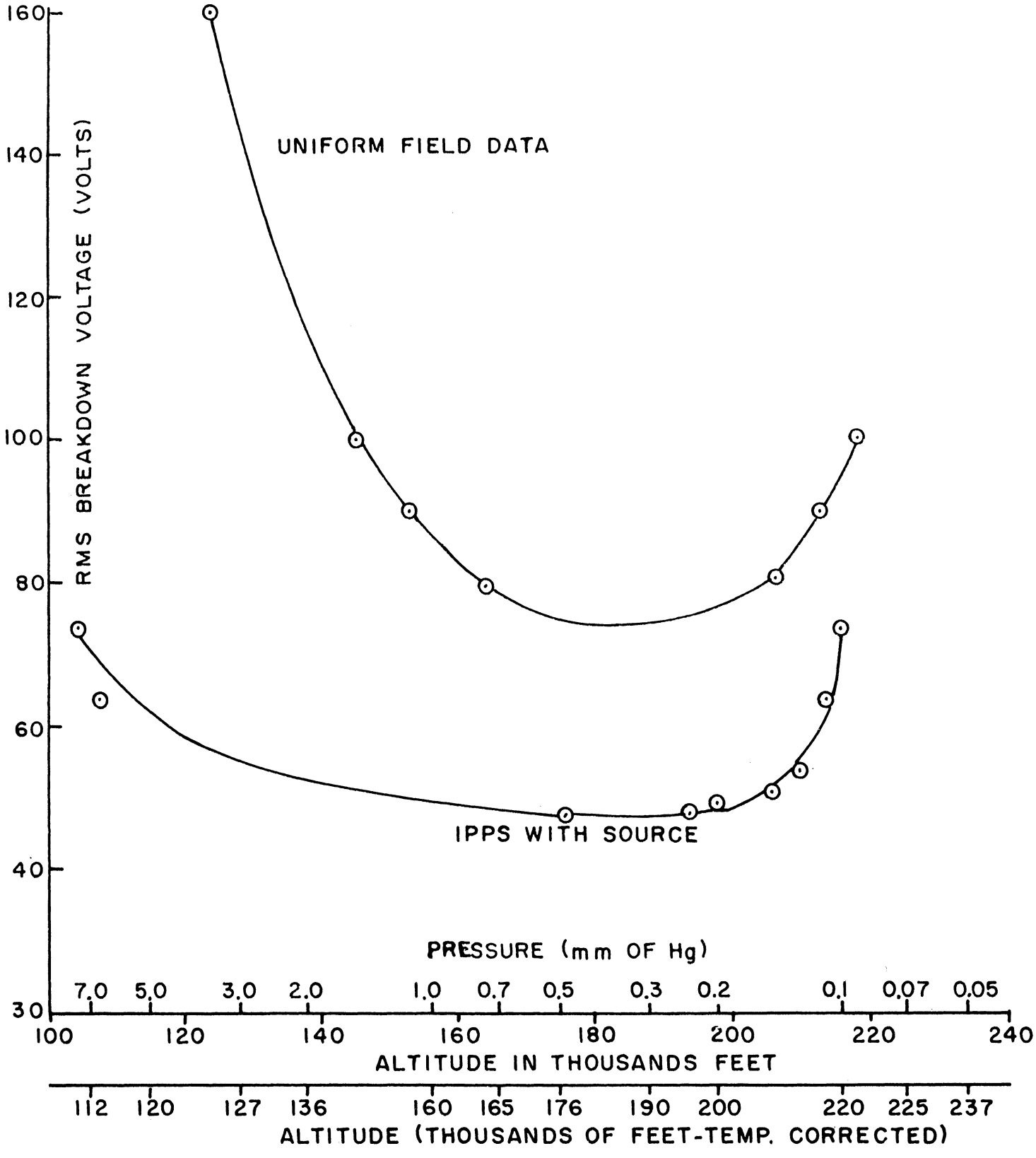

CALC			REVISED	DATE	COMPARISON OF BREAKDOWN VOLTAGES FOR IPPS WITH SOURCE AND THAT FROM UNIFORM FIELD DATA	FIG.12
CHECK						
APR						
APR						
					BOEING AIRPLANE COMPANY SEATTLE 24, WASHINGTON	PAGE

References

1. Jones, L. M., and Bartman, F. L., "Satellite Drag and Air-Density Measurements," in: Van Allen, J. (ed.), Scientific Uses of Earth Satellites (Ann Arbor: University of Michigan Press, 1956), pp. 95-98.

2. Meteorological Rocket Soundings in the Arctic, IGY Bulletin No. 14, pp. 4-5, August, 1958.

3. IGY Rocket Report No. 1, p. 47, July 30, 1958.

4. MacDonald, A. D., and Brown, S. C., "Limits for the Diffusion Theory of High Frequency Gas Discharge Breakdown," Phys. Rev., 76, 1629 (1949).

5. Brown, S. C., "Microwave Gas Discharge Breakdown," Appl. Sci. Res. B, 5, 97 (1955).

6. Rose, D. J., and Brown, S. C., "Microwave Gas Discharge Breakdown, in Air, Nitrogen and Oxygen," J. Appl. Phys., 28, 561 (1957).

7. Worth, F., A Study of Voltage Breakdown in the Cavity Fed Slot Antenna, Lockheed Internal Report, MSD 2030.

8. Gould, L., and Roberts, L. W., "Breakdown of Air at Microwave Frequencies," J. Appl. Phys., 22, 1162 (1956).

9. MacDonald, A. D., "High Frequency Breakdown in Air at High Altitudes," Proc. IRE, 47, 436 (1959).

APPENDIX B

NIKE-CAJUN FLIGHTS
AM 6.02, 6.03, 6.05

AM 6.02

Fort Churchill 1-25-58 1312 CST

Accelerometer Recycle Period, Seconds

Upleg		Downleg		Minimum	Transit
Upper Limit	Lower Limit	Upper Limit	Lower Limit	Transit Time	Distance x 2 Feet
.92000	1.01000	.92000	1.01000	.00800	.0313

Threshold Acceleration		Mean Acceleration, Ft/Sec^2		Elapsed Time	
Upleg	Downleg	Upleg	Downleg	Upleg	Downleg
.40	.40	1.60	1.30	13.	10.

g_o Ft/Sec^2	r_o Feet	cos ∅	sin ∅	cos Θ	sin Θ
32.2270	20903520.	.51877000	.85491000	-.60182000	.79864000

M/A $Slugs/Ft^2$
1.3400

Balloonsonde Data

Altitude Feet	Pressure Lb/Ft^2	Temperature Deg Fahr	Density $Slug/Ft^3$
.	2105.	-4.0	.00269146
1214.	2007.	5.7	.00251239
3281.	1846.	15.4	.00226381
6693.	1612.	8.6	.00200586
7283.	1574.	6.4	.00196817
7874.	1537.	11.5	.00190064
9514.	1441.	7.1	.00179834
10417.	1388.	7.0	.00173385
13369.	1232.	-5.8	.00158161
14107.	1194.	-6.9	.00153701
16371.	1088.	-14.8	.00142489
18077.	1010.	-23.3	.00134935
18766.	981.	-23.3	.00131032
22464.	835.	-39.5	.00115815
28149.	643.	-62.5	.00094350
29494.	605.	-66.1	.00089648
30511.	576.	-64.3	.00084932
34186.	484.	-67.0	.00071883
34973.	467.	-61.1	.00068370
35761.	449.	-62.5	.00065861
37040.	421.	-59.5	.00061406
41043.	350.	-59.8	.00051116
42847.	321.	-61.1	.00047004
43930.	307.	-59.8	.00044726
49540.	236.	-58.4	.00034258
57414.	162.	-64.9	.00024035
60892.	137.	-65.4	.00020365
67224.	102.	-67.4	.00015196
78260.	60.	-77.8	.00009239
98293.	20.	-100.3	.00003385
101846.	18.	-92.8	.00002984

AM 6.02

Raw accelerometer data, upleg and downleg, time in seconds

45.77000	45.86286	46.77000	47.77000	47.87782	48.77000	48.88802	49.75000
50.74000	50.87881	51.72000	51.87011	52.69000	53.69000	53.86733	54.67000
54.86651	55.65000	55.85394	56.63000	56.85718	57.61000	58.59000	58.84649
59.57000	59.86091	60.55000	61.53000	61.87933	62.53000	62.92681	63.49000
63.92415	64.47000	64.92212	65.44000	65.95826	66.41000	66.91972	67.41000
67.98283	68.39000	69.00702	69.37000	70.11741	70.35000	71.09827	71.33000
72.06819	72.31000	73.06142	73.29000	74.04219	74.27000	75.02202	75.25000
76.00350	76.23000	76.98492	77.21000	77.96539	78.20000	78.95541	.00000
299.8330	300.6163	300.8270	301.6111	301.8240	302.6041	302.8120	303.5893
303.8000	304.5808	304.7900	305.5731	305.7860	306.5706	306.7840	307.5664
307.7740	308.5552	308.7630	309.5389	309.7550	310.5286	310.7360	311.4681
311.7270	312.4068	312.7220	313.4709	313.7070	314.2862	314.6900	315.2511
315.6630	316.2554	316.6370	317.1099	317.6180	318.0673	318.6000	319.0657
319.5880	319.9872	320.5730	320.9442	321.5610	321.9195	322.5400	322.8422
323.5300	323.8229	324.5200	324.7942	325.5000	325.7364	326.4800	326.7050
327.4600	327.6716	328.4400	328.6268	329.4100	330.3900	330.5559	331.3700
331.5182	332.3000	332.4418	333.3300	333.4592	334.3100	334.4283	335.3000
335.4107	336.2700	336.3707	337.2500	337.3430	338.2200	338.3063	339.2000
339.2790	340.1800	340.2509	341.1600	341.2239	342.1600	342.2181	343.1500
343.2027	344.1400	344.1890	345.1300	345.1734	346.1300	346.1691	347.1200
347.1549	348.0500	348.0812	349.0900	349.1178	350.0700	350.0948	351.0700
351.0924	352.0600	352.0800	353.0500	353.0681	354.0400	354.0562	355.0300
355.0595	356.0300	356.0436	357.0200	357.0326	358.0200	358.0317	359.0100
360.0000	360.0212	360.9800	361.0230	361.9700	361.9808	362.9400	362.9508
363.9200	363.9310	364.9000	364.9281	365.8800	365.8915	366.8500	366.8621
367.8200	367.8325	368.8100	368.8358	369.7800	369.7935	370.7600	370.7744
371.7400	371.7552	372.7300	372.7460	373.7200	373.7368	374.6900	374.7078
375.6800	375.7596	376.6700	376.6890	377.6600	377.6817	378.6400	378.6629
379.6300	379.6537	380.6200	380.6435	381.6100	381.6329	382.5900	382.6143
383.5800	383.6056	384.5600	384.5859	385.5300	385.5557	386.5100	386.5358
387.4900	387.5149	388.4700	388.4958	389.4500	389.4751	390.4300	390.4569
391.4000	391.4269	392.3800	392.4068	393.3600	393.3861	394.3400	394.3671
395.3200	395.3467	396.3100	396.3378	397.2900	397.3172	398.2800	398.3057
399.2600	399.2865	400.2400	400.2668	.00000	.00000	.00000	.00000

AM 6.02 Acceleration ft/sec^2 vs time, upleg and downleg

45.81643	3.63295	300.2247	.05106	351.0812	62.26898
47.82391	2.69471	301.2191	.05095	352.0700	78.00676
48.82901	2.24903	302.2140	.05149	353.0591	95.52225
50.80941	1.62581	303.2006	.05185	354.0481	119.37855
51.79506	1.39026	304.1904	.05139	355.0447	35.99690
53.77867	.99619	305.1816	.05108	356.0368	170.38515
54.76826	.81122	306.1783	.05089	357.0263	198.91299
55.75197	.75320	307.1752	.05117	358.0259	228.07389
56.74359	.60698	308.1646	.05133	360.0106	69.83772
58.71825	.47618	309.1510	.05203	361.0015	16.91888
59.71546	.37017	310.1418	.05234	361.9754	270.6056
61.70467	.25671	311.1020	.05845	362.9454	266.1053
62.72841	.19895	312.0669	.06779	363.9255	258.4615
63.70708	.16620	313.0964	.05586	364.9140	39.72966
64.69606	.15325	313.9966	.09338	365.8858	237.28984
65.69913	.11663	314.9705	.09951	366.8561	213.28203
66.66486	.12057	315.9592	.08926	367.8263	200.49439
67.69642	.09547	316.8735	.14008	368.8229	47.13599
68.69851	.08228	317.8426	.15521	369.7868	170.88963
69.74371	.05608	318.8329	.14443	370.7672	151.08179
70.72414	.05595	319.7876	.19658	371.7476	135.95225
71.69910	.05749	320.7586	.22733	372.7380	121.92052
72.68571	.05548	321.7403	.24369	373.7284	110.46529
73.66610	.05537	322.6911	.34291	374.6989	98.53980
74.64601	.05539	323.6764	.36520	375.7198	4.95162
75.62675	.05517	324.6571	.41668	376.6795	86.41996
76.60746	.05497	325.6182	.56041	377.6708	66.83723
77.58770	.05490	326.5925	.61880	378.6515	59.58425
78.57771	.05490	327.5658	.69946	379.6419	55.67851
		328.5334	.89785	380.6318	56.48401
		330.4729	1.13876	381.6215	59.63384
		331.4441	1.42652	382.6022	52.92415
		332.3709	1.55841	383.5928	47.76287
		333.3946	1.87782	384.5730	46.59326
		334.3691	2.23996	385.5429	47.28285
		335.3553	2.55682	386.5229	46.91700
		336.3204	3.08740	387.5024	50.64775
		337.2965	3.62202	388.4829	47.06288
		338.2631	4.20720	389.4626	49.56610
		339.2395	5.01816	390.4434	43.35838
		340.2155	6.23020	391.4135	43.13161
		341.1919	7.67681	392.3934	43.61795
		342.1891	9.27082	393.3731	45.95208
		343.1763	11.29253	394.3536	42.62633
		344.1645	13.05285	395.3333	44.07469
		345.1517	16.62428	396.3239	40.56570
		346.1496	20.46005	397.3036	42.34284
		347.1374	25.79432	398.2929	47.43031
		348.0656	32.24318	399.2732	44.60935
		349.1039	40.53516	400.2534	43.64900
		350.0824	51.10130		

Time in seconds (x10)
of rejected data points

3550'
3600'
3610'
3649'
3688'
3757''

AM 6.02

45.82 325.62 10. 10. ← Points used in peak time calculation

Time	a_D ft/sec^2	Vert.Vel.	Horiz.Vel.	Alt.	C_D	Density slugs/cu ft x 10^3	Pressure lbs/sq ft x 10^3	Temp. ^oF
191.649	.000	.	500.	494902.				
191.649	.000	.	500.	516103.				
191.649	.000	.	500.	515108.				
191.649	.000	.	500.	515101.				
311.102	.058	-3684.	515.	295870.	1.424	.00000795		
312.067	.068	-3714.	515.	292301.	1.380	.00000937	5.8	-99.8
313.097	.056	-3746.	516.	288462.	1.431	.00000732	6.8	80.4
313.997	.093	-3774.	516.	285078.	1.282	.00001345	7.8	-119.6
314.971	.099	-3804.	516.	281388.	1.261	.00001435	9.4	-75.6
315.959	.089	-3835.	516.	277612.	1.289	.00001240	11.0	59.2
316.874	.140	-3864.	516.	274093.	1.213	.00002037	12.8	-93.3
317.843	.155	-3894.	517.	270334.	1.202	.00002243	15.3	-61.4
318.833	.144	-3925.	517.	266463.	1.208	.00002045	17.9	51.5
319.788	.197	-3955.	517.	262702.	1.178	.00002813	20.8	-29.2
320.759	.227	-3985.	517.	258848.	1.163	.00003245	24.4	-20.8
321.740	.244	-4015.	517.	254922.	1.155	.00003450	28.5	23.0
322.691	.343	-4045.	518.	251090.	1.122	.00004927	33.5	-62.7
323.676	.365	-4076.	518.	247090.	1.117	.00005193	39.9	-11.6
324.657	.417	-4106.	518.	243079.	1.108	.00005888	46.9	4.6
325.618	.560	-4136.	518.	239119.	1.083	.00007987	55.5	-54.8
326.593	.619	-4166.	518.	235075.	1.076	.00008745	66.1	-18.9
327.566	.699	-4196.	519.	231006.	1.068	.00009823	78.0	3.2
328.533	.898	-4225.	519.	226933.	1.047	.00012681	92.4	-35.1
330.473	1.139	-4284.	519.	218681.	1.031	.00015899	129.4	14.7
331.444	1.426	-4314.	519.	214506.	1.012	.00020008	153.0	-14.2
332.371	1.558	-4342.	519.	210496.	1.007	.00021700	179.4	21.9
333.395	1.878	-4372.	519.	206036.	.992	.00026168	213.0	14.5
334.369	2.240	-4401.	519.	201762.	.979	.00031250	251.7	9.5
335.355	2.557	-4430.	519.	197408.	.969	.00035563	297.6	27.9
336.320	3.087	-4457.	519.	193120.	.963	.00042670	350.5	18.9
337.297	3.622	-4485.	519.	188756.	.961	.00049589	414.0	26.8
338.263	4.207	-4512.	519.	184409.	.958	.00057074	487.3	37.8
339.240	5.018	-4538.	519.	179991.	.955	.00067508	574.2	35.9
340.216	6.230	-4563.	518.	175550.	.951	.00083228	679.9	16.3
341.192	7.677	-4588.	518.	171083.	.947	.00101966	810.5	3.5
342.189	9.271	-4611.	517.	166497.	.943	.00122447	973.2	3.4
343.176	11.292	-4632.	516.	161935.	.939	.00148475	1168.6	-1.1
344.165	13.053	-4651.	515.	157349.	.936	.00170788	1400.6	18.1
345.152	16.624	-4668.	514.	152750.	.930	.00217265	1682.5	-8.5
346.150	20.460	-4681.	512.	148086.	.925	.00267373	2040.2	-15.2
347.137	25.794	-4690.	510.	143458.	.920	.00337908	2483.3	-31.6
348.066	32.243	-4692.	507.	139104.	.914	.00424397	3008.5	-46.7
349.104	40.535	-4688.	504.	134235.	.909	.00537863	3750.1	-53.5
350.082	51.101	-4674.	499.	129655.	.906	.00684169	4636.2	-64.9
351.081	62.269	-4650.	493.	124999.	.906	.00842643	5763.6	-61.2
352.070	78.007	-4612.	486.	120420.	.906	.01073020	7153.4	-71.3
353.059	95.522	-4558.	478.	115886.	.906	.01345402	8892.9	-74.6
354.048	119.379	-4484.	467.	111415.	.906	.01737796	11077.9	-88.4
356.037	170.385	-4261.	438.	102720.	.909	.02739075	17178.7	-94.4
357.026	198.913	-4110.	419.	98579.	.913	.03420754	21232.3	-98.1
358.026	228.074	-3930.	398.	94561.	.918	.04266738	26143.1	-102.8
361.975	270.605	-3076.	301.	80728.	.946	.08028461	52434.5	-79.2
362.945	266.105	-2848.	276.	77855.	.954	.09132650	60306.6	-75.0
363.926	258.461	-2623.	251.	75174.	.968	.10308824	68631.9	-71.9
365.886	237.290	-2202.	206.	70446.	1.010	.12875716	86099.2	-70.1
366.856	213.282	-2016.	186.	68400.	1.010	.13819482	94836.7	-59.9
367.826	200.494	-1847.	167.	66527.	1.010	.15479974	103613.1	-69.8
369.787	170.890	-1547.	135.	63201.	1.010	.18819224	121818.7	-82.6
370.767	151.082	-1421.	122.	61747.	1.010	.19723407	130795.2	-73.4
371.748	135.952	-1312.	110.	60408.	1.010	.20822276	139491.4	-69.4

AM 6.03

Fort Churchill 1-29-58 1306 CST

Accelerometer Recycle Period, Seconds

Upleg		Downleg		Minimum	Transit
Upper Limit	Lower Limit	Upper Limit	Lower Limit	Transit Time	Distance x 2 Feet
1.09000	1.21000	1.09000	1.21000	.00800	.0313

Threshold Acceleration		Mean Acceleration, Ft/Sec^2		Elapsed Time	
Upleg	Downleg	Upleg	Downleg	Upleg	Downleg
.10	.20	.60	.60	14.	10.

g_o Ft/Sec^2	r_o Feet	cos ∅	sin ∅	cosΘ	sin Θ
32.2270	20903520.	.51877000	.85491000	-.60182000	.79864000

M/A $Slugs/Ft^2$
1.3360

Balloonsonde Data

Altitude Feet	Pressure Lb/Ft^2	Temperature Deg Fahr	Density $Slug/Ft^3$
.	2121.	1.9	.00267792
1066.	2034.	-4.3	.00260171
1936.	1963.	6.4	.00245369
4298.	1783.	5.7	.00223265
5905.	1668.	1.6	.00210761
6266.	1649.	5.0	.00206853
8005.	1537.	5.0	.00192714
10417.	1390.	-4.0	.00177829
11729.	1319.	-7.9	.00170162
14961.	1148.	-21.1	.00152580
21325.	866.	-48.4	.00122734
22195.	835.	-48.1	.00118246
23589.	785.	-49.0	.00111394
25623.	710.	-55.9	.00102435
30381.	572.	-58.9	.00083180
36089.	438.	-53.2	.00062848
40682.	355.	-52.9	.00050832
43143.	317.	-54.8	.00045672
45275.	288.	-54.4	.00041429
53182.	196.	-61.6	.00028730
55413.	179.	-59.7	.00026155
68405.	96.	-69.7	.00014351
89239.	35.	-97.6	.00005712
98780.	20.	-85.9	.00003255

Raw accelerometer data, upleg and downleg, time in seconds

51.05000	52.22000	53.39000	53.54193	54.56000	55.73000	56.89000	57.09534
58.06000	59.23000	59.50903	60.40000	61.57000	62.73000	63.11052	63.90000
65.07000	65.54575	66.24000	66.73547	67.40000	68.56000	69.07136	69.73000
70.41241	70.90000	71.64093	72.06000	72.69300	73.22000	73.91000	74.39000
75.28078	75.56000	76.39237	76.72000	77.61167	77.88000	78.77689	79.05000
79.94047	80.21000	81.10746	81.37000	82.26349	82.54000	83.43527	83.70000
84.52065	84.86000	85.75528	86.01000	86.74982	87.18000	87.79655	88.33000
89.04384	89.49000	90.08779	90.65000	91.54829	91.81000	92.70724	92.97000
93.86311	.00000	.00000	.00000	.00000	.00000	.00000	.00000

301.7700	302.6584	302.8800	303.7633	304.0000	304.8796	305.1100	305.5881
306.2300	306.5817	307.3400	308.2236	308.4600	309.3451	309.5800	310.4688
310.6900	311.5780	311.8100	312.6948	312.9200	313.8039	314.0400	314.9245
315.1600	316.0221	316.2700	317.1544	317.3800	317.9239	318.5000	319.3852
319.6200	320.5069	320.7300	321.6160	321.8500	322.7330	322.9600	323.8467
324.0700	324.8015	325.1900	325.7800	326.3000	327.1823	327.4200	328.0747
328.5400	329.3436	329.6500	330.3185	330.7700	331.3553	331.8800	332.3579
332.9900	333.4646	334.1100	334.5654	335.2200	335.9149	336.3300	336.7191
337.4500	337.8062	338.5600	338.8473	339.6800	339.9463	340.7800	341.0321
341.9000	342.1375	343.0100	343.2246	344.1300	344.3214	345.2400	345.4067
346.3500	346.4977	347.4700	348.5800	349.6900	349.7972	350.8000	350.8987
351.9100	352.0006	353.0200	353.1019	354.1400	354.2130	355.2500	355.3150
356.3600	356.4189	357.4700	357.5235	358.5800	358.6288	359.7000	359.7453
360.8100	360.8511	361.9200	361.9576	363.0300	363.0642	364.1300	364.1610
365.2500	365.2780	366.3600	366.3858	367.4600	367.4834	368.5700	368.5907
369.6900	369.7166	370.7900	370.8060	371.9000	371.9143	373.0100	373.0227
374.1300	374.1420	375.2400	375.2510	376.3500	376.3603	377.4600	378.5800
378.5903	379.6900	379.7102	380.8000	380.8108	381.9200	381.9311	383.0300
383.0417	384.1400	384.1676	385.2600	385.2731	386.3700	386.3837	387.4700
387.4846	388.5800	388.5957	389.7000	389.7165	390.8100	390.8275	391.9200
391.9385	393.0300	393.0495	394.1400	394.1616	395.2400	395.2630	396.3500
396.3738	397.4600	397.4845	398.5600	398.5847	399.6700	399.6952	400.7800
400.8059	401.8800	401.9056	402.9900	403.0163	404.0900	404.1167	405.2000
405.2261	406.3100	406.3364	407.4100	407.4365	408.5100	408.5711	409.6300

AM 6.03 Acceleration ft/sec^2 vs time, upleg and downleg

53.46597	1.35713	302.2142	.03970	356.3895	9.01756
56.99267	.74295	303.3217	.04015	357.4967	10.95703
59.36952	.40236	304.4398	.04049	358.6044	13.17626
62.92026	.21635	305.3491	.13704	359.7226	15.30645
65.30788	.13841	306.4059	.25321	360.8306	18.52726
66.48774	.12761	307.7818	.04013	361.9388	22.20597
68.81568	.11980	308.9026	.03999	363.0471	26.78330
70.07121	.06727	310.0244	.03966	364.1455	32.61942
71.27047	.05706	311.1340	.03973	365.2640	39.93013
72.37650	.07818	312.2524	.04001	366.3729	47.13599
73.56500	.06580	313.3620	.04010	367.4717	57.50877
74.83539	.03948	314.4823	.04005	368.5804	72.82991
75.97619	.04522	315.5911	.04215	369.7033	44.17577
77.16584	.03940	316.7122	.04005	370.7980	122.67845
78.32845	.03894	317.6520	.10589	371.9071	153.40977
79.49524	.03951	318.9426	.03998	373.0164	192.71299
80.65873	.03889	320.0634	.03983	374.1360	217.92141
81.81675	.03924	321.1730	.03990	375.2455	261.3062
82.98764	.03909	322.2915	.04018	376.3552	293.0149
84.11033	.04652	323.4033	.03985	378.5851	297.0565
85.30764	.03909	324.4358	.05354	379.7001	76.47081
86.37991	.05724	325.4850	.08998	380.8054	266.6204
87.48828	.08241	326.7411	.04025	381.9256	252.4346
88.68692	.06148	327.7473	.07309	383.0358	230.43056
89.78890	.08766	328.9418	.04851	384.1538	41.21374
91.09915	.03882	329.9842	.07010	385.2665	183.67431
92.25862	.03892	331.0627	.09144	386.3768	167.89611
93.41656	.03928	332.1190	.13716	387.4773	147.36944
		333.2273	.13909	388.5878	127.42437
		334.3377	.15108	389.7083	114.92491
		335.5675	.06487	390.8187	102.76076
		336.5246	.20691	391.9293	91.43284
		337.6281	.24691	393.0397	82.81397
		338.7036	.37957	394.1508	67.33466
		339.8131	.44191	395.2515	59.48039
		340.9060	.49302	396.3619	55.44648
		342.0188	.55532	397.4723	52.06345
		343.1173	.68028	398.5724	51.35025
		344.2257	.85495	399.6826	49.33000
		345.3233	1.12770	400.7930	46.73739
		346.4239	1.43598	401.8928	47.98776
		349.7436	2.72394	403.0032	45.32419
		350.8493	3.21834	404.1033	43.97713
		351.9553	3.81470	405.2131	45.91851
		353.0609	4.67377	406.3232	44.84783
		354.1765	5.88013	407.4232	44.67680
		355.2825	7.42595	408.5405	8.40516

Time in seconds (x10)
of rejected data points

3254'
3267'
3289'
3352'
3696'
3796'
3841''

53.47 336.52 6. 10. ← Points used in peak time calculation

Time	a_D ft/sec^2	Vert.Vel.	Horiz.Vel.	Alt.	C_D	Density slugs/cu ft x 10^3	Pressure lbs/sq ft x 10^3	Temp. °F
199.861	.000	.	500.	539251.				
199.861	.000	.	500.	557685.				
199.861	.000	.	500.	556961.				
199.861	.000	.	500.	556974.				
322.292	.040	-3762.	516.	327546.	1.522	.00000489		
323.403	.040	-3796.	516.	323344.	1.521	.00000477	3.5	-24.3
324.436	.058	-3829.	516.	319409.	1.410	.00000743	4.3	-122.7
327.747	.073	-3932.	517.	306561.	1.336	.00000929	7.6	19.4
329.984	.070	-4001.	517.	297689.	1.341	.00000858	10.1	227.8
331.063	.091	-4035.	518.	293356.	1.262	.00001170	11.5	112.3
332.119	.137	-4068.	518.	289077.	1.208	.00001804	13.4	-25.4
333.227	.139	-4103.	518.	284550.	1.205	.00001803	16.5	74.1
334.338	.151	-4137.	519.	279976.	1.196	.00001941	19.2	116.8
336.525	.207	-4205.	519.	270855.	1.164	.00002645	25.7	106.8
337.628	.247	-4240.	519.	266196.	1.146	.00003155	29.9	93.4
338.704	.379	-4273.	520.	261618.	1.104	.00004959	35.7	-40.3
339.813	.442	-4307.	520.	256859.	1.088	.00005764	43.7	-18.0
340.906	.493	-4341.	520.	252134.	1.077	.00006401	52.7	20.3
342.019	.555	-4375.	520.	247285.	1.066	.00007170	63.0	52.9
343.117	.680	-4409.	520.	242460.	1.051	.00008776	75.1	39.2
344.226	.855	-4443.	521.	237554.	1.033	.00011048	90.4	17.0
345.323	1.128	-4477.	521.	232660.	1.011	.00014676	110.1	-22.7
346.424	1.436	-4510.	521.	227715.	.992	.00018771	136.0	-37.5
349.744	2.724	-4608.	521.	212583.	.961	.00035241	260.9	-28.4
350.849	3.218	-4639.	521.	207471.	.958	.00041190	322.4	-3.6
351.955	3.815	-4670.	521.	202324.	.956	.00048318	395.1	16.7
353.061	4.674	-4700.	521.	197144.	.952	.00058655	482.4	19.5
354.177	5.880	-4730.	520.	191885.	.948	.00073192	591.7	11.3
355.283	7.426	-4757.	520.	186639.	.944	.00091761	728.0	2.5
356.390	9.017	-4783.	519.	181359.	.941	.00110610	896.7	12.6
357.497	10.957	-4807.	518.	176050.	.938	.00133530	1101.5	20.9
358.605	13.176	-4829.	517.	170714.	.934	.00159807	1348.9	32.1
359.723	15.306	-4849.	516.	165303.	.931	.00184813	1644.0	58.6
360.831	18.527	-4865.	514.	159923.	.927	.00223196	1991.3	60.1
361.939	22.206	-4878.	512.	154525.	.923	.00267301	2410.4	65.7
363.047	26.783	-4886.	510.	149115.	.918	.00323024	2916.1	66.3
364.146	32.619	-4888.	507.	143748.	.913	.00395186	3526.6	60.2
365.264	39.930	-4883.	503.	138284.	.908	.00487443	4290.5	53.1
366.373	47.136	-4870.	498.	132876.	.906	.00580070	5206.4	63.2
367.472	57.509	-4848.	493.	127537.	.906	.00714343	6302.3	54.3
368.580	72.830	-4811.	486.	122183.	.906	.00918617	7687.1	27.8
370.798	122.678	-4666.	465.	111675.	.906	.01645602	11863.1	-39.7
371.907	153.410	-4549.	450.	106565.	.906	.02165408	14949.4	-57.5
373.016	192.713	-4394.	431.	101606.	.906	.02916847	18941.0	-81.4
374.136	217.921	-4200.	409.	96795.	.909	.03595489	23923.2	-72.1
375.245	261.306	-3971.	384.	92263.	.916	.04788107	29950.1	-95.3
376.355	293.015	-3700.	355.	88007.	.925	.06127617	37334.5	-104.8
378.585	297.056	-3117.	293.	80407.	.945	.08578713	55033.4	-86.0
380.806	266.620	-2564.	235.	74101.	.974	.11032657	74710.4	-65.2
381.926	252.434	-2311.	209.	71371.	1.000	.12530007	84989.8	-64.6
383.036	230.430	-2079.	185.	68935.	1.010	.13995839	95323.9	-62.9
385.267	183.674	-1690.	145.	64731.	1.010	.16888414	116049.2	-59.4
386.377	167.896	-1532.	128.	62943.	1.010	.18815238	126264.4	-68.8
387.477	147.369	-1394.	114.	61334.	1.010	.19945666	136252.2	-61.8
388.588	127.424	-1277.	102.	59851.	1.010	.20545136	145869.7	-46.1

AM 6.05

Fort Churchill 3-4-58 1330 CST

Accelerometer Recycle Period, Seconds

Upleg Upper Limit	Upleg Lower Limit	Downleg Upper Limit	Downleg Lower Limit	Minimum Transit Time	Transit Distance x 2 Feet
1.02000	1.11000	1.02000	1.11000	.00800	.0313

Threshold Acceleration Upleg	Threshold Acceleration Downleg	Mean Acceleration, Ft/Sec^2 Upleg	Mean Acceleration, Ft/Sec^2 Downleg	Elapsed Time Upleg	Elapsed Time Downleg
.20	.20	2.70	1.20	14.	13.

g_o Ft/Sec^2	r_o Feet	cos ∅	sin ∅	cos θ	sin θ
32.2270	20903520.	.51877000	.85491000	-.44932000	.89337000

M/A Slugs/Ft^2
1.3290

Balloonsonde Data

Altitude Feet	Pressure Lb/Ft^2	Temperature Deg Fahr	Density Slug/Ft^3
.	2128.	-19.2	.00281420
394.	2090.	-21.9	.00278153
853.	2055.	-21.9	.00273429
1280.	2015.	-16.9	.00265098
2231.	1938.	-13.4	.00252981
4068.	1791.	-16.6	.00235608
4495.	1762.	-13.4	.00230082
5971.	1654.	-12.5	.00215472
8186.	1507.	-17.4	.00198585
8989.	1457.	-15.0	.00190974
10236.	1382.	-16.0	.00181492
13878.	1182.	-24.4	.00158187
20407.	885.	-50.1	.00125946
21699.	835.	-52.3	.00119447
24869.	720.	-60.4	.00105112
28740.	601.	-60.4	.00087746
36975.	413.	-52.3	.00059126
51506.	208.	-58.9	.00030358
56693.	162.	-62.2	.00023872
58268.	152.	-64.3	.00022464
63386.	119.	-62.5	.00017461
78576.	58.	-68.8	.00008715
92815.	29.	-65.8	.00004324
96139.	25.	-61.0	.00003661

AM 6.05

Raw accelerometer data, upleg and downleg, time in seconds

45.88000	45.95086	46.98000	47.05931	48.07000	48.15885	49.16000	49.25786
50.24000	50.34962	51.32000	51.44318	52.40000	52.46592	53.48000	53.63752
54.57000	54.74340	55.66000	56.74000	56.95245	57.82000	58.91000	59.18196
59.99000	61.07000	61.37614	62.15000	63.24000	63.59721	64.32000	65.41000
65.86722	66.49000	66.87460	67.57000	68.19445	68.66000	69.08394	69.74000
70.57207	70.82000	71.36152	71.90000	72.69661	72.99000	73.69966	74.06000
74.59400	75.14000	75.75628	76.22000	76.83205	77.30000	77.80142	78.38000
79.02905	79.45000	79.91135	80.53000	81.31215	.00000	.00000	.00000
328.8300	329.6635	329.8800	330.7131	330.9300	331.7189	331.9800	332.6463
333.0300	333.5504	334.0800	334.7308	335.1300	335.7609	336.1800	336.6152
337.2400	338.0689	338.2800	338.7077	339.3300	339.9770	340.3800	341.0503
341.4300	342.2417	342.4800	342.9808	343.5300	344.1544	344.5800	345.0437
345.6300	346.1840	346.6800	347.3800	347.7300	348.3293	348.7800	349.4655
349.8300	350.2619	350.8700	351.3390	351.9200	352.3084	352.9700	353.3716
354.0200	354.3767	355.0700	355.4422	356.1200	357.1600	357.4563	358.2200
359.2600	359.4924	360.3100	360.5300	361.3600	361.5744	362.4000	362.7639
363.4500	363.6139	364.5000	364.6444	365.5500	365.6810	366.6000	366.7160
367.6400	367.7442	368.6900	368.8537	369.7400	370.7900	370.8679	371.8400
371.9102	372.8900	372.9536	373.9400	373.9969	374.9800	375.0317	376.0300
376.0767	377.0800	377.1219	378.1200	378.1578	379.1700	379.2040	380.2200
380.2504	381.2700	381.2973	382.3200	382.3444	383.3600	383.3811	384.4100
384.4294	385.4600	385.4772	386.5000	386.5154	387.5500	387.5642	388.6000
388.6131	389.6500	389.6716	390.6900	390.7012	391.7400	391.7506	392.7900
392.8317	393.8400	393.8502	394.8900	394.9002	395.9500	395.9603	396.9900
397.0006	398.0400	399.0900	399.1014	400.1400	400.1521	401.1800	401.1925
402.2300	402.2433	403.2800	403.3025	404.3300	404.3442	405.3800	405.4292
406.4400	406.4568	407.4700	407.4880	408.5200	408.5386	409.5600	409.5805
410.6000	410.6219	411.6500	411.6728	412.6900	412.7132	413.7300	413.7533
414.7800	414.8049	415.8300	415.8546	416.8700	416.8941	417.9100	417.9360
418.9600	418.9865	420.0000	420.0265	421.0400	421.0663	422.0900	422.1166
423.1300	423.1554	424.1800	424.2060	425.2200	425.2463	426.2700	426.2972
427.3100	427.3359	428.3500	428.3771	429.3900	429.4173	430.4300	430.4574
-395.3333							

AM 6.05 Acceleration ft/sec^2 vs time, upleg and downleg

45.91543	6.23892	329.2468	.04510	381.2836	42.18878
47.01966	4.98035	330.2965	.04514	382.3322	52.83707
48.11443	3.96819	331.3245	.05033	383.3705	70.63062
49.20893	3.27117	332.3131	.07056	384.4197	82.89541
50.29481	2.60697	333.2902	.11570	385.4686	106.26017
51.38159	2.06459	334.4054	.07397	386.5077	131.58465
52.43296	7.20899	335.4455	.07870	387.5571	155.81302
53.55876	1.26252	336.3976	.16537	388.6065	184.23872
54.65670	1.04187	337.6545	.04559	389.6608	67.08522
56.84623	.69406	338.4938	.17128	390.6956	247.95690
59.04598	.42355	339.6535	.07484	391.7453	278.2972
61.22307	.33424	340.7151	.06973	392.8108	18.04120
63.41861	.24550	341.8358	.04755	393.8451	299.3873
65.63861	.14986	342.7304	.12490	394.8951	304.0752
66.68230	.21178	343.8422	.08036	395.9552	296.4501
67.88223	.08034	344.8118	.14571	396.9953	280.4104
68.87197	.17431	345.9070	.10207	399.0957	240.23184
70.15604	.04525	347.0300	.06394	400.1460	216.12991
71.09076	.10683	348.0297	.08721	401.1862	200.83140
72.29831	.04937	349.1228	.06666	402.2366	177.37610
73.34483	.06221	350.0460	.16792	403.2913	61.93656
74.32700	.10986	351.1045	.14245	404.3371	155.37377
75.44814	.08248	352.1142	.20767	405.4046	12.92575
76.52603	.08362	353.1708	.19425	406.4484	111.39695
77.55071	.12459	354.1983	.24627	407.4790	97.12171
78.70453	.07436	355.2561	.22618	408.5293	90.55366
79.68068	.14718	357.3081	.35692	409.5702	74.76314
80.92108	.05121	359.3762	.58002	410.6110	65.13920
		360.4200	.64748	411.6614	60.10310
		361.4672	.68149	412.7016	58.30182
524''		362.5820	.23659	413.7417	57.70669
		363.5319	1.16644	414.7924	50.69045
		364.5722	1.50339	415.8423	51.76523
		365.6155	1.82462	416.8821	53.84888
		366.6580	2.32846	417.9230	46.16438
		367.6921	2.88462	418.9733	44.57719
		368.7718	1.16928	420.0132	44.77998
		370.8290	5.15689	421.0532	45.18643
		371.8751	6.36589	422.1033	44.37588
		372.9218	7.75926	423.1427	48.59543
		373.9685	9.67931	424.1930	46.37795
		375.0059	11.72495	425.2332	45.22241
		376.0533	14.39488	426.2836	42.34284
		377.1009	17.88697	427.3230	46.69961
		378.1389	21.89024	428.3636	42.56336
		379.1870	27.17897	429.4036	42.03270
		380.2352	33.91979	430.4437	41.66514

Time in seconds (x10)
of rejected data points

3625'
3687'
3896'
3928'
4032'
4054''

AM 6.05

45.91 355.26 10. 10. ← Points used in peak time calculation

Time	a_D ft/sec^2	Vert.Vel.	Horiz.Vel.	Alt.	C_D	Density slugs/cu ft x 10^3	Pressure lbs/sq ft x 10^3	Temp. °F
208.756	.000	.	500.	587283.				
208.756	.000	.	500.	594264.				
208.756	.000	.	500.	594290.				
348.030	.087	-4273.	520.	298153.	1.251	.00001000		
349.123	.067	-4307.	520.	293465.	1.324	.00000711	7.3	137.2
350.046	.168	-4336.	520.	289476.	1.180	.00001984	8.8	-200.3
351.104	.142	-4369.	521.	284870.	1.194	.00001638	11.4	-52.6
352.114	.208	-4400.	521.	280443.	1.157	.00002430	14.2	-118.4
353.171	.194	-4433.	521.	275777.	1.162	.00002230	17.6	1.4
354.198	.246	-4465.	521.	271206.	1.139	.00002846	21.2	-24.3
355.256	.226	-4498.	522.	266467.	1.145	.00002560	25.3	115.8
357.308	.357	-4561.	522.	257173.	1.100	.00004093	34.8	36.2
359.376	.580	-4625.	523.	247674.	1.053	.00006761	50.7	-22.6
360.420	.647	-4658.	523.	242830.	1.046	.00007488	61.5	19.4
361.467	.681	-4690.	523.	237936.	1.046	.00007778	73.3	89.6
363.532	1.166	-4753.	524.	228189.	1.003	.00013520	105.2	-6.2
364.572	1.503	-4784.	524.	223229.	.983	.00017552	129.4	-30.2
365.616	1.825	-4815.	524.	218222.	.969	.00021342	160.0	-22.9
366.658	2.328	-4846.	524.	213186.	.962	.00027079	198.3	-33.0
367.692	2.885	-4876.	524.	208160.	.959	.00033263	246.0	-28.7
370.829	5.157	-4962.	524.	192731.	.949	.00058001	463.1	5.5
371.875	6.366	-4989.	523.	187527.	.946	.00071094	569.0	6.6
372.922	7.759	-5015.	523.	182292.	.943	.00086071	698.9	13.4
373.969	9.679	-5039.	522.	177030.	.939	.00106781	859.0	9.0
375.006	11.725	-5061.	521.	171792.	.935	.00128772	1054.0	17.2
376.053	14.395	-5080.	520.	166481.	.931	.00157637	1294.3	18.7
377.101	17.887	-5097.	519.	161151.	.926	.00195614	1591.9	14.4
378.139	21.890	-5109.	517.	155855.	.922	.00239367	1956.3	16.5
379.187	27.179	-5117.	515.	150497.	.917	.00298044	2411.7	11.7
380.235	33.920	-5118.	512.	145134.	.911	.00374014	2982.0	4.8
381.284	42.189	-5111.	509.	139772.	.906	.00469144	3697.5	-.5
382.332	52.837	-5095.	504.	134421.	.906	.00591419	4596.0	-7.0
383.371	70.631	-5064.	498.	129147.	.906	.00800331	5755.2	-40.8
384.420	82.895	-5018.	490.	123859.	.906	.00957031	7230.8	-19.5
385.469	106.260	-4952.	481.	118631.	.906	.01259539	9065.1	-40.4
386.508	131.585	-4862.	470.	113532.	.906	.01618156	11391.1	-49.6
387.557	155.813	-4745.	455.	108492.	.906	.02011756	14296.8	-45.7
388.607	184.239	-4601.	439.	103588.	.906	.02530533	17834.4	-49.1
390.696	247.957	-4218.	397.	94377.	.908	.04043283	27327.1	-66.0
391.745	278.297	-3977.	371.	90076.	.916	.05065621	33557.8	-73.8
393.845	299.387	-3440.	316.	82290.	.933	.07150974	48610.3	-63.7
394.895	304.075	-3158.	287.	78827.	.943	.08526302	57269.6	-68.4
395.955	296.450	-2875.	258.	75630.	.953	.09924970	66686.9	-68.3
396.995	280.410	-2609.	232.	72778.	.969	.11208361	76316.9	-63.0
399.096	240.232	-2132.	184.	67800.	1.010	.13816167	96182.9	-54.1
400.146	216.130	-1926.	164.	65670.	1.010	.15223278	106081.6	-53.8
401.186	200.831	-1744.	146.	63762.	1.010	.17272870	115999.5	-68.5
402.237	177.376	-1579.	129.	62017.	1.010	.18601999	126020.0	-65.0
404.337	155.374	-1298.	101.	58996.	1.010	.24133294	146587.0	-105.9